The Seismic Velocity Structure of the Crust and Uppermost Mantle in Sudan and East Africa

By

Nada Bushra El Tahir

June 2014

A thesis submitted to the
Faculty of Science, University of the Witwatersrand, Johannesburg,
in fulfillment of the requirements for the degree of
Doctor of Philosophy

DECLARATION

I declare that this thesis is my own. It is being submitted for the degree of Doctor of Philosophy at the University of the Witwatersrand, Johannesburg. It has not been submitted before for any degree or examination in any other University

Signed in Khartoum, Sudan on the 25th of June 2014.

Nada Bushra El Tahir Ahmed

Nada Bushra

Abstract

In this thesis the crustal structure beneath two areas of Africa is investigated. In Sudan, the new constraints on the crustal structure beneath the northern part of the Khartoum basin have been obtained. In East Africa, the size of the Tanzania Craton, and the differences between the Eastern and Western branches of the East African Rift System (EARS) have been determined. In southern Tanzania, the debate on the secular variation between Proterozoic and Archean crust has been investigated. The approach used in this thesis involves different data sets and methods.

In first part of the thesis, the crustal structure of the northern part of the Mesozoic Khartoum basin is investigated by using two modelling methods: H-k stacking of receiver functions, and a joint inversion of receiver functions and Rayleigh wave group velocities. H-k stacking indicated that the crust is 33-37 km thick with an average of 35 km, and the crustal Vp/Vs ratio is 1.74-1.81 with an average of 1.78. Similar results were obtained from the joint inversion for Moho depth, as well as an average shear wave velocity of 3.7 km/s for the crust. These results provide the first seismic estimates of Moho depth for a basin in Sudan. When compared to average crustal thickness for unrifted Proterozoic crust in eastern Africa, our results indicate that only a few kilometers of crustal thinning may have occurred beneath the Khartoum basin. This finding is consistent with estimates of effective elastic plate thickness, which indicate little modification of the Proterozoic lithosphere beneath the basin, and suggests that there may be insufficient topography on the lithosphere-asthenosphere boundary beneath the Sudanese basins to channel plume material westward from Ethiopia.

In the second part of the thesis, the uppermost mantle structure beneath East Africa is investigated by using a standard singular value decomposition algorithm model. Results reveal fast Pn velocities beneath the Mozambique Belt to the east of the craton, the Kibaran Belt west of the craton, and beneath the northern half of the Ubendian Belt to the southwest of the craton. These results indicate that the cold, thick lithosphere of the Tanzania Craton extends beneath the Proterozoic mobile belts and the areal extent of the cratonic lithosphere is much larger than is indicated

by the mapped boundaries of the craton. The results also show that the Pn velocities beneath the volcanic provinces along the Western Branch are not anomalously slow, which indicates little, if any, perturbation of the uppermost mantle beneath them. This is in contrast to the upper mantle structure at depths ≥ 70 km beneath the volcanic regions, which is clearly perturbed. The fast Pn velocities beneath the Western Branch contrast with the slow Pn velocities (7.5-7.8 km/s) beneath the Eastern Branch in Kenya, indicating that the upper mantle beneath the Eastern Branch has been altered more than beneath the Western Branch.

In the third part, the crustal structure beneath two Proterozoic mobile belts, the Usagaran and the Ubendian belts, is investigated by using the Non-Dominated Genetic Algorithm method. In the Usagaran belt, results show an average Moho depth of 35 km for station MAFI and 41 and 42 km for stations MOGR and MIKU, respectively. In the Ubendian Belt, results showed an average Moho depth of 43 km beneath the Ufipa sub-terrane compared to 39 km for Wakole sub-terrane. These results indicate localized thickening in the Ufipa sub-terrane, but not beneath the entire Ubendian Belt. These results indicate that is no clear evidence that Paleoproterozoic crust in East Africa is substantially thicker than Archaean crust.

Acknowledgements

First and foremost I thank God for being my strength and guide in the writing of this thesis. He was always there when I needed his support, peace and blessing.
This study was mostly done at the School of Earth and Mineral Sciences, Penn State University, as part of my PhD programme at the Witwatersrand University; Johannesburg, South Africa. This PhD programme was sponsored by Schlumberger Foundation's Faculty for the Future program and AfricaArray organization. I am very grateful to these organizations.

At Penn State University, the work has been done under the guidance of Prof. Andrew Nyblade, who was my co-supervisor. I am heartily thankful to him for the constant advice, help, encouragement, care, and support. I am very grateful to my supervisor, Prof. Ray Durrheim of the School of Geosciences at the University of the Witwatersrand, Johannesburg, South Africa. He provided valuable advice and orientation needed in this work.

I am also grateful to Prof. Charles Ammon, Dr. Jordi Julià and Dr. Brazier of Penn State University for their codes which I made extensive use of.

During my stay at Penn State, I received the support of the AfricaArray group at the Department of Geosciences, School of Earth and Mineral Sciences. My sincere thanks to the former and present members of the 444 Geophysics Lab namely, G. Mulibo, F. Tugume, S. Hansen, A. Adams, A. Raveloson, C. Ramirez, M. Kachingwe, J. P. O'Donnell, E. Emry, C. Johnson, G. Arroyo, A. Gaynor and K. Homman, with whom I shared knowledge and problems concerning our research during weekly group meetings. Many thanks go to Antonia Mooney, the administrative assistant for her support and much assistance during my period of stay. I still remember that moment in my first day in State college, USA, when she met me at the airport.

During my stay at the Witwatersrand University, I acknowledge the support of the corresponding AfricaArray group, School of Geosciences, especially Dr Alain Tokam Kamga and Dr Musa Manzi. I would like to also thank Prof. Paul Dirks, the former Head of the School of Geosciences at the University of the Witwatersrand, for organizing my first stint at Penn State University. I am grateful to Dalena Prentice, Leza Prentice and Sharon Ellis, the administrative assistants at the University of the Witwatersrand, for their assistance and help in solving all the practical problems. During my stay at the Witwatersrand University, I had a great chance to visit and stay at the Council for Geosciences for three months, I am very grateful to the Manager of the Seismological Unit, Michelle Grobbelaar, for allowing me to stay over. I am very grateful to the staff at the council, Dr V. Midzi and Dr E. Kgaswane, with whom I have had stimulating discussions valuable to my work.

I would like to mention my family whose sacrifice enabled me to complete my studies. My husband, Osman, I thank him for allowing me to carry out this study, something that is not common in my country Sudan, and for being patient with me for the whole time he has been alone with the children, my deepest gratitude to him for the support and encouragement that kept me going. To our kids, Ahmed and Rayan, who endured so much time separate from their mother without complaining, I thank them for that gift. Thanks also to all the social and moral support, which I have received from my family and my family-in-law as well as friends; they were so helpful in the accomplishment of my task.

List of personal publications

- El Tahir, N.A., Nyblade, A.A., Julià, J., and Durrheim, R.J., 2013, Crustal structure of the Khartoum Basin, Sudan. Tectonophysics, 593, 151–160.
- Abd Alhadi Ibrahim Alhassan, Amani Elkhidir Belail, Hatim Siddig Hag Elbashir, Indira Abdel Rahman Mohamed, Mustafa Bashir Mohammed, Nada Bushra Eltahir, and Jens Havskov, 2007, The Sudanese Seismic Network, Seismological Research Letters, 78, 498-501.
- Data Base from the Sudan Seismic Network for the period November 2003 to April 2006 and the Seismic Catalog for Sudan, Nada Bushra Eltahir and Amani Elkhidir Belail, published at www.sudan.mnfa.uib.no
- Seismotectonics of Sudan and the implication of the fault plane solutions on the stress of the area, by Nada Bushra El Tahir, published at www.sudan.mnfa.uib.no.
- Location and Magnitude of Abu Delig Earthquake in Central Sudan, by Nada Bushra El Tahir, published at www.sudan.mnfa.uib.no.
- Data Base status until April 2007, by Nada Bushra El Tahir and Hatim Siddig Hag Elbashir, published at www.sudan.mnfa.uib.no.
- O.M. Abudaltif, N.B. El Tahir, S.H.Osman and S.H Abass, Engineering geology, mining and environmental aspects: A case study from tropical Sudan, Symposium on Engineering Geology and Environment, Athens 1997.

Workshops and Conferences

- Attended and presented paper about the Seismicity in Sudan at the Eighth Annual Africa Array Workshop held in School of Geosciences, Witwatersrand University, Johannesburg, South Africa, 14–17 January 2014.
- Attended and presented a poster at The American Geophysical Union Fall Meeting, San Francisco, USA, 3-7 December 2012.
- Attended the First Geodynamics Processes at Rifting and Subduction Margins Workshop in New Jersey, USA, October 2012.
- Attended the Second Workshop for the Global Earth Model (GEM) in North Africa, Tunis, May 2012.
- Attended and presented a paper about Seismicity in Sudan at the Seventh Annual Africa Array Workshop, School of Geosciences, Witwatersrand University, Johannesburg, South Africa, 19-21November 2011.
- Attended and presented a paper in the First Workshop for the Global Earth Model (GEM) in North Africa, Rabat, Morocco, May 2011.
- Attended and presented a paper about the Seismicity in Sudan at the Sixth Annual Africa Array Workshop, School of Geosciences, Witwatersrand University, Johannesburg, South Africa, 19-21 November 2010.
- Attended workshop on Three-Dimensional Modeling of Seismic Waves Generation, Propagation and their Inversion, Abdus Salam International Centre for Theoretical Physics, Trieste, Italy, 27 September - 8 October 2010.
- Attended and presented a paper about Seismic Hazard Mitigation in Sudan at the UNESCO Workshop on Reducing Earthquake Losses in the Extended Mediterranean (RELEMR), Luso-American Foundation, Lisbon, Portugal, 26-29 October 2009.
- Attended IASPEI Summer School, Cape Town, South Africa, 19-23 January 2009.

- Attended and presented a poster on Seismicity and Seismotectonics of Sudan at the IASPEI General Assembly, Cape Town, South Africa, 11-16 January 2009.
- Attended a workshop on Three-Dimensional Modeling of Seismic Wave Generation, Propagation and their Inversion, Abdus Salam International Centre for Theoretical Physics, Trieste, Italy, 22 September to 4 October 2008.
- Attended and presented a paper about the Seismicity in Sudan at the Fourth Annual AfricaArray workshop, School of Geosciences, Witwatersrand University, Johannesburg, South Africa, 17-18 June 2008.
- Attended and a presented paper about the Sudanese Seismic Network at the IUGG XXIV General Assembly, Perugia, Italy, 2-13 July 2007.
- Attended workshop in Seismology held at Geological Research Authority of Sudan, April 2007-May, 2007.
- Attended workshop in seismology held at the Geological Research Authority of Sudan, 7-18 December 2006.
- Attended a workshop in seismology held at the Geological Research Authority of Sudan, 24 April 2006 – 8 May 2006.
- Attended a workshop in Earthquakes held at Natural Research Centre, Ministry of Science and Technology, December 2002 - January 2003.
- Attended and contributed with a poster about the Probabilistic Seismic Hazard Assessment for Sudan in the Conference held at the Institute of Solid Earth Physics, University of Bergen, Norway, August 1999.
- Attended a seismological seminar in Turkey to evaluate the damage caused by the big earthquake in May 1998.

TABLE OF CONTENTS

LIST OF FIGURES

LIST OF TABLES

1 INTRODUCTION

1.1 Motivation for Research

In comparison to many other continents, little is known about the structure of the crust and uppermost mantle beneath Africa. This thesis makes contributions to our knowledge of the crustal structure in two areas of eastern Africa, *viz* central Sudan and southern Tanzania (fig 1-1), as well as to our understanding of the uppermost mantle structure beneath the East African Plateau. Crustal structure across Africa has been recently reviewed by Tugume et al. (2013), who found little evidence for secular variations in crustal thickness for terrains spanning some four Ga of the Earth's history, in contrast to findings for other Precambrian terrains. Results presented in this thesis fill in some of the gaps in knowledge of the crustal structure identified by Tugume et al. (2013), and so contributes to the continuing debate on reality of secular variations in the evolution of the crust. As yet there are no comparable reviews of uppermost mantle structure across Africa.

1.2 Previous studies of the crust and uppermost mantle in east Africa

1.2.1 Experiments

As reviewed in Tugume et al. (2013), over the past two decades, there have been several broadband seismic experiments in eastern, southern and western Africa that have provided data for investigating crustal and mantle structure. In eastern Africa these experiments include the Tanzania Broadband Seismic Experiment (TBSE) (Nyblade et al., 1996), the AfricaArray permanent seismic network (africaarray.org), three phases of the AfricaArray East African Seismic Experiment (AAEASE) (Tugume et al., 2012, 2013), the Southeastern Tanzania Basin Experiment (AASTBE) (Mulibo, 2013) and the Ethiopia/Kenya Broadband Seismic Experiments (Nyblade and Langston, 2002). In southern Africa these experiments

include the Southern Africa Experiment (SASE; Carlson et al., 1996) and permanent AfricaArray stations. In Western Africa, a broadband seismic experiment was conducted in Cameron between 2005- 2007 (Tokam et al., 2010).

1.2.2 Crust

Seismic investigations of crustal and upper mantle structure in eastern Africa, western Africa and southern Africa using data from these experiments have yielded important new information, helping to fill in gaps in our knowledge of crustal and mantle structure beneath these areas and improve our understanding of the ongoing geological process (e.g., Last et al., 1997; Brazier et al., 2000; Nyblade and Brazier, 2002; Dugda et al., 2005, 2009; Kgaswane et al., 2009; Tokam et al., 2010; Adams et al., 2012; Tugume et al., 2012, 2013; O'Donnell et al., 2013; Mulibo and Nyblade, 2013; Hosney and Nyblade, 2014). Dugda et al. (2005) revealed that the crust beneath areas of Ethiopia and Kenya away from the Cenozoic rift borders has not been modified significantly by the Cenozoic rifting and magmatism, while the crust beneath the rifted regions has been thinned in several places and greatly modified by the addition of mafic rock. In addition, Dugda et al. (2007) suggested that the shear velocity structure of the Ethiopian Plateau lithosphere can be explained by a plume model and the uplift in Ethiopia can be attributed to the thermally perturbed lithospheric structure.

Tugume et al. (2012, 2013) investigated crustal structure beneath seismic stations in Tanzania and Uganda, and compared the results to those of other Precambrian areas of Africa. The main results are that the average crustal structure is similar across all Precambrian terrains, but there exists variability in lower crustal structure, depending on the local geological history of each terrain. This finding is consistent with crustal structure in southern Africa investigated by Kgaswane et al. (2009), in Cameroon by Tokam et al. (2010) and in Egypt by Hosney and Nyblade (2014). All of these studies showed that many Precambrian terrains of all ages have a mafic lower crust that can be up to ~20 km thick, and that crustal thickness averages between 35 and 45 km. These results are used to understand whether or not

the crustal structure in central Sudan and southern Tanzania are anomalous in any way.

The East African plateau comprises a substantial part of one of the largest topographic anomalies on Earth, the African Superswell (Nyblade and Robinson 1994). There is continuing controversy about the origin of the Africa Superswell, and in particular the influence of upper mantle and the uplift of the East Africa Plateau. The tectonic framework of the East Africa Plateau includes the Archean Tanzania craton in the center surrounded by the Proterozoic mobile belts to the west, south and east.

1.2.3 Uppermost mantle

A number of previous tomographic studies have examined the upper mantle structure in different areas of east Africa using both body and surface wave tomography. In Kenya, a Low Velocity Zone (LVZ) dipping to the west beneath the Tanzania craton has been imaged by Park and Nyblade (2006), consistent with earlier tomographic model from the KRISP project (Achauer et al., 1994). The LVZ has also been imaged beneath the Eastern Branch of the East Africa Rift System (EARS) dipping to the west under the Tanzania craton and extending to ≥ 400 km depth by Ritsema et al. (1998). Adams et al. (2012) imaged a LVZ under the Tanzania craton that also extends into the transition zone and beneath the Western Branch. Recently, a shear wave velocity study by Mulibo and Nyblade (2013) showed evidence of a LVZ in the upper mantle extending to depths of 300-350 km beneath the Tanzania craton. In contrast, fast velocities in the uppermost mantle beneath the Tanzania craton have been imaged, indicating that the lithospheric keel of the craton extends to a depth of ~ 200 km (Ritsema et al. 1998). Other studies investigating the uppermost mantle suggested that there are no broad (~100 km wide) thermal anomalies in the uppermost mantle beneath areas of rifting in northern Tanzania, suggesting that the thermal anomalies that exist deeper in the mantle have not yet reached the base of the crust (Brazier et al., 2000; O'Donnell et al., 2013).

1.3 Methodology

This thesis consists of three main chapters that focus on investigating the crust and upper mantle structure using different methods and data sets to understand the process of crustal deformation and evolution through geological history.

1.3.1 Receiver functions

In Chapter Two, modelling of receiver functions method was used. Receiver functions are time series computed from three-component seismograms, which show the relative response of earth structure near the receiver site (Ammon et al., 1990; Ammon, 1997), and are composed of a direct P wave plus P-to-S conversions. Figure 1-2 shows a simplified and ideal representation of ray propagation resulting in a receiver function. Basically, the S waves travel more slowly than the P waves, so, a direct measure of the depth of the discontinuity is calculated by the time difference in the arrival of the direct P wave and the converted phase (Ps), provided the velocity model is known. In addition to the direct Ps converted phases, the multiples resulting from the discontinuity and free surface (Fig. 1-2), are also seen on the receiver function traces. Modelling of the receiver functions was performed using two techniques: the H-k stacking algorithm (Zhu and Kanamori, 2000), and a joint inversion with Rayleigh wave group velocities (Julià et al., 2000, 2003). The advantage of the H-k stacking method is that there is no need to pick the arrival times of the direct conversion from the Moho and its multiples, because the algorithm stacks the amplitudes of receiver functions at the predicted arrival time for the Moho conversion (Ps) and its multiples (PpPs and PpSs+PsPs) for different crustal thicknesses H and Vp/Vs ratios. The H-k stacking technique also provides better constraints on thickness estimates and crustal Vp/Vs, whilst inverting surface wave dispersion curves and receiver functions provides better constraints on shear velocities.

1.3.2 Pn tomography

In Chapter Three, a standard singular value decomposition algorithm (Wiggins, 1972; Menke, 1989) was used. In this method, the Pn phases correspond to raypaths that are critically refracted at the Moho discontinuity. Thus, Pn travel times are sensitive to the uppermost mantle P-wave velocities. In this approach, Pn travel times of local and regional earthquakes were tomographically inverted to determine velocity variations in the uppermost mantle. The tomographic inversion of travel times solves for crustal time delays at each event, crustal time delays at each station, and lateral variations in mantle. The event delays serve mostly to accommodate errors in event depth and origin time so some structural information can be derived from them. The inversion was set up to include only the mantle ray path following the procedure outlined by Hearn (1984), where the travel times used in the inversion are adjusted for contributions from the crustal legs. This procedure minimizes the influence of crustal structure on the model results (Hearn, 1984).

To account for the varying crustal thicknesses and event depths across the study area, event and station corrections were calculated. After the inversion was initially performed, the residual travel time from the observed and predicted travel times were calculated by subtracting the predicted travel times from the observed travel times for each station-event pair. The residuals for each station and event were then averaged to yield a correction that was then subtracted from the observed travel times and the inversion was performed again.

1.3.3 Waveform inversion

In Chapter Four, a Non-Dominated Sorting Genetic Algorithm (NSGA-II) (Deb et al., 2002) was used to invert waveforms. The “genetic algorithms” are named as such as the ideas are borrowed from evolutionary biology, in which the best, or fittest, individuals in a population survive. The genetic algorithm (Fig. 1-3) works in such a way that an initial population of a fixed size is generated from

random numbers. Each member of this population is a possible solution to the problem being posed, however, these solutions would not be very close. This is the parent generation, from which all other solutions will evolve. NSGA-II is able, for most problems, to find a much better spread of solutions and better convergence near the true Pareto-optimal front compared to the Pareto-archived evolution strategy and the strength-Pareto evolutionary algorithm. The greatest advantage of this technique is that it is a guided search of the model space, provides estimates of the uncertainty of the solution, and allows different sources of data to be combined.

1.4 Thesis summary

1.4.1 Khartoum basin

The work presented in Chapter Two, which is already published (El Tahir et al., 2013), presents new constrains on the crustal structure beneath the northern part of the Khartoum basin. The Khartoum basin is one of several Mesozoic rift basins in Sudan associated with the Central Africa Rift System. Results presented in this chapter provide the first seismic estimates of Moho depth for a basin in Sudan. The data used were obtained from the Sudan Seismic Network (SSN), which consists of 3 permanent seismic stations within 40 km of Khartoum. As mentioned previously, two modelling methods were used, the H-k stacking of receiver functions (Zhu and Kanamori, 2000) and a joint inversion of receiver functions and Rayleigh wave group velocities (Julià et al, 2000, 2003). The main objective of this study was to image velocity discontinuities beneath the three seismic stations around the Khartoum basin and estimate Moho depth. The results show crustal thinning of at most a few kilometers beneath the basin compared to unrifted Proterozoic crust of the same age in Africa. Although the outcome of this study sheds new light on the crustal structure of the Khartoum basin, more detailed studies are needed to further elucidate the nature of the crustal thinning more broadly beneath the Sudan basins.

1.4.2 Uppermost mantle beneath East Africa

In Chapter Three, the uppermost mantle structure beneath East Africa is investigated by inverting Pn travel times. This work expands on work previously conducted by Brazier et al. (2000) and Nyblade and Brazier (2002) using a combined large data set from three different networks, the Tanzania Broadband Seismic Experiment (TBSE), the AfricaArray East African Seismic Experiment (AAEASE) and the AfricaArray Tanzania Basin Seismic Experiment (AATBSE). In this study, P-wave arrival times from regional earthquakes recorded on at least seven stations at distances greater than 200 km were used. The final data compilation yielded good ray coverage across East Africa. The Pn travel times were inverted to determine the uppermost mantle velocity structure using the standard singular value decomposition algorithm (Wiggins, 1972; Menke, 1989), whilst assuming an isotropic medium. The inversion was set up to include only the mantle ray path, following the procedure outlined by Hearn (1984). The main objective was to investigate the velocity variations in the uppermost mantle across the region, which was then used to address two outstanding questions on East African tectonics:

1) To what extent does the cold, thick lithosphere of the Tanzania craton extend beneath the Proterozoic mobile belts that surround it?
2) Do the thermal anomalies in the deeper mantle previously imaged beneath the Cenozoic volcanic provinces in the Western Rift extend upward to the base of the crust?

Answering the first question is important for understanding the size of the Tanzania craton, and the answer to the second question is important for understanding differences between the Eastern and Western branches of the East African Rift System (EARS). Results indicate that the uppermost mantle beneath the volcanic regions of the Western branch of the EARS is not anomalously perturbed.

1.4.3 Crustal structure beneath the Usagaran and Ubendian Belts

In Chapter Four, results are presented of an investigation of the crustal structure beneath two Proterozoic mobile belts, the Usagaran and the Ubendian belts. This was done by modelling regional seismograms from the Karonga earthquakes of 6 and 9 December 2009 recorded on AAESE stations using the Non-Dominated Genetic Algorithm method (NSGA II) (Deb et al., 2002). There has been a long standing debate about secular variation in Precambrian crustal structure, as recently reviewed in Tugume et al. (2012, 2013), Arndt and Davaille (2013) and Abbott et al. (2013). Whether or not Proterozoic crust is thicker than Archaean crust is at the core of this debate. A contribution was made to this debate in this study by examining the crustal structure in these two Paleoproterozoic terranes, and comparing the thickness of the crust beneath these terranes to average Precambrian crustal structure across Africa.

The Proterozoic Usagaran and Ubendian mobile belts formed at about 2.05 to 1.8 Ga and have a genetic relation, as suggested by many authors (e.g., Gabert and Wendt, 1974; Daly et al., 1989). However, they were affected by different tectonic process, including several phases of reactivation since the Paleoproterozoic (Theunissen 1988; Theunissen et al., 1992; Ring 1993). Previous crustal thickness estimates beneath the Ubendian Belt in SE Tanzania craton showed slightly thicker crust than the other Proterozoic mobile belts in East Africa (Last et al., 1997; Julià et al., 2005; Tugume et al., 2012). Results from this study agree that the Ufipa sub-terrane crust has been thickened more than other sub-terranes within the Ubendian Belt.

1.5 Thesis structure

Chapter two, three and four are each written in the format of independent journal articles. For this reason, there is some repetition of content in the description of data and the background sections in these chapters.

Also included in the thesis are three appendices that give additional information. Appendix A contains plots of the H–k stacks of receiver functions for the stations near Khartoum used in the analysis in Chapter 2. Appendix B provides a list of event locations used to study the uppermost mantle structure in Chapter three. Appendix C provides plots of the azimuthal anisotropy for stations used for waveform inversion in Chapter four.

References

Abbott, H., Mooney, W. D., and VanTongeren, A. (2013), The character of the Moho and lower crust within Archean cratons and the tectonic implications, Tectonophysics, 609, 690-705.

Achauer, U. and the KRISP Teleseismic Working Group (1994), New ideas on the Kenya rift based on the inversion of the combined dataset of the 1985 the Kenya rift based on the inversion of the combined dataset of the 1985 and 1989/90 seismic tomography experiments, Tectonophysics, 236(1–4), and 305–329.

Adams, A., Nyblade, A. A. and Weeraratne, D. (2012), Upper mantle shear wave velocity structure beneath the East African plateau: evidence for a deep, plateau wide low velocity anomaly, Geophysical Journal Intentional, 189(1), 123–142.

Al Hassan A. A. I., Khidir Belail A., El Bashir H.S.H, Mohamed I. A. R., Mohammed M. B., El Tahir N. B. and Havskov, J. (2007), The Sudanese Seismic Network, Seismological Research Letters, 78, 498-501.

Arndt, N. and Davaille, A. (2013), Episodic Earth evolution, Tectonophysics, 609. 661-674.

Ammon, C. J. (1997), Receiver functions, http://eqseis.geosc.psu.edu/~cammon /HTML/RftnDocs.

Ammon, C. J., G.E. Randall and G. Zandt (1990), On the non-uniqueness of receiver functions inversions, Journal of Geophysical Research, 95, 15303 – 15318.

Ammon, C. and Simiyu, S. (2005), Crustal Structure in Ethiopia and Kenya from receiver function analysis: Implications for Rift development in eastern Africa, Journal of Geophysical Research, 110, B01303, doi:10.1029/2004JB003065.

Brazier, R. A., Nyblade, A.A. and Langston, C.A. (2000), Pn wave velocities beneath the Tanzania Craton and adjacent rifted mobile belts, East Africa, Geophysical Research Letter, 27(16), 2365–2368.

Carlson, R. W., T. L. Grove, M. J. de Wit, and Gurney J. J. (1996), Program to study crust and mantle of the Archean Craton in southern Africa, Eos, Transactions, American, Geophysical, Union, 77(29), 273–277, doi:10.1029/96EO00194.

Daly, M. C., Chorowicz, J. and Fairhead, J. D. (1989), Rift basin evolution in Africa: the influence of reactivated steep basement shear zones. Special Publication, Geological Society London, 309-334, doi:10.1144/GSL.SP.1989.044.01.17.

Deb K., Agrawl, A., Pratap, A. and Meyarivan, T. (2002). A fast elitist non-dominated sorting genetic algorithm for multi-objective optimization: NSGA-II, IEEE Transactions on Evolutionary Computation, 6, 182-197.

Dugda, M. T., Nyblade, A. A., Julià, J., Langston, C. A., Ammon, C. and Simiyu, S. (2005), Crustal Structure in Ethiopia and Kenya from receiver function analysis: Implications for Rift development in eastern Africa, Journal of Geophysics Research, 110: B01303, doi:10.1029/2004JB003065.

Dugda, M. T., Nyblade, A. A. and Julià, J. (2007), Thin lithosphere beneath the Ethiopian Plateau revealed by a joint inversion of Rayleigh wave group velocities and receiver functions, Journal of Geophysical Research, 112, B08305, doi:10.1029/2006JB004918.

Dugda, M. T., Nyblade, A. A. and Julia, J. (2009), S-wave velocity structure of the crust and upper mantle beneath Kenya in comparison to Tanzania and Ethiopia: Implication or the formation of the East African and Ethiopian plateaus, South African Journal of Geology, 112, 241-250, doi:10.2113/gssajg.112.3-4.241.

El Tahir, N. A., Nyblade, A. A., Julià, J., and Durrheim, R. J. (2013), Crustal structure of the Khartoum Basin, Sudan, Tectonophysics, 593, 151–160.

Gabert, G. and Wendt, I. (1974), Datierung von granitischen Gesteinen im Dodoman- und Usagaran-System und in der Ndembera-Serie (Tanzania), Geologische Jahrbuch B 11, 3-55.

Hearn, T. M. (1984), Pn Travel times in southern California Journal of Geophysical Research, 89, 1843-1855.

Hosney A. and Nyblade A. (2014), Crustal structure in southeastern Egypt: Symmetric thinning of the northern Red Sea rifted margins, Geology, 34726, 1, doi:10.1130/G34726.1.

Julià, J., Ammon, C., Herrmann, R. B. and Correig, A. M. (2000), Joint inversion of receiver functions and surface wave dispersion observations, Geophysical Journal International, 143, 99– 112.

Julià, J., Ammon, C. and Herrmann, R. B. (2003), Lithospheric structure of the Arabian Shield from the joint inversion of receiver functions and surface wave group velocities, Tectonophysics, 371: 1 – 21, doi:10.1016/ S0040-1951(03)00196-3.

Julia, J., Ammon, C.J. and Nyblade, A.A. (2005), Evidence for mafic lower crust in Tanzania, East Africa, from joint inversion of receiver functions and Rayleigh wave dispersion velocities, Geophysical Journal International, 162, 555-569.

Kgaswane, E. M, Nyblade, A. A., Julià, J., Dirks, P.H.G.M., Durrheim R. J. and Pasyanos, M. E. (2009), Shear wave velocity structure of the lower crust in southern Africa: evidence for compositional heterogeneity within Archaean and Proterozoic terrains, Journal of Geophysical Research,114: B12304, doi:10.1029/2008JB006217.

Langston, C. A., Nyblade, A. A. and Owens, T. J. (2002), Regional wave propagation in Tanzania, East Africa, Journal of Geophysical Research, 107 (B1), doi:10.1029/ 2001JB000167.

Last, R.J., Nyblade, A. A., Langston, C.A. and Owens, T.J. (1997), Crustal structure of the East African Plateau from receiver functions and Rayleigh wave phase velocities, Journal of Geophysical Research, 102, 24469–24483.

Lenoir, J. L., Liegeois, J. P., Theunissen, K. and Klerkx, J. (1994), The palaeoproterozoic Ubendian shear belt in Tanzania; geochronology and structure, Journal of African Earth Sciences, 19, 160-184.

Menke, W. (1989), Geophysical Data Analysis: Discrete Inverse Theory, International Geophysics series, 45, p 40.

Mulibo, G.D. and Nyblade, A. A. (2013), The P and S wave velocity structure of the mantle beneath eastern Africa and the African superplume anomaly, Geochemistry Geophysics Geosystems, 14, 2696-2715.

Nyblade, A. and S. Robinson (1994), The African superswell, Geophysical Research Letters, 21, 765-768.

Nyblade, A. A. and Brazier, R. A. (2002), Precambrian lithospheric controls on the development of the East African rift system, Geology, 30, 755–758.

Nyblade, A. A. and Robinson, S.W. (1994), The African superswell, Geophysical Research Letters, 21, 765–768.

Nyblade, A. A., Langston, C.A., Last, R. J., Birt, C. and Owens, T.J. (1996), Seismic experiment reveals rifting of craton in Tanzania, EOS, Transactions, American, Geophysical Union, 77(51), 517–521.

O'Donnell, J., Adams, A., Nyblade, A. A., Mulibo, G., Tugume, F. and Weeraratne, D. (2013), The uppermost mantle shear wave velocity structure of eastern Africa from Rayleigh wave tomography: Constraints on rift evolution, Geophysical Journal International, 194, 961-978.

Park, Y. and Nyblade, A. A. (2006), P-wave tomography reveals a westward dipping low velocity zone beneath the Kenya Rift, Geophysical Research Letters, 33(4), doi:10.1029/2005 GL 025605.

Ring, U. (1993), Aspects of the kinematic history and mechanisms of superposition of the Proterozoic mobile belts of eastern central Africa (northern mobile belts of eastern central Africa (northern mobile belts of eastern central Africa (northern Malawi and southern Tanzania), Precambrian Research, 62, 207-226.

Ritsema, J., Nyblade, A. A., Owens, T.J., Langston, C.A. and VanDecar, J.C. (1998), Upper mantle seismic velocity structure beneath Tanzania, east Africa: implications for the stability of cratonic lithosphere, Journal of Geophysical Research, 103(B9), 21201–21213.

Theunissen, K. (1988), The Ufipa shear zone in the Ubende belt at Karema (W. Tanzania): a NW oriented left lateral strike-slip of postulated late Ubende belt at Karema (W. Tanzania): a NW Kibaran age. In: UNESCO/IUGS GARS Program in Africa (Edited by Lavreau, J. and Bardinet, C.), Séries 8, Sciences géologiques 96, Musée Royal Afrique Centrale, Tervuren, Belgium, pp. 63-77.

Theunissen., K., Lenoir., J. I., Liegeois., J. P. Delvaux, D. and Mnrma., A. (1992), Major Pan-African imprint in the Ubendian belt of SW Tanzania: U-Pb on zircon geochronology and structural context, Comptes rendus Academie Sciences Paris 314 (II), 1355-1362.

Tokam, A.P, Tabod, C.T., Nyblade, A. A., Julià, J., Wiens, D.A. and Pasyanos, M. E. (2010), Structure of the crust beneath Cameroon, West Africa, from the joint inversion of Rayleigh wave group velocities and receiver functions, Geophysical Journal International, 183: 1061-1076, doi:10.1111/j.1365- 246X.2010.04776.x.

Tugume, F., Nyblade, A. A. and Julià, J. (2012), Moho depths and Poisson's ratios of Precambrian crust in East Africa: evidence for similarities in Archean and Proterozoic crustal structure, Earth and Planetary Science Letters, 355–356, 73–81.

Tugume, F., Nyblade, A. A., Julià, J., Meijde M. (2013), Precambrian crustal structure in Africa and Arabia: Evidence lacking for secular variation, Tectonophysics, 609, 250-266.

Wiggins, R. (1972), The general linear inverse problem: Implications of surface waves and free oscillations for Earth structure, Reviews of Geophysical and space Physics, 10, 251-285.

Zhu, L., and Kanamori, H. (2000), Moho depth variation in southern California from teleseismic receiver functions, Journal of Geophysical Research, 105: 2969–2980.

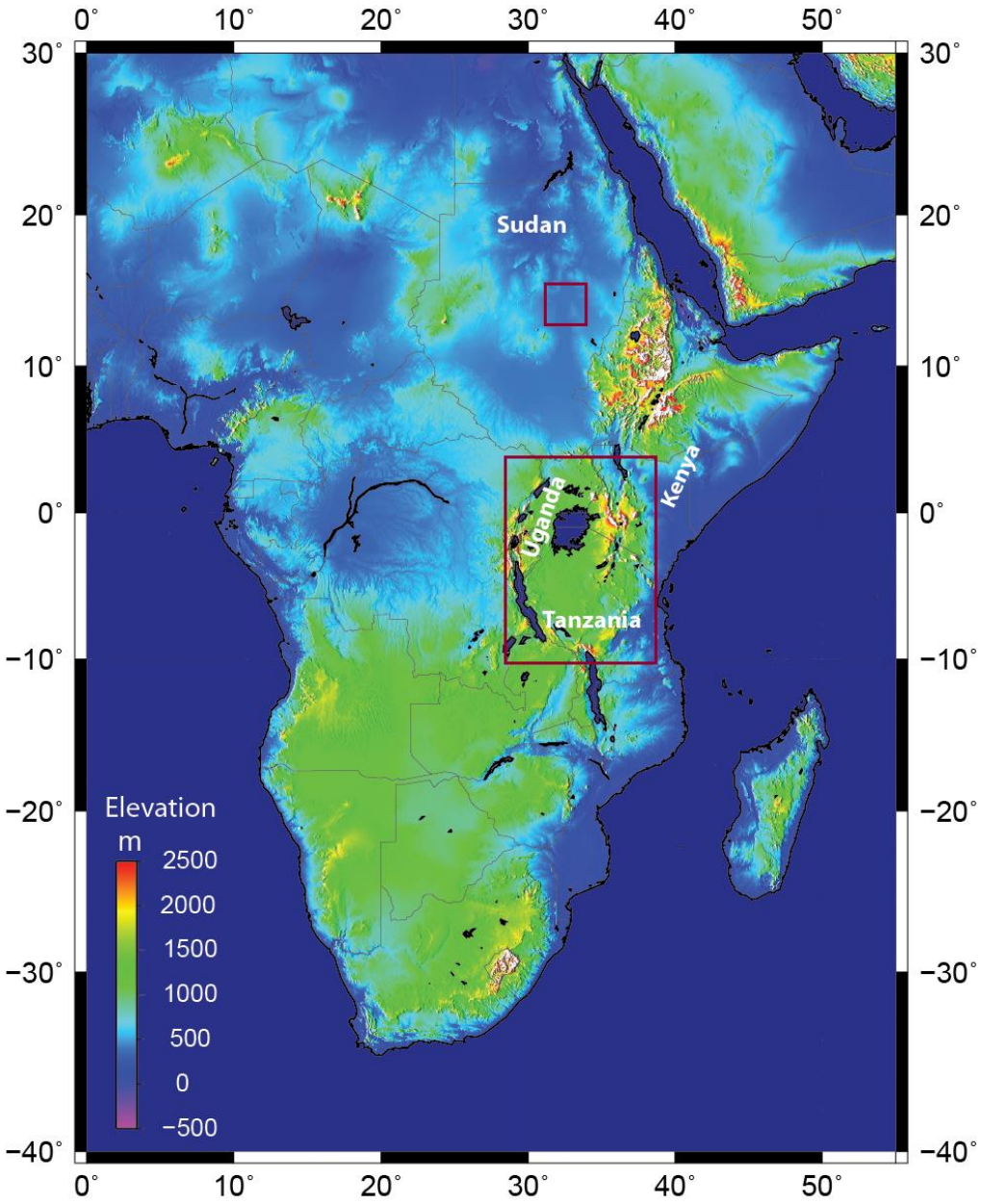

Figure 1-1. Location of the study area (red box) in Sudan and eastern Africa.

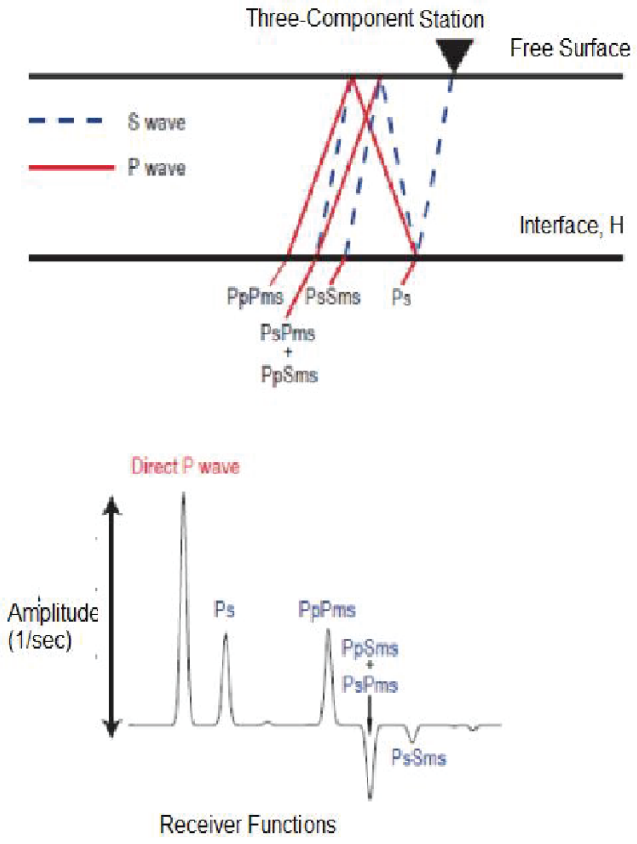

Figure 1-2. (Top) Ray diagram showing the legs of the major phase arrivals that comprise the receiver function using a single layer over a half-space model. (Bottom) the corresponding waveforms calculated using the model above. The figure is modified from Ammon et al. (1990).

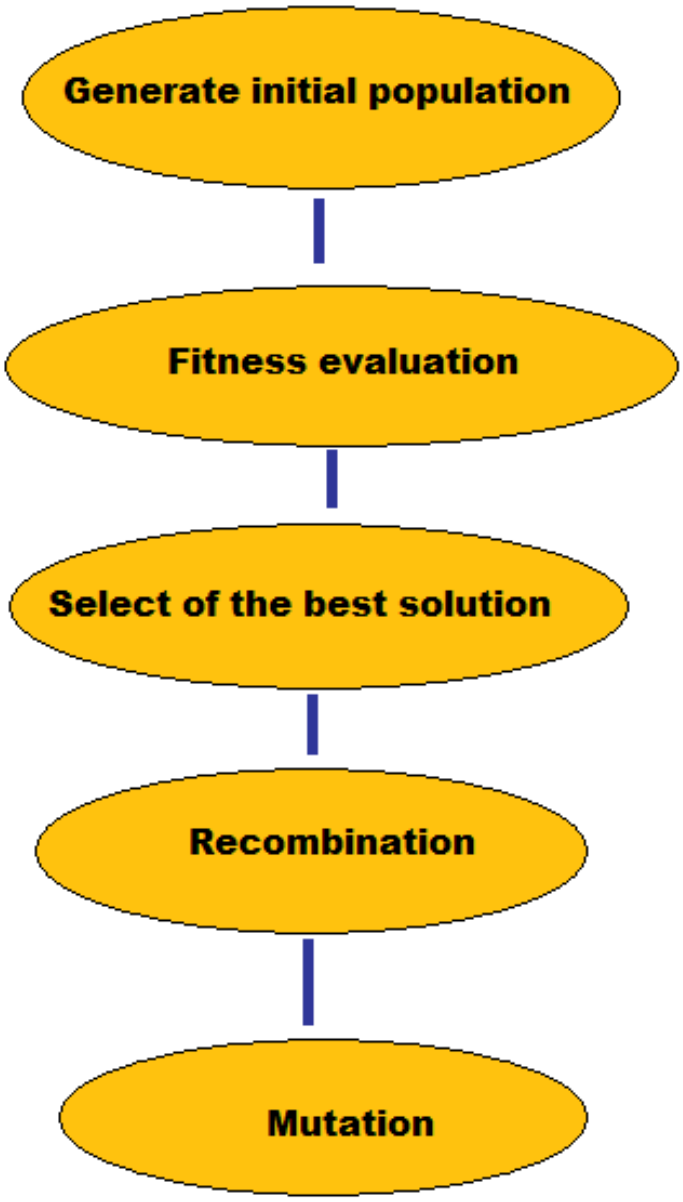

Figure 1-3. The flowchart of Non-Dominated Sorting Genetic Algorithm (NSGA-II) adopted in this study. The individual steps are discussed in the text.

2 CRUSTAL STRUCTURE OF THE KHARTOUM BASIN

2.1 Introduction

The Khartoum basin is one of several Mesozoic rift basins in Sudan associated with the Central Africa Rift System (CARS) (Figure 2-1). The initial development of the Sudanese basins has been linked to extension throughout the Afro-Arabian region associated with the separation of east and west Gondwana and sea-floor spreading of the proto-Indian Ocean in the Jurassic (Reynolds, 1993). A second phase of rift development occurred in the Cretaceous during the opening of the South Atlantic (Browne et al., 1985; Fairhead and Green, 1989) and faulting along the Central African Shear Zone (Figure 2-1) (Browne and Fairhead, 1983; Browne et al., 1985; Fairhead, 1986; Bosworth, 1989).

The structure of the Sudan rift basins, which align in a northwest to southeast direction (Figure 2-1), have been investigated previously using potential field data, seismic reflection data and well logs (e.g., Schull, 1988; Mann, 1989; Hussein, 1992). The basins are bounded by listric normal faults (Mann, 1989; Reynolds, 1993), and the amount of extension is variable among them. In the Muglad rift, for example, about 45 km of crustal extension is documented (Browne and Fairhead, 1983; Jorgensen and Bosworth, 1989), while in the White Nile rift basin about 10 km of extension has occurred (Brown et al., 1980). Similarly, sediment thickness also varies between the basins, with up to 15 km of fill in the Muglad basin (Schull, 1988) and possibly as little as 1 km in the Blue Nile rift (Jorgensen and Bosworth, 1989).

Little is known about the deep structure under the basins, in particular the depth of the Moho, limiting our understanding of their tectonic development. The only information on deep crustal structure comes from regional gravity studies (Browne and Fairhead, 1983; Bermingham et al., 1983; Browne et al., 1985; Jorgensen and Bosworth 1989) and continental scale tomography models (e.g., Pasyanos and Nyblade, 2007), but in these studies crustal thickness is not well constrained. In this paper, we present the first estimates of Moho depth for a Mesozoic rift basin in Sudan determined using receiver functions and Rayleigh wave

group velocities, along with estimates of crustal Poisson's ratio and the shear wave velocity structure of the crust. We then comment on the tectonic implications of our findings for lithospheric extension within the CARS, as well as the development of Cenozoic volcanic fields in central Africa vis-à-vis the channeling of plume material from Ethiopia.

2.2 Background

2.2.1 Geology and tectonic setting of the Khartoum basin

The Khartoum basin is part of the Blue Nile rift basin system, which lies in the north between the White Nile and the Blue Nile, and stretches to the southeast across the Blue Nile (Figure 2-1) (Awad, 1994). The basin may be a 'sag' basin because its edges do not appear to be controlled by major bounding faults, and it may be quite shallow, with a maximum sediment thickness of not more than a few kilometers (Mohammed, 1997).

The basin sediments lie uncomformably on Pan-African (Neoproteozoic) metamorphic and igneous rocks of the Mozambique Belt, which are exposed north of Khartoum in the Sabaloka area (Figure 2-2). Kröner et al. (1987) suggested that the gneisses found there formed along an ancient continental margin onto which juvenile arc assemblages were accreted. The Albian age Omdurman formation crops out across much of the study area (Schrank and Awad, 1990; Awad, 1994) (Figure 2), and consists of the Umm Badda and Merkhiyat members (Awad, 1994). Within these members, the dominant lithology is the Nubian Sandstone, which is composed of sandstones, pebbly sandstones, and conglomerates, often capped by ferruginous beds (Whiteman, 1971). The late Tertiary and Quaternary Gezeria formation crops out in the area between the White Nile and the Blue Nile and on the east bank of the Blue Nile (Awad, 1994) (Figure 2-2). The formation consists of sandstones, silts and clays (Andrew, 1948; Adamson and Williams, 1980). Quaternary deposits in the area include the Nile Silt and Wadi deposits (Figure 2-2).

2.2.2 Seismic Stations

Data used for this study come from the Sudan Seismic Network (SSN), which consists of 3 seismic stations, MRKH, SLAT and JAWL, installed in 2001 within 40 km of Khartoum (Al Hassan et al., 2007) (Figure 2-2). The stations are equipped with intermediate period LE-3D/20 sensors, which have a flat frequency response from 0.05 to 20 Hz, Mars-88 data loggers with 24-bit digitizers, GPS clocks for timing and bidirectional RF telemetry. Until recently, data were recorded in trigger mode. The MRKH station is located on an outcrop of Nubian sandstone at Jebel Merkhiyat. The JAWL station is located on an outcrop of Nubian sandstone at Jebel Aulia, and the SLAT station is located on a ridge of Nubian sandstone to the north-east of Khartoum (Figure 2-2).

2.3 Methods

2.3.1 Receiver functions

Receiver functions are time series obtained from teleseismic P-waveforms recorded at single seismic stations after deconvolving the vertical component of ground motion from the corresponding horizontal components. The deconvolution isolates the seismic response of the local structure beneath the recording station and removes the signature of the instrument response and source time function (Langston, 1979). Modeling receiver functions has become a standard procedure for investigating Moho depth and the shear wave velocity structure of the crust (e.g. Owens and Zandt, 1987; Ammon et al., 1990; Julià et al., 2000).

For this study, we have used data from seismic sources located at epicentral distances between 30˚and 90˚ and with moment magnitude greater than 5.5. (See Table 2-1 and Figure 2-3) recorded between 2003 and 2010. Before computing the receiver functions, the data were windowed 10 s before and 40 s after the P wave. The data were then de-trended, tapered and band pass filtered between 0.05 – 8 Hz to remove low-frequency noise and avoid aliasing before being decimated to 10

samples per second. The horizontal seismograms were rotated into the great circle path to obtain the corresponding radial and transverse components, and the iterative time-domain deconvolution method of Ligorría and Ammon (1999) was employed to compute the receiver functions using 500 iterations. For each teleseismic event, receiver functions were computed at two overlapping frequency bands, one with a Gaussian filter width of 1.0 ($f < 0.5$ Hz) and the other with a filter width of 2.5 ($f < 1.2$ Hz).

To evaluate the quality of the deconvolved traces, a least-squares-misfit criterion was utilized, in which the radial waveform for each receiver function is reconstructed by convolving the receiver function back with the corresponding vertical waveform and comparing it with the original radial waveform. Only receiver functions that were recovered at a 85% level or higher were further considered for analysis (Ligorria and Ammon, 1999).

The degree of lateral heterogeneity and isotropy of the propagation medium can be assessed by examining transverse receiver function amplitudes (Cassidy, 1992). Small amplitudes on the transverse component indicate a homogeneous and isotropic medium beneath the station, which is assumed in both the H-k stacking and joint inversion modeling procedures. Therefore, in cases where we obtained transverse receiver functions with amplitudes similar to the radial receiver function, the data were rejected.

2.3.2 H-k stacking technique

Receiver functions have been modeled using the H-k stacking technique of Zhu and Kanamori (2000) to estimate crustal thickness (H) and crustal Vp/Vs ratio (k). The stacking procedure transforms the receiver function waveforms from the time-amplitude domain into the H-k parameter space through a weighted sum along theoretical phase moveout curves obtained for given values of H and k and an assumed value of P-wave velocity. The weighted sum is given by

$$s(H,\kappa) = \sum_{j=1}^{N} w_1 r_j(t_1) + w_2 r_j(t_2) - w_3 r_j(t_3) \qquad (2\text{-}1)$$

where w_1, w_2 and w_3 are the a priori weights for the Ps, PpPs, and PpSs phases, respectively, with summation equal to 1, $r_j(t_i)$, i=1, 2, 3 are the receiver function amplitude values for the j-th receiver function at the predicted arrival times t_i , and N is the number of receiver functions used.

The basic idea behind the H-k algorithm is that the stacked amplitudes will attain its maximum value when there is coherent stacking along the phase moveout curves resulting from H and k values consistent with the location of a subsurface discontinuity (Zhu and Kanamori, 2000). Moreover, if lateral variations in Earth structure are moderate, by stacking receiver functions from different back azimuths and different distances, the effects of lateral structural variation are reduced and an average crustal thickness can be obtained.

In applying the H-k technique, it is necessary to select weights w1, w2 and w3 (Eq. 2-1). The choice for weights is somewhat subjective. A trial and error approach was used to come up with the combinations of phase weights that produced the most consistent stacks. If one of the phases was poorly defined, its weight was decreased, and vice versa. I give more weight to the phases that are most clearly observed and less weight to phases that are not clearly identified or inconsistent among receiver functions. For stations SLAT and MRKH, for instance, all three phases are clearly seen in the receiver function waveforms, so we give similar weight to each of them by using w_1=0.4, w_2=0.3 and w_3=0.3. On the other hand, for JAWL the PsPs multiple is not as clear as the other two phases, and so the weights are re-adjusted to w_1=0.5, w_2=0.1 and w_3=0.4.

In the stacking procedure, a mean Vp for the crust must be assumed. An average crustal P-wave velocity of 6.5 km/s was used, which is representative of Precambrian crust worldwide (e.g., Christensen and Mooney, 1995). However, as explained below, other values of Vp were investigated in order to determine uncertainties in H and k due to this assumption.

Following the approach of Julià and Mejía (2004), we estimate formal uncertainties in H and k by bootstrapping the receiver function dataset for each station using 200 replications (Efron and Tibshirani, 1991). The uncertainties for each station using a mean crustal Vp of 6.5 km/s for the H-k stacking are given in Table 2-2 and shown in Figure 2-4. For evaluating the uncertainty in H and k arising from the choice of mean crustal Vp, the H-k stacks were recomputed using a range of Vp between 6.3 and 6.8 km/s (Table 2-2; and also shown in the Supplementary material, Appendix A). To obtain an overall uncertainty in H and k, the formal uncertainty obtained from the bootstrap method was combined with the range of H and k values obtained when using the range of mean crustal Vp values. The overall uncertainties are ±3-4 km in Moho depth and ± 0.05 in Vp/Vs for each station.

Figure 2-4 shows the H-k results for each station and Table 2-2 provides a summary of the results. Crustal thicknesses are 35, 37 and 33 km for stations SLAT, MRKH and JAWL, respectively, and the average is 35 km. Vp/Vs ratios are 1.81, 1.74 and 1.81 for stations SLAT, JAWL and MRKH, respectively, with an average of 1.78.

2.3.3 Joint inversion technique

To investigate the shear wave velocity structure of the crust, we have used the method of Julià et al. (2000, 2003) to jointly invert the receiver functions with Rayleigh-wave group velocities. The combination of surface-wave dispersion curves and receiver functions provides better constraints on the shear velocity of the crust compared to modeling either data set independently (Özalaybey et al., 1997; Julià et al., 2000, 2003, 2005; Dugda et al., 2007). This method makes use of a linearized inversion procedure that minimizes a weighted combination of least squares norms for each data set (i.e., receiver functions and group velocities). In the joint inversion method, the two data sets must be consistent (i.e., they should sample the same study area). To make the contribution of each data set to the joint least squares misfit comparable, a normalization of the data sets is necessary, and this is done using the number of data points and variance for each of the data sets. An influence factor is

assigned prior to the joint inversion. Its role is to maintain balance between the two data sets (the receiver functions and the group velocity dispersion curves) so that no set dominates over the other. An influence factor of 0.5 was used in this study. It provides a good compromise between fitting the receiver functions and the dispersion velocities. Previous applications or studies that used the same method and the same influence factor produced good results.

Because the velocity models are parameterized as a stack of thin layers, a smoothness constraint is necessary to stabilize the inversion process. The velocity models obtained are, therefore, a compromise between fitting the observations, model simplicity and a priori constraints (Julià et al., 2003).

Dispersion curves for each station were obtained from a revised version of the Rayleigh wave group velocity model published by Pasyanos and Nyblade (2007). Rayleigh wave group velocities between 20 to 75 s were used. As the original dispersion curve showed large variability between periods, a 3-point running average were applied to the dispersion curve to smooth it out before using it in the inversion. Dispersion velocities in the 20-50 s period range constrain crustal and uppermost mantle velocity structure; however, dispersion velocities at periods up to 75 s were included to model velocity structure down to ~100 km depth during the inversion.

The starting model used in the joint inversion consisted of a 37.5 km thick crust with a linear shear wave velocity increase from 3.4 km/s at the surface to 4.0 km/s at the Moho, and a flattened PREM (Preliminary Reference Earth Model; Dziewonski and Anderson, 1981) model for the mantle. Following the approach of Kgaswane et al. (2009), Tokam et al. (2010), Tugume et al. (2013), the model parameterization consists of a stack of constant velocity layers that increase in thickness with depth. Thicknesses at the top of the model were 1 and 2 km, respectively, 2.5 km for layers between 3 and 60.5 km depth, and 5 km between 60.5 and 260.5 km depth. Poisson's ratio was fixed to 0.25 for the crust during the inversions (Dimitrova and Haines, 2013) and to PREM values for deeper structure. Densities were obtained from P wave velocities using the empirical relation of

Berteussen (1977). Velocities below a depth of 100 km were fixed to PREM values to account for the partial sensitivity of the longer periods to deeper structure.

In order to investigate lateral variations in crustal structure around the stations, receiver functions were first sorted by backazimuth and ray parameter and then averaged within groups. Grouping by backazimuth was done by overlapping individual receiver function waveforms and visually correlating waveform shapes, while groupings by ray parameter was done by limiting ray parameter values to a maximum variation of 0.01 s/km within the backazimuth groups. Four or five groups of receiver functions were obtained for each station. For each group, receiver functions with both lower ($f < 0.5$ Hz) and higher ($f < 1.25$ Hz) frequencies were computed and stacked with a minimum of two receiver functions per stack. Each receiver function group for each station was then jointly inverted with the corresponding group velocity curve to obtain a shear wave velocity model. The results (Figure 2-5) show that comparable models with similarly good fits to the data are obtained for each group and for each station, indicating little variability in crustal structure around the stations. Therefore, a best average velocity model for each station was obtained by jointly inverting all receiver function averages for a given station with the group velocity curve.

Following the approach of Julià et al. (2005), uncertainties in the shear wave models have been assessed by repeatedly performing the inversions with a range of inversion parameters, such as weighting parameters and Poisson's ratios. Poisson's ratio was allowed to vary between 0.25 and 0.28. We obtain an uncertainty of approximately 0.1–0.2 km/s for the velocity in each layer, which translates into an uncertainty of ~2–3 km in the depth of any crustal boundary observed in the model, including the Moho.

2.4 Discussion and conclusions

Following the approach of Kgaswane et al. (2009), Tokam et al. (2010), and Tugume et al. (2012), crustal thickness is determined from the shear wave velocity models in Figure 2-5 by placing the Moho at the depth where the shear wave

velocity exceeds 4.3 km/s. Shear wave velocities for typical lower crust lithologies are not higher than 4.3 km/s (Christensen and Mooney, 1995; Christensen, 1996). Hence, we take shear wave velocities above 4.3 km/s to indicate the presence of lithologies with mantle composition. At station SLAT, a marked velocity increase occurs at 38 km depth, where velocities increase to values > 4.3 km/s (Figure 2-5). However, at stations MRKH and JAWL, the velocity increase with depth is gradational and a sharp velocity discontinuity is not imaged (Figure 2-5).

The crustal thickness beneath all three stations determined from the station average models is 38 km (Figure 2-5 and Table 2-2), and the average shear wave velocity for stations SLAT, MRKH and JAWL is 3.6, 3.7 and 3.7 km/s, respectively. The Moho depths determined from the joint inversion models are uniformly deeper than those obtained from the H-k stacking procedure (Table 2-2), but still comparable within the reported uncertainties (i.e., 3 to 4 km for the H-k stacking estimates and ±2.5 km for the joint inversion estimates).

To summarize, our results indicate that crustal thickness beneath the Khartoum basin is between 33 and 38 km, with an average of 35 km; the crustal Vp/Vs ratio is on average 1.78 (Poisson's ratio of 0.27); and the average Vs of the crust is 3.7 km/s. In the remainder of this section, we compare these results to other estimates of crustal structure in Sudan and then investigate their implications for lithospheric thinning and the channeling of plume material.

A number of gravity studies have reported estimates of Moho depth in Sudan that are in agreement with our results. Browne et al. (1985) and Mohamed et al. (2001) estimated a crustal thickness of about 35 km beneath much of Sudan, Jorgensen and Bosworth (1989) reported Moho depths of 32 to 37 km for central Sudan, and a crustal thickness map in Tedla et al. (2011) shows Moho depths of 33 to 36 km for central Sudan.

As discussed previously, the Pan-African basement beneath the Khartoum basin belongs to the Mozambique Belt. To estimate the amount of crustal thinning beneath the Khartoum basin, therefore, we compare our results to estimates of Moho depth in areas of east Africa where the Proterozoic Mozambique Belt has not been rifted. The crustal structure of Mozambique Belt in Kenya has been studied by the

Kenya Rift International Seismic project (KRISP) using seismic refraction profiling (Prodehl et al., 1994; Fuchs et al., 1997 and references therein), and by Dugda et al. (2005) using receiver functions. Results from these studies show that crustal thickness is 40 to 42 km away from the Kenya rift. The Mozambique Belt in Tanzania has been also investigated using receiver functions and Rayleigh wave group and phase velocities (Last et al., 1997; Julià et al., 2005; Dugda et al., 2005). Moho depths were found to range from 37 to 42 km. If these results are averaged, then a mean crustal thickness of 38 ± 2 km is obtained (Tugume et al., 2012). If we compare our estimated average crustal thickness of 35 km for the Khartoum basin with the average crustal thickness from these studies, then at most there has been only a few kilometers of crustal thinning. This small amount of crustal thinning is similar to the amount of thinning in the southern part of the Kenya rift (Birt et al., 1997), but is significantly less than that in northern Kenya where the Cenozoic rift and the Mesozoic Anza graben coincide (Figure 2-1). In this region, the 20-25 km thick crust (Benoit et al., 2006) is probably the result of two episodes of thinning, one during Mesozoic rifting and then again in the Cenozoic.

Given the similarity between our crustal thickness estimates for the Khartoum basin and estimates of crustal thickness elsewhere in central and southern Sudan from gravity models, it follows that only small amounts of crustal thinning have occurred throughout the CARS in Sudan. And similarly, it can be inferred that the lithosphere has also undergone only minor amounts of extension, if any. This conclusion is supported by estimates of effective elastic plate thickness (Te). Pèrez-Gussinye et al. (2009) obtained Te estimates of 80 to 100 km for the region beneath the Khartoum basin, as well as for several of the other basins in central and southern Sudan, including the Muglad basin, the largest one. A Te of 80 to 100 km is similar to or greater than estimates for the Mozambique Belt in parts of eastern Africa where the lithosphere has not been affected by the Cenozoic East African rift system. Pèrez-Gussinye et al. (2009) show a narrow region within central Sudan where Te is between 50 and 60 km, but this region does not encompass any of the larger rift basins. Thus, the Te estimates for the basins are consistent with our conclusion that there has been little thinning of the crust or lithosphere beneath them.

The conclusion that the crust and lithosphere under the Sudan basins have not been thinned to any significant extent has important implications for understanding Cenozoic volcanism in central Africa. Pèrez-Gussinye et al. (2009) and Ebinger and Sleep (1998) have proposed that thinned lithosphere beneath the Sudan basins created a channel in the lithosphere-asthenosphere boundary for magma from the Afar/Ethiopia region to migrate to the west, reaching as far as the Cameroon Volcanic Line. Our results showing little crustal thinning, combined with the Te estimates from Pèrez-Gussinye et al. (2009), indicate that there may be insufficient topography on the lithosphere-asthenosphere boundary, at least beneath the basins, to create a channel for the migration of plume material. Consequently, Cenozoic volcanism in regions like the Darfur and the Cameroon Volcanic Line might not result from plume material migrating from the Ethiopia/Afar region to the west beneath thinned lithosphere.

References

Adamson, D.A. and Williams, F. (1980), Structural geology, tectonics and the control of drainage in the Nile Basin, in The Sahara and the Nile, Williams, M.A.J. and Faure, H. (editors), Balkema, Rotterdam, pp. 225-252.

Al Hassan A.A.I., Khidir Belail A., El Bashir H.S.H, Mohamed I. A. R., Tahir N. Mohammed M. B., El B. and Havskov, J. 92007), The Sudanese Seismic Network. Seismological Research Letters, 78, 498-501.

Ammon, C., Randall, G.E. and Zandt, G. (1990), On the nonuniqueness of receiver functions inversions, Journal of Geophysical Research, 95, 15, 303-15, 318.

Andrew, F.M. (1948), The geology of the Sudan: London, Oxford University.

Awad, M.Z. (1994), Stratigraphic, Palynological and Paleoecological studies in the East-Central Sudan (Khartoum and Kosti Basins), Late Jurasic to Mid-Tertiary, Ph.D thesis, Free Uni. Berlin, pp. 149.

Benoit, M.H., Nyblade, A.A. and Pasyanos, M.E. (2006), Crustal thinning between the Ethiopian and East African plateaus from modelling Rayleigh wave dispersion. Geophyical Research Letters, 33: L13301, doi:10.1029/2006GL025687.

Bermingham, P.M., Fairhead, J.D. and Stuart, G.W. (1983), Gravity Study of the Rift Central African System: A model of Continental Distribution 2. The Darfour Domal Uplift and Associated Cainozoic Volcanism, Tectonophysics, 94: 205-222.

Berteussen, K.A. (1977), Moho depth determinations based on spectral ratio analysis, Physics of the Earth Planetary Interiors, 31: 313– 326.

Bosworth, W. (1989), Detachment geometries and kinematics in continental rifts, 28th International Geological Congress, Washington,D.C., abstract 45.

Birt, C.S., Maguire, P.K.H., Khan, M.A., Thybo, H., Keller, G.R. and Patel, J. (1997), The influence of pre-existing structures on the evolution of the Southern Kenya rift valley – evidence from seismic and gravity studies, Tectonophysics, 278: 211-242.

Brown, C., Girdler, R.W. and Rehner, R.G.B. (1980), A gravity traverse across north Africa, Journal of Geophysical Research, 85: 6436-6442.

Browne, S.E., Fairhead, J.D. and Mohamed, I.I. (1985), Gravity study of the White Nile Rift, Sudan and its regional tectonic setting, Tectonophysics, 113: 123-137.

Browne, S.E. and Fairhead, J.D. (1983), Gravity study of the Central African Rift: a model of continental disruption, Tectonophysics, 94: 187-203.

Cassidy, J. (1992), Numerical experiments in broadband receiver functions analysis, Bulletin of the Seismological Society of America, 82: 1453– 1474.

Christensen, N.I. and Mooney, W.D. (1995), Seismic velocity structure and composition of the continental crust: A global view, Journal of Geophysical Research, 100: 9761– 9788.

Christensen, N.I. (1996), Poisson's ratio and crustal seismology, Journal of Geophysical Research, 101: 3139–3156.

Dimitrova, L.L and Haines, A.J. (2013), Constraining the Long Term Poisson's Ratio of the Martian Lithosphere From 2D and 3D Dynamic Modeling of Lithospheric Stress and the Surface Faulting Record, 44Th Lunar and Planetary Science Conference.

Dugda, M.T., Nyblade, A.A., Julià, J., Langston, C.A., Ammon, C. and Simiyu, S. (2005), Crustal structure in Ethiopia and Kenya from receiver function analysis: Implications for Rift development in eastern Africa, Journal of Geophysics Research, 110: B01303, doi:10.1029/2004JB003065.

Dugda, M.T., Nyblade, A.A. and Julià, J. (2007), Thin lithosphere beneath the Ethiopian Plateau revealed by a joint inversion of Rayleigh wave group velocities and receiver functions, Journal of Geophysical Research, 112, B08305, doi:10.1029/2006JB004918.

Dziewonski, A. and Anderson, D.L. (1981), Preliminary reference Earth model, Physics of the Earth Planetary Interiors, 25: 297-356.

Ebinger, C.J. and Sleep, N.H. (1998), Cenozoic magmatism throughout east Africa resulting from impact of a single plume, Nature, 395: 788-971.

Efron, B. and Tibshirani, R. (1991), Statistical data analysis in the computer age. Science, 253: 390–395.

Fairhead, J.D. (1986), Geophysical controls on sedimentation within the African rift systems. In: L.E. Frostick, R.W. Renault, I. Reid and I.I. Tiercelin (Editors), Sedimentation in the African Rifts, Geological Society of London Special Publication, 25: 19-27.

Fairhead, J.D. and Green, C.M. (1989), Control on rifting in Africa and the regional tectonic model for the Niger rift basins, Journal of Africa Earth Sciences, 8: 231-249.

Fuchs, K., Altherr, B., Muller, B. and Prodehl, C. (1997), Structure and dynamics processes in the lithosphere of the Afro-Arabian rift system, Tectonophysics, 278: 1-325.

Hussein M, T. (1992), On the depositional framework of the Cretaceous Omdurman formation in Khartoum area, Sudan, Journal of Africa Earth Sciences 14: 559-566.

Jorgensen, G.J and Bosworth, B. (1989), Gravity modelling in the central Africa Rifts System, Sudan: rift geometries and tectonic significance, Journal of Africa Earth Sciences, 8: 283-306

Julià, J., Ammon, C., Herrmann, R.B. and Correig, A.M. (2000), Joint inversion of receiver functions and surface wave dispersion observations, Geophysical Journal International, 143: 99–112.

Julià, J., Ammon, C. and Herrmann, R.B. (2003), Lithospheric structure of the Arabian Shield from the joint inversion of receiver functions and surface wave group velocities, Tectonophysics, 371: 1 – 21, doi: 10.1016/ S0040-1951(03)00196-3.

Julià, J., Ammon, C. and Nyblade, A.A. (2005), Evidence for mafic lower crust in Tanzania, East Africa, from joint inversion of receiver functions and Rayleigh wave dispersion velocities, Geophysical Journal International, 162: 555-569.

Julià, J. and Mejia, J. (2004), Thickness and Vp/Vs ratio variation in the Iberian crust, Geophysical Journal International, 156: 59–72.

Kgaswane, E.M, Nyblade, A.A., Julià, J., Dirks, P.H.G.M., Durrheim R.J. and Pasyanos, M.E. (2009), Shear wave velocity structure of the lower crust in southern Africa: evidence for compositional heterogeneity within Archaean and Proterozoic terrains, Journal of Geophysical Research, 114B12304, doi:10.1029/2008JB006217.

Kröner, A., Stern R.J., Dawoud, A.S., Compston, W. and Reischmann, T. (1987), The Pan-African continental margin in northeastern Africa: evidence from a study of granulites at Sabaloka, Sudan, Earth Planetary Science Letters, 85: 91-104.

Langston, C.A. (1979), Structure under Mount Rainier, Washington, inferred from teleseismic body waves, Journal of Geophysical Research, 84: 4749 – 4762.

Last, R.J., Nyblade, A.A., Langston C.A. and Owens, T.J. (1997), Crustal structure of the East Africa Plateau from receiver functions and Rayleigh wave velocities, Journal of Geophysical Research, 102: 24,469-24,483.

Ligorria, J.P. and Ammon, C. (1999), Iterative deconvolution and receiver functions estimation, Bulletin of the Seismological Society of America, 89: 1395–1400.

Mann, D.C. (1989), Thick-skin and thin-skin detachment faults in continental Sudanese rift basins, Journal of Africa Earth Sciences, 8: 307-322.

Mohamed, A.Y., Ashcroft, W.A. and Whiteman, A. (2001), Structure development and crustal stretching in the Muglad basin, southern Sudan, Journal of Africa Earth Sciences, 32:179-191.

Mohammed, I.A. (1997), Geology and structures of the area west of the White Nile as deduced from gravity measurements, M.Sc. Thesis, Khartoum University. (Unpublished).

Owens, T.J. and Zandt, G. (1987), Implication of crustal property variations for models of the Tibetan Plateau, Nature, 387, 37-43.

Özalaybey, S., Savage, M.K., Sheehan, A.F., Louie, J.N. and Brune, J.N. (1997), Shear-wave velocity structure in the northern Basin and Range province from the combined analysis of receiver functions and surface waves, Bulletin of the Seismological Society of America, 183-199.

Pasyanos, M. E. and Nyblade, A.A. (2007), A top to bottom lithospheric study of Africa and Arabia, Tectonophysics, 444, 27-44.

Pèrez-Gussinye, M., Metois, M., Fernandez, M., Verges, J., Fullea, J. and Lowry, A. (2009), Effective elastic thickness of Africa and its relationship to other proxies for lithospheric structure and surface tectonics, Earth Planetary Science Letters, 287, 152-167.

Prodehl, C., Keller, G.R. and Khan, M.A. (Eds.) (1994), Crustal and upper mantle structure beneath Kenya rift, Tectonophysics (Special Issue), pp 236, 483.

Reynolds P.O. (1993), Plate tectonic aspects of continental rift basin formation in Central and Western Sudan. In: Thorweihe U, Schandelmeier H (editors) Geoscientific Research in Northeast Africa, Balkema, Rotterdam, pp 207-212.

Schull, T.J. (1988), Rift basins of interior Sudan. Petroleum exploration and discovery, American Association of Petroleum Geologist Bulletin, 72, 1128-1142.

Schrank, E. and Awad, M.Z. (1990), Palynological evidence for the age and depositional Berliner environment of the Cretaceous Omdurman Formation in the Khartoum area, Sudan – Geowiss. Abh., A 120.1, 169-182, Berlin.

Tedla, G.E., Meijde, M.V., Nyblade, A.A. and Meer, F.D. (2011), A crustal thickness map of Africa derived from a global gravity field model using Euler deconvolution, Geophysical Journal International, 187, 1-9, doi:10.1111/j. 1365-246X. 2011.05140.x.

Tokam, A-P. K Tabod, C.T., Nyblade, A.A., Julià, J., Wiens, D.A. and Pasyanos, M.E. (2010), Structure of the crust beneath Cameroon, West Africa, from the joint inversion of Rayleigh wave group velocities and receiver functions, Geophysical Journal International, 18, 1061-1076, doi:10.1111/j.1365-246X.2010.04776.x.

Tugume, F., Nyblade, A.A. and Julià, J. (2012), Moho depths and Poisson's ratios of Precambrian crust in East Africa: Evidence for similarities in Archean and Proterozoic crustal structure, Earth and Planetary Science Letters, 355/6, 73-81.

Tugume, F., Nyblade, A., Julià, J., Meijde M. (2013), Precambrian crustal structure in Africa and Arabia: Evidence lacking for secular variation, Tectonophysics, 609, 250-266.

Whiteman, A.J. (1971), The Geology of the Sudan Republic: Oxford, Claredon Press.

Zhu, L., and Kanamori, H. (2000), Moho depth variation in southern California from teleseismic receiver functions, Journal of Geophysical Research, 105, 2969–2980.

Table 2-1: Events with magnitude Mb > 5.5 recorded on the Sudan Seismic Network (SSN) used in this study.

Event date	Event time	Latitude	Longitude	Magnitude	Ray parameter	Backazimuth
yyyy/mm/dd	(h.min.s)	(deg.)	(deg.)	(Mw)	(s/km)	(deg.)
2003/12/10	04:38:11.6	23.039	121.362	6.8	0.046	68.08
2004/10/8	14:36:6.10	13.925	120.534	6.4	0.045	77.11
2004/11/17	20:58:22.3	39.189	71.857	5.7	0.073	47.92
2004/12/26	00:59:6.40	3.295	95.9 82	9.0	0.059	94.11
2005/5/14	05:05:18.5	0.587	98.459	6.7	0.057	96.03
2006/1/2	06:10:54.8	-60.934	-21.575	7.4	0.043	203.27
2007/7/25	23:37:31.5	7.157	92.518	5.5	0.062	90.66
2007/8/20	22:42:49.29	29.2	-39.248	6.3	0.055	273.22
2007/9/6	17:51:26.2	24.340	122.219	6.1	0.046	66.69
2008/4/14	09:45:19.7	-56.02	-28.03	6.0	0.042	209.25
2008/5/23	19:35:35.0	7.33	-34.90	6.5	0.057	271.42
2009/8/10	19:55:35.6	14.10	92.89	7.5	0.062	82.93
2009/8/20	06:35:04.4	72.20	00.94	6.0	0.062	349.26
2009/9/30	10:16:09.2	-0.72	99.87	7.5	0.056	97.09
2009/10/1	15:2:27.3	-02.52	101.50	6.6	0.054	98.39
2009/10/3	17:36:06.1	23.63	121.45	6.1	0.046	67.49
2009/10/29	17:44:31.2	36.39	70.72	6.2	0.074	51.46
2009/10/30	07:03:39.1	29.22	129.78	6.8	0.046	68.17
2009/11/10	02:48:46.7	08.08	91.90	6.0	0.062	90.03
2010/1/5	04:55:38.9	-58.170	-14.700	6.8	0.046	203.00
2010/2/18	01:13:19.5	42.59	130.70	6.9	0.043	47.13
2010/3/2	02:51:21.3	18.18	122.40	5.8	0.045	72.64
2010/3/3	00:18:51.2	22.92	120.79	6.3	0.047	68.42
2010/3/5	16:07:07.6	-3.76	100.99	6.8	0.050	99.96
2010/3/14	20:33.10.8	-2.75	83.68	5.8	0.065	105.58
2010/3/30	16:54:46.7	13.67	92.83	6.7	0.062	83.43
2010/4/6	22:15:01.5	2.38	97.05	7.8	0.058	94.75
2010/4/26	02:59:52.2	22.18	123.73	6.5	0.044	68.36
2010/5/5	16:29:03.2	-4.05	101.10	6.6	0.054	100.05
2010/5/9	05:59:42.4	03.75	096.03	7.2	0.059	93.61

Table 2-2. Crustal thickness and Vp/Vs ratios for the Khartoum basin.

Station	Weight	H (1) (km)	k (1)	H (2) (km)	k(2)	H (3) (km)	k (3)	H J(km)	Vs J (km/s)
SLAT	w_1=0.4, w_2=0.3, w_3 =0.3	34.5 ± 1.1	1.81 ± 0.05	36.4	1.80	33.2	1.82	38 ± 2.5	3.7
MRKH	w_1=0.4, w_2=0.3, w_3=0.3	36.9 ± 1.2	1.74 ± 0.05	38.7	1.74	35.6	1.75	38 ± 2.5	3.7
JAWL	w_1=0.5, w_2=0.1, w_3=0.4	32.7 ± 1.4	1.81 ± 0.07	34.4	1.81	31.6	1.82	38 ± 2.5	3.6
Average		**35**	**1.78**					**38**	**3.7**

H (1, 2, 3,), k (1, 2, 3): average of Vp used for H-k stack method. (1) Vp= 6.5 kms^{-1}, (2) Vp= 6.8 kms^{-1} (3) Vp= 6.3 kms^{-1}

HJ= Depth from joint inversion method.

VsJ= Shear velocity from joint inversion method.

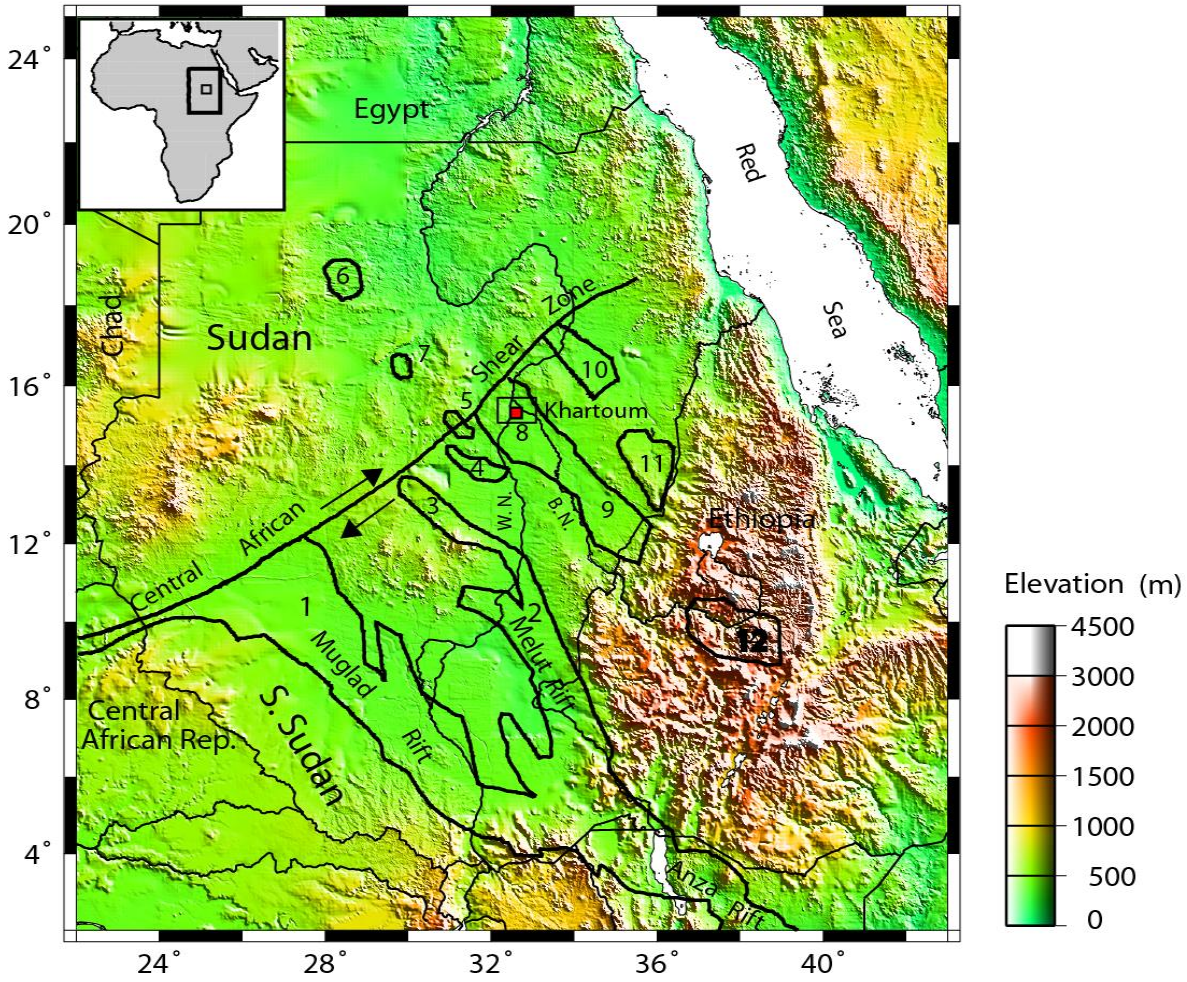

Figure 2-1. Topographic map showing the locations of Mesozoic rift basins of central Sudan and the Central African Shear Zone (modified from Awad, 1994). 1 Muglad Rift, 2 Melut Rift, 3 Bara Basin, 4 Kosti Basin, 5 Bagbag Basin, 6 Abyad Basin, 7 Humar Basin, 8 Khartoum Basin, 9 Blue Nile Basin, 10 Atbara Basin, 11 Gedarif Basin, 12 Abbay River Basin, B.N. Blue Nile, W.N. White Nile.

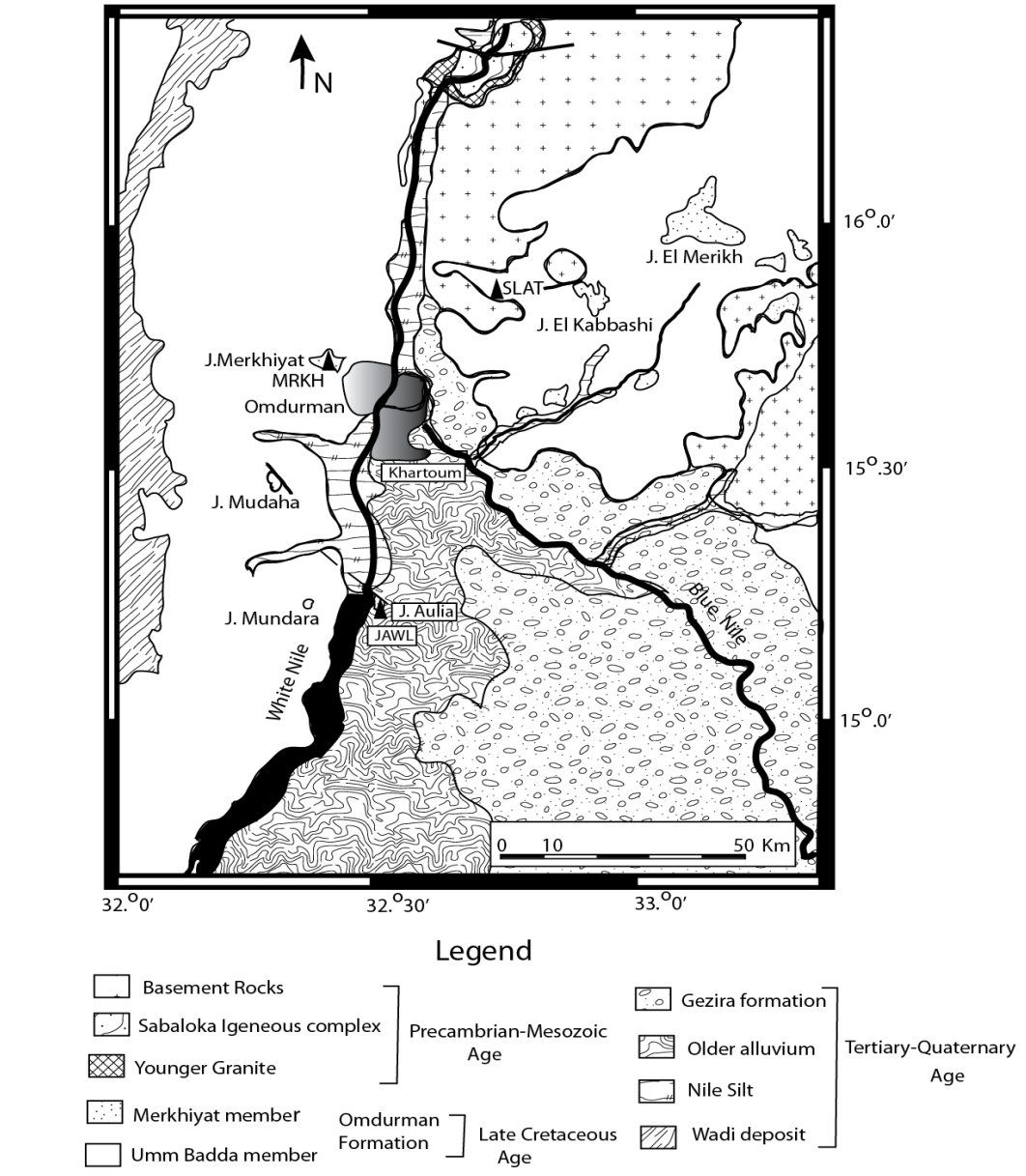

Figure 2-2. Geological and tectonic map of the Khartoum area with seismic stations shown by black triangles. Map redrawn from Awad (1994).

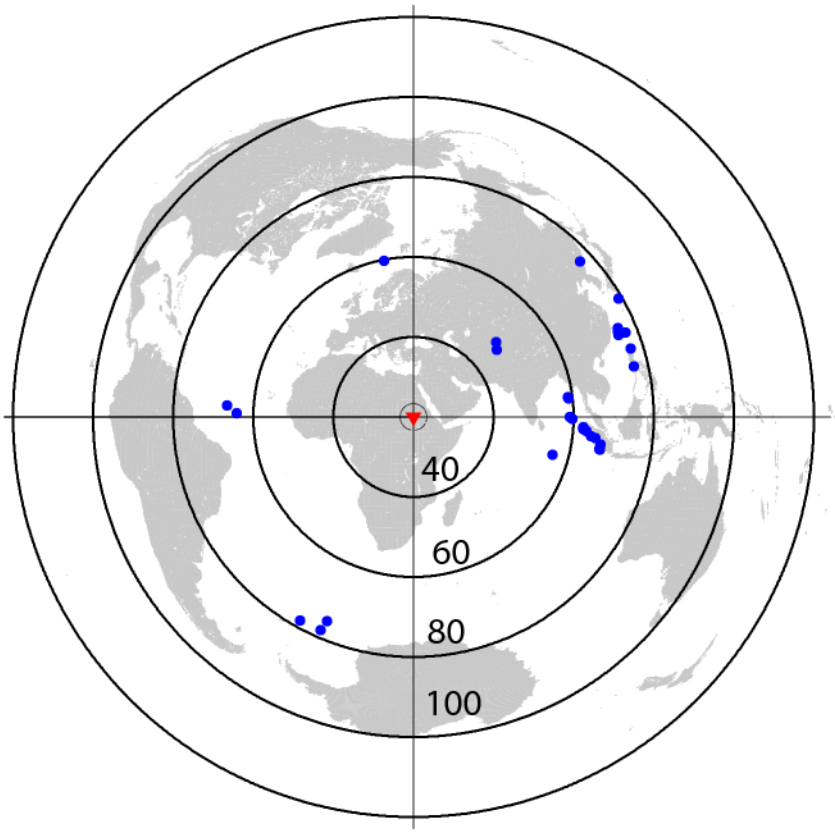

Figure 2-3. Distribution of teleseismic earthquakes used for this study (small blue circles). The triangle shows the center of the SSN network. Circles show distance in 20˚ increments from the center of the network.

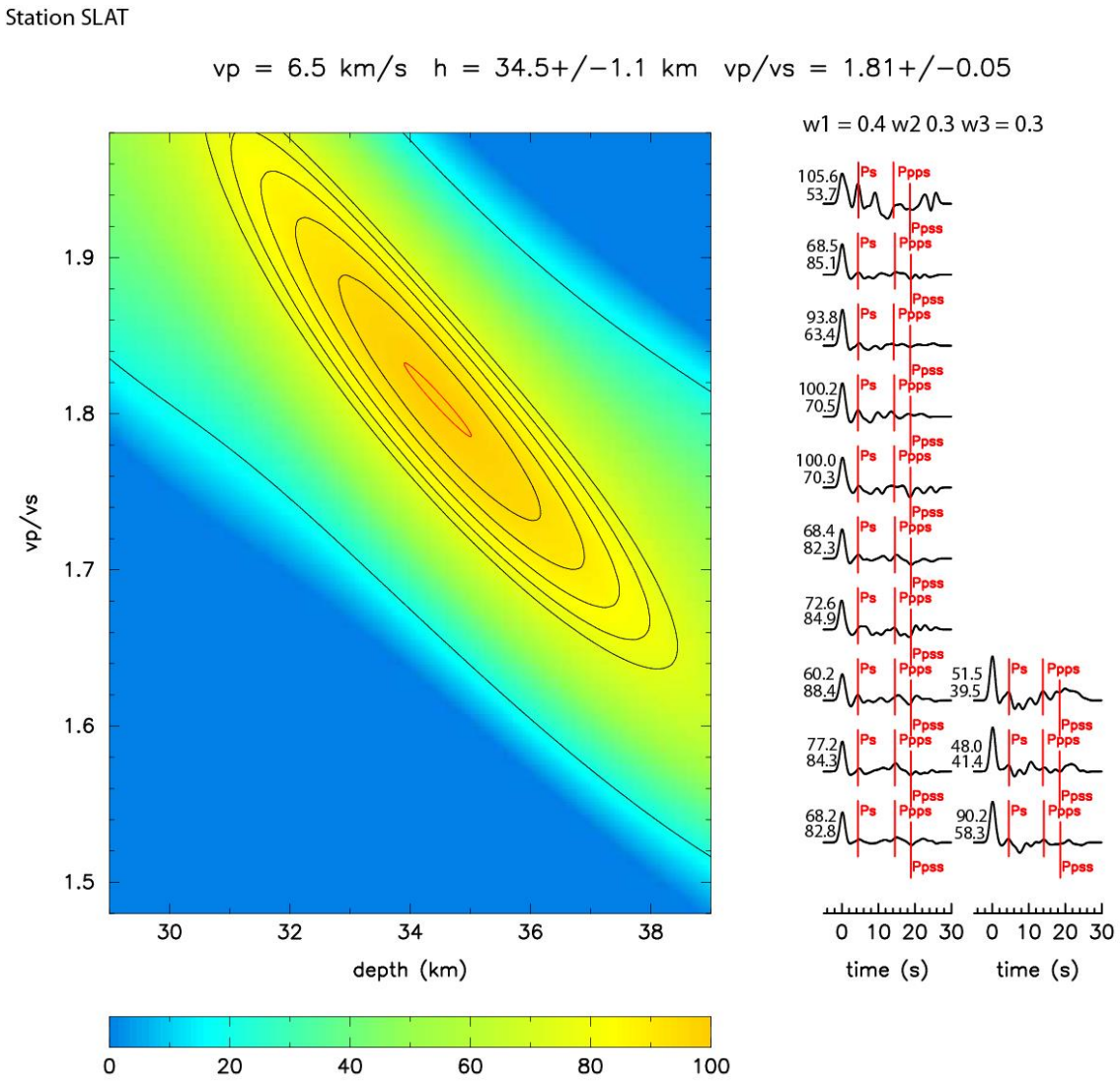

Figure 2-4 (a). H–k stack of receiver functions for stations SLAT for a mean crustal Vp of 6.5 km/s. To the left of each receiver function, the top number gives the event azimuth and the bottom number gives the event distance in degrees. Contours map out percentage values of the objective function given in the text.

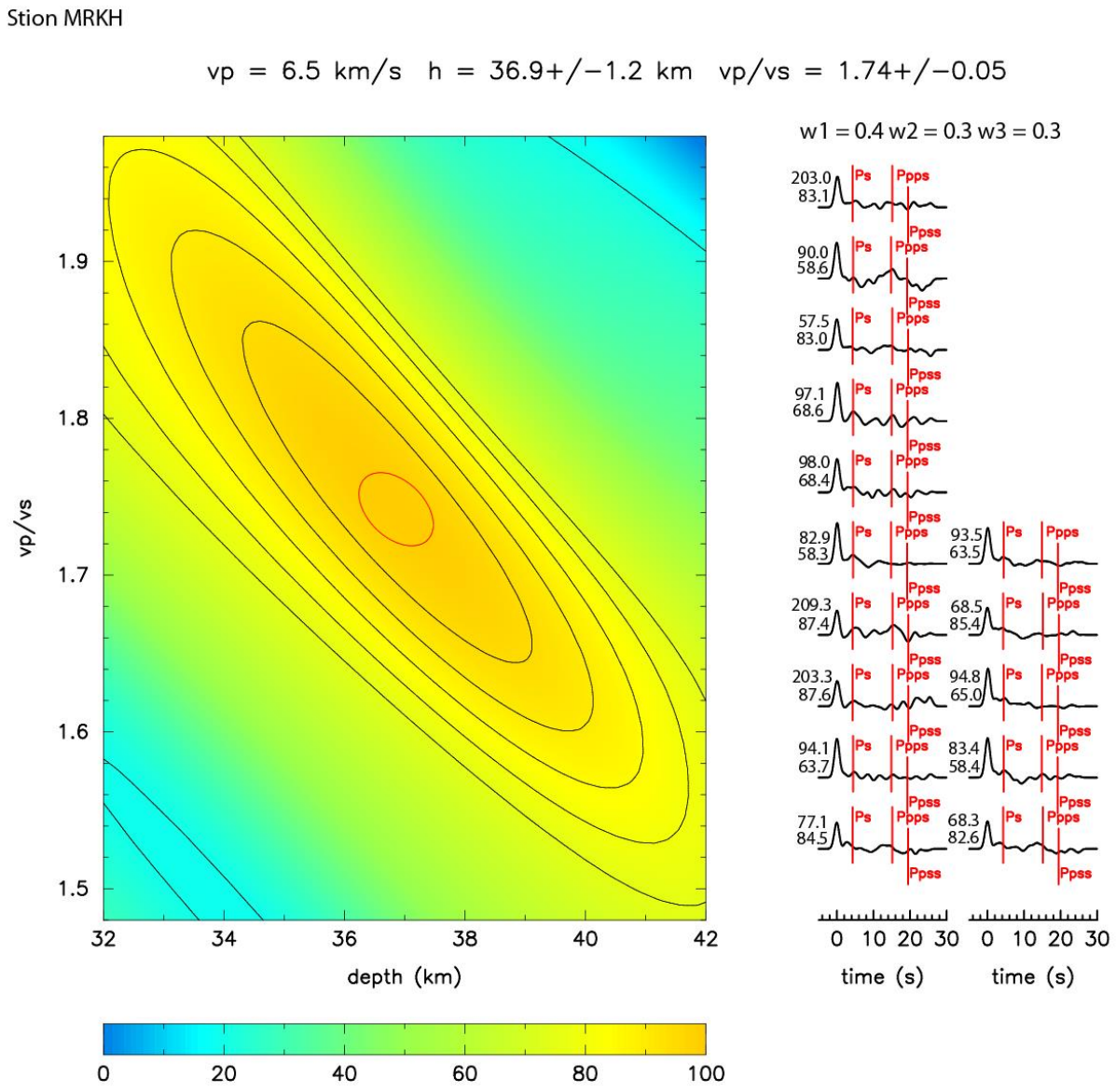

Figure 2-4 (b). H–k stack of receiver functions for station MRKH for a mean crustal Vp of 6.5 km/s. To the left of each receiver function, the top number gives the event azimuth and the bottom number gives the event distance in degrees. Contours map out percentage values of the objective function given in the text.

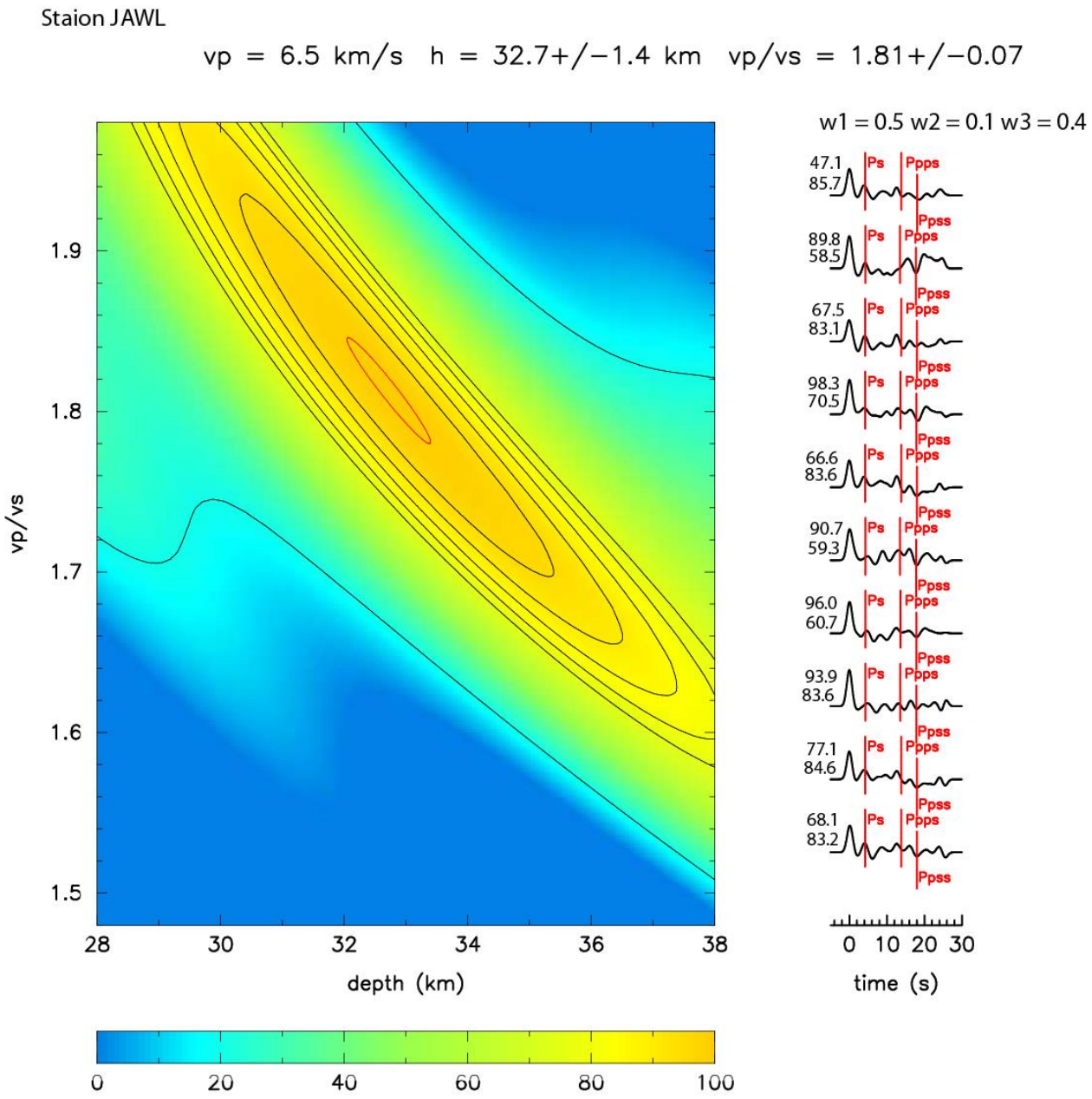

Figure 2-4 (c). H–k stack of receiver functions for station JAWL for a mean crustal Vp of 6.5 km/s. To the left of each receiver function, the top number gives the event azimuth and the bottom number gives the event distance in degrees. Contours map out percentage values of the objective function given in the text.

Figure 2-5 Joint inversion results for stations (a) SLAT, (b) MRKH and (c) JAWL. The top, middle and bottom panels in each column display receiver functions, smoothed dispersion curves for Rayleigh wave group velocities, and shear wave velocity models, respectively. For the receiver functions, observations are shown in black and predictions in red. Above each group of receiver functions is given in sequence the number of waveforms (N), average back azimuth (degrees) ± one standard deviation (baz ± sbaz) and average ray parameter (s km−1) ± one standard deviation. For the group velocity plots, the observations are shown with triangles and the model results are shown with the solid red line. For the velocity models, the grey line is the starting model and the red line is the model obtained from the inversion. The panel to the right shows the shear wave velocity model obtained by jointly inverting all groups of receiver functions with the group velocity curve. The dashed line shows the Moho depth.

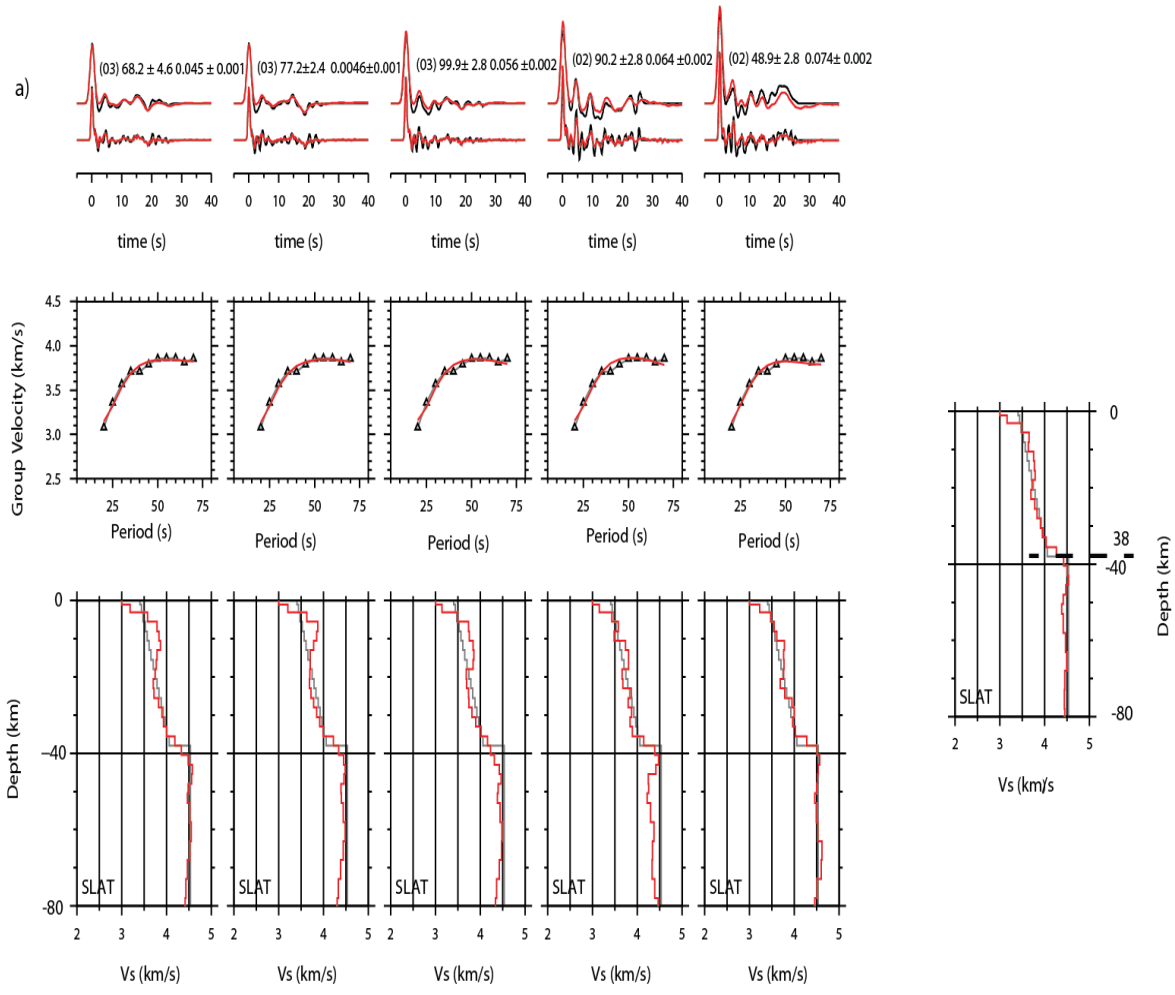

Figure 2-5 (a). Joint inversion results for station SLAT.

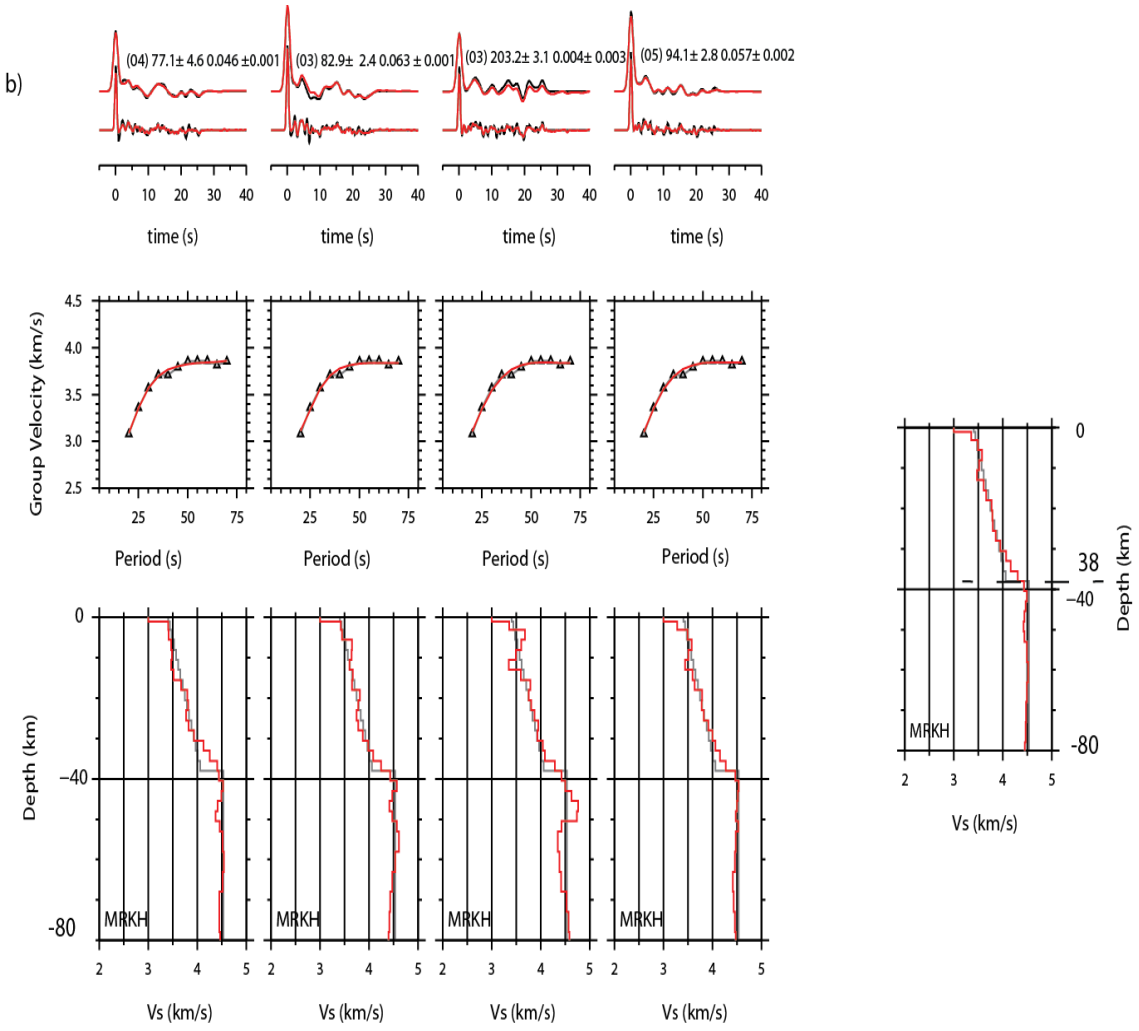

Figure 2-5 (b). Joint inversion results for station MRKH.

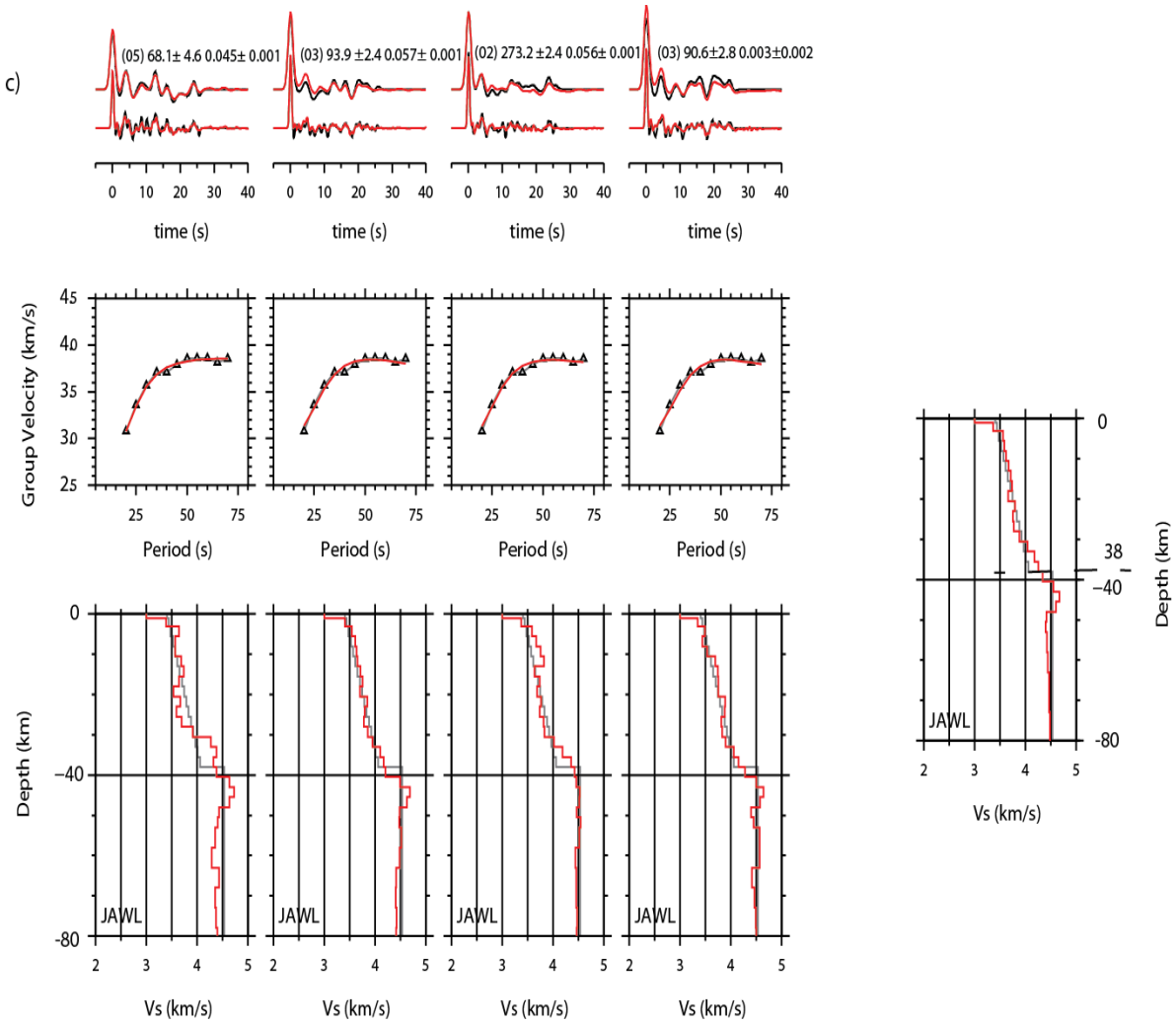

Figure 2-5 (c). Joint inversion results for station JAWL.

3 VELOCITY STRUCTURE OF THE UPPERMOST MANTLE BENEATH THE TANZANIAN CRATON AND THE SURROUNDING PROTEROZOIC MOBILE BELTS FROM Pn TOMOGRAPHY

3.1 Introduction

In this chapter, the uppermost mantle structure beneath East Africa is investigated by inverting Pn traveltimes to obtain a model of P wave velocities. The new Pn tomography model shows variations in uppermost mantle velocities across the region which can be used to address two outstanding questions about East African tectonics:

1) To what extent does the cold, thick lithosphere of the Tanzania Craton extend beneath the Proterozoic mobile belts that surround it?
2) Do the thermal anomalies in the deeper mantle previously imaged beneath the Cenozoic volcanic provinces in the Western Rift extend upward to the base of the crust?

The answer to the first question is important for understanding the size of the Tanzania Craton, while the answer to the second question is important for understanding differences between the Eastern and Western branches of the East African Rift System (EARS).

To address these questions, the previous Pn tomography models of the region by Brazier et al. (2000) and Nyblade and Brazier (2002) have been expanded. A total of 2870 new Pn travel time measurements have been made and modelled, improving the resolution of the uppermost mantle velocity structure across much of East Africa.

3.2 Background and previous studies

3.2.1 Geology and tectonic setting

The tectonic framework of East Africa is comprised of the Archean Tanzania Craton and several Proterozoic mobiles belts that have experienced Karoo (Permian-Jurassic) and Cenozoic rifting (fig. 3-1). The Tanzania Craton lies in the center of the region surrounded to the east by the Neoproterozoic Mozambique Belt, to the northwest and north respectively by the Mesoproterozoic Kibaran and Rwenzori Belts, to the southwest by the Paleoproterozoic Ubendian Belt and to the southeast by the Paleoproterozoic Usagaran Belt.

Low grade greenstone belts and granitoids are found in the northern and central parts of the Tanzania Craton, while high-grade gneisses, granodiorites and migmatites comprise the southern part of the craton (Cahen et al., 1984; Schlüter, 1997).

- The Ubendian Belt formed during the Ubendian Orogeny (2.1-2.2 Ga), and consists of northwest-oriented fold belts of high-grade metamorphic rocks that separate the northern-eastern margin of the Bangweulu Block in northern Zambia from the Tanzanian Craton (Cahen et al., 1984; Lenoir et al., 1994; Schlüter, 1997).
- The Usagaran Belt formed by island arc accretion to the Tanzania Craton during the Usagaran orogeny between 2.1-1.8 Ga (Fritz et al., 2005) and was subsequently reworked during Pan-African (615-650 Ma) collisional events (Moller et al., 1995).
- The Kibaran Belt was formed c. 1.3 Ga during the Kibaran Orogeny (Cahen et al., 1984) and consists of metasedimentary rocks and granitic intrusions (Cahen et al., 1984). The general structural orientation of the belt is NE-SW directed (Schlüter, 1997).
- The Rwenzori Belt (1.86-1.78 Ga) is comprised of metasedimentary rocks of passive margin origin and tholeites that were thrust onto the northern margin of the Tanzania Craton (Begg et al. 2009).

- The Mozambique Belt formed through several collisions between 1.2 Ga and 450 Ma, resulting in largely N-S striking structures (e.g., Cahen, 1984; Key et al., 1989). The northern portion of the Mozambique Belt in Tanzania consists of juvenile terrains of reworked Archean to Mesoproterozoic continental crust while the southern portion (i.e., southern Tanzania and northern Mozambique) consists of Paleoproterozoic to Neoproterozoic gneisses metamorphosed during the Pan-African Orogeny (Begg et al., 2009).

Karoo rifting began in the Permian with the initial breakup of Gondwana and ended in the Jurassic with the separation of Madagascar from Africa (Schlüter, 1997). In the study area, Karoo rift basins formed mostly within the Mozambique Belt and consist of several NNE-SSW to NE-SW striking half grabens (Schlüter, 1997). The Karoo basins may reach maximum depths of 6 to 10 km and are filled primarily with mudstones and sandstones (Schlüter, 1997; Verniers et al., 1989).

The Cenozoic rifting is concentrated in the eastern and western branches of the EARS, which bifurcate around the Tanzanian Craton (Ebinger, 1989; Tesha et al., 1997; Huerta et al., 2009; Nyblade and Barazier, 2002) (fig. 3-1). The EARS extends southward from the Afar Triple junction through Ethiopia and Kenya and into northern Tanzania. In northern Tanzania, the Eastern Branch spreads into a 300-km wide zone of block faulting known as the Tanzanian Divergence Zone (TDZ) (Foster et al., 1997; Dawson, 1992), which surficially extends west to east from the eastern margin of the Tanzania Craton to the Pangani rift (Ebinger et al. 1997; Foster et al. 1997; Chorowicz, 2005). The Eastern Branch propagated from north to south and reached the craton margin as early as c. 10-12 Ma (Lubala and Rafoni, 1987; Dawson, 1992; Nyblade and Brazier, 2002). The divergence of the rift in northern Tanzania may be due to the existence of cratonic lithosphere at depth beneath the Mozambique Belt crust (Smith & Mosley, 1993; Ebinger et al., 1997; Nyblade and Brazier, 2002; Mana et al., 2012). There is less seismicity in the Eastern Branch compared to the Western Branch (Fairhead and Girdler, 1971; Nyblade and Langston, 1995; Foster and Jackson, 1998; Brazier et al., 2005).

The southward extension of the Eastern Branch from the TDZ is debated. Båth (1975) suggested that it continues to the south from the Kenya rift through east-

central Tanzania joining the Western Branch at the northern end of the Lake Malawi rift. Mougenot et al. (1986) and Chorowicz (2005) suggested that the Eastern Branch trends south-eastwards across eastern Tanzania linking offshore with the Davie Ridge, in agreement with a recent tomography study by O'Donnell et al. (2013). Seismicity studies in southeastern Tanzania by Mulibo (2012) also revealed a pattern of seismicity that is consistent with the Eastern Branch extending offshore rather than connecting to the Western Branch at the northern end of the Lake Malawi rift.

The Western Branch of the EARS is comprised of several fault-bounded basins (Ebinger, 1989) extending through the Lake Albert, Lake Edward, Lake Kivu, and Lake Tanganyika rifts, and further south through the Lake Rukwa and Lake Malawi rifts. The Western Branch is thought to be considerably younger than the Eastern Branch, with rift initiation at c. 12 Ma (Ebinger, 1989; Pasteels et al., 1989; Kampunzu et al., 1998). However, Roberts et al. (2012) suggested that rifting in southern Tanzania may have begun as early as c. 25 Ma, contemporaneously with rifting in Kenya. High levels of seismicity in the Western Branch correlate with the major rift basins (e.g., De Bremaecker 1959; Wohlenberg, 1969; McKenzie et al., 1970; Kebede and Kulhánek, 1991; Langston et al., 2002; Brazier et al., 2005; Kim et al., 2009).

Cenozoic volcanism in East Africa is found in several areas. In Kenya and northern Tanzania, a large volcanic province is found along the eastern margin of the Craton (Dawson, 1992; Foster et al., 1997). In southern Tanzania, the Rungwe volcanic province lies to the south of the craton. The other main volcanic province along the Western Branch is the Virunga/Kivu (Bellon and Pouclet, 1980; Ebinger, 1989; Kampunzu et al., 1998) (fig. 3-1).

Topographically, the study area is part of the East African Plateau, which spans an area of c. 1.8 x 10^6 km^2 with a mean elevation of 1 km (Nyblade and Robinson, 1994). The plateau includes the previously mentioned Precambrian terranes that have endured Cenozoic rifting, as well as the Cenozoic volcanic provinces.

3.2.2. Previous studies of uppermost mantle structure

Previous geophysical studies in East Africa have mainly provided information about many aspects of crust and mantle structure. Here we review results from relevant studies on uppermost mantle structure. Pn velocities have been used to study the uppermost mantle structure in a number of locations. Results from the seismic refraction profiles carried out by the Kenya Rift International Seismic project (KRISP) across Kenya found low Pn velocities of 7.5-7.8 km/s beneath the rift axis, Pn velocities between 8.1 to 8.2 km/s beneath the unrifted areas of Mozambique Belt, and a Pn velocity of 8.3 km/s beneath the Tanzania Craton (Prodehl et al., 1994; Fuchs et al., 1997 and references therein) (fig. 3-10). Pn velocity studies in Tanzania using earthquake traveltimes by Brazier et al. (2000) and Nyblade and Brazier (2002) inferred Pn velocities of 8.3 to 8.35 km/s beneath the Mozambique Belt and 8.4 to 8.45 km/s beneath the Tanzania Craton (fig. 3-11), slightly faster than the KRISP results. These reported Pn velocities fall at the high end of the range (8.0 to 8.6 km/s) of upper mantle values for other Precambrian terranes (e.g. Finland and western Russia; King and Calcagnile, 1976; the Canadian shield, LeFevre and Helmberger, 1989; the Kaapvaal Craton, Simon et al., 2002). The high Pn velocities beneath the thick and cold Tanzanian Craton indicate that the uppermost mantle away from the rift has not been extensively disrupted by the Cenozoic tectonism.

Uppermost mantle structure beneath East Africa has also been studied by Langston et al. (2002) using regional wave phase travel times. Their results showed fast Pn velocities of 8.32 to 8.45 km/s beneath the Tanzanian Craton and velocities of 8.1 to 8.2 km/s beneath the Mozambique Belt, in agreement with results from Brazier et al. (2000) and Nyblade and Brazier (2002).

Surface-waves have been used widely to image the velocity variations in the deeper upper mantle. Weeraratne et al. (2003), Adams et al. (2012) and O'Donnell et al. (2013) used Rayleigh waves to model shear velocity structure using a variety of data sets and obtained similar results. Their models show fast shear velocities of 4.65 to 4.7 km/s at depths less than 100 km beneath the Tanzanian Craton, which extend to depths between 150 to 200 km. Fast velocities were also evident beneath the

Kibaran Belt, consistent with the previous study by Nyblade and Brazier (2002). Fast velocities were also imaged beneath the Mozambique Belt to the east of the craton in northern Tanzania, in agreement with the results of Brazier et al. (2000). The most recent surface wave tomography model by O'Donnell et al. (2013) shows low velocities (4.2 to 4.4 km/s) beneath the centers of the Rungwe and Virunga/Kivu volcanic provinces at a depth of ~70 km. O'Donnell et al. (2013) also imaged a region of somewhat low shear velocities beneath the Usagaran Belt to the southeast of the Tanzania Craton.

The upper mantle structure beneath the Western Branch has been investigated by Nolet and Mueller (1982) using body wave travel times and surface wave group and phase velocities. They modelled a high velocity lid that is ~20 km thick underlain by a low velocity channel. The upper mantle structure beneath East Africa has also been studied using body wave tomography by Mulibo and Nyblade (2013), Park and Nyblade (2006), and Ritsema et al. (1998), but none of these models has good resolution of mantle structure above ~100 km depth. The model by Mulibo and Nyblade (2013) at 100 km depth shows regions of low velocities beneath the Cenozoic volcanic provinces along the Western Branch, similar to the surface wave tomography models.

3.3 Method and data

3.3.1 Data

The data used in this study came from three networks. The first network is the 1994-1995 Tanzania Broadband Seismic Experiment (TBSE) which consisted of 20 broadband seismic stations spread across Tanzania (Nyblade et al., 1996) (fig. 3-2). Pn arrival times from regional earthquakes recorded at these stations were used by Brazier et al. (2000) and Nyblade and Brazier (2002) to model variations in Pn velocities in northern and central Tanzania, as described previously. The Pn arrival times from Brazier et al. (2000) and Nyblade and Brazier (2002) are used in this study.

The second network is the Africa Array East African Seismic Experiment (AAEASE) network (fig. 3-2), which was deployed in two stages. The first stage, from August 2007 to December 2008, consisted of 20 stations installed in Uganda and northwestern Tanzania. The second stage ran from December 2008 to June 2010. In this stage 18 stations were taken from Uganda and northwestern Tanzania (the first stage), and reinstalled with a spacing of 100 to 150 km in southern Tanzania.

The third network was the Africa Array Tanzania Basin Seismic Experiment (AATBSE) network. For this experiment eight stations were installed in basins in southeastern Tanzania from February 2010 to July 2011 (fig. 3-2).

All of the networks used broadband seismometers (Guralp CMG-3T, Guralp EPS, or STS-2), 24 bit data loggers and Global Position System (GPS) clocks. Data were recorded continuously at either 20 or 40 samples per second. Local and regional events recorded on the Africa Array stations were initially located by Mulibo (2012) using the HYPOELLIPSE event location code (Lahr, 1999). Events in southeastern Tanzania and the Western Branch from Mulibo (2012) were selected to improve the seismic coverage provided by the Brazier et al. (2000) and Nyblade and Brazier (2002) data sets. Prior to picking Pn arrival times, the data were filtered using a Butterworth 1-5 Hz bandpass filter. The uncertainty in picking the P arrivals is 0.1 s. These events were relocated using the crust and upper mantle model from Langston et al. (2002) (Table 3-1) and the HYPOELLIPSE code (Lahr, 1999). An example of event used in this study is shown in Figure 3-3. Event locations used for this study are provided in Appendix (B).

The combined data set consists of 4035 Pn phases, 1165 from the previous studies by Brazier et al. (2000) and Nyblade and Brazier (2002) and 2870 are from this study. The average crustal thickness and P wave velocity across the East African Plateau is 37 km and 6.5 km/s, respectively (Last et al., 1997), giving a cross-over distance between Pg and Pn arrivals of ~200 km. Thus arrivals from distances less than 200 km were not included in the data compilation. For the inversion, Pn arrival times have been used between distances of 200 and 1200 km for events recorded on seven or more stations. These selection criteria reduce the combined data set to 3364

Pn arrival times. By extending data coverage into southern and southeast Tanzania (fig. 3-4), regions that were not well imaged by previously published studies using similar methodologies (Brazier et al. 2000; Nyblade and Brazier 2002), we address these issues using an improved and expanded regional-scale tomographic image of the uppermost mantle Pn wave velocity structure of eastern Africa. Firstly, the image allows us to track the extension of the Tanzanian Craton beneath the mobile belts that surround it; secondly, we are able to image the development of the Eastern and Western Rifts beyond the well-studied segments which skirt the flanks of the Tanzania Craton; and lastly, the image of the uppermost mantle affords us the opportunity to examine whether the thermal anomalies along the Western Branch have reached the base of the crust.

Before inverting the Pn arrival times, they were first checked for evidence of azimuthal anisotropy by plotting the traveltime residuals versus azimuth for each station. No sinusoidal variations were observed at any station, as illustrated for station MGOR in Figure 3-5, indicating that azimuthal anisotropy is not well developed. Similar plots for all stations are provided in Appendix (C).

3.3.2 Method

A standard singular value decomposition algorithm (Wiggins, 1972; Menke, 1989) was used to invert the Pn travel times for uppermost mantle velocity variations assuming an isotropic medium. The Pn ray path consists of three legs: an initial crustal leg, a leg along the crust/mantle boundary (traveling at upper mantle velocity), and a crustal leg returning to the receiver (Brazier et al. 2000) (fig. 3-6). The inversion was set up to include only the mantle ray path, following the procedure outlined by Hearn (1984). To do this a crust with a thickness of 37 km and an average P wave velocity of 6.5 km/s velocity was assumed. Several studies of crustal structure in East Africa show that 37 km is a good representative value for crustal thickness (Last et al. 1997; Tugume et al., 2012, 2013), and 6.5 km/s is a

good representative value for average crustal P wave velocity (Prodehl et al. 1994; Fuchs et al. 1997 and references therein, Julia et al. 2005).

To account for the varying crustal thickness and event depths across the study area, event and station corrections were calculated. The delays attributed to the crust depend on crustal thickness and the crustal velocity structure. If we assume a constant crustal velocity, a one second delay corresponds to about 10 km of crustal thickness change. Conversely, if we assume a constant crustal thickness, one second of delay corresponds to a change in mean crustal velocity of about 1.6 km/s. The tomographic inversion algorithm we used is able to take variations in crustal thicknesses and event depths across the study area into account.

The starting upper mantle velocity for the inversion was obtained from the average Pn velocity for the study area. The best fitting line to the data yields a Pn velocity of 8.3 km/s (fig. 3-7). To evaluate how much bias the stating model might introduce into the inversion, different starting velocities of 8.1 km/s and 8.2 km/s were used. Comparable velocity patterns were obtained for each starting model (fig. 3-8) indicating that the inversion result is not significantly influenced by the choice of the starting velocity.

Because small errors in the traveltimes can affect the stability of the inversion, constraints such as damping or smoothing need to be applied to regularize the inversion. The selection of the appropriate degree of regularization is determined by balancing the inversion stability versus the Root Mean Square (RMS) data misfit. Based on the method of Menke (1989), we found that the parameters that maximized the stability and least affected the resolution, as discussed below, was a small amount of damping and smoothing. Using the equation for damped least squares,

$$||\mathbf{Gm-d}||^2+\gamma^2||\mathbf{m-ma}||^2 \qquad (3\text{-}1)$$

where **G** contains the model parameters (i.e. crustal thickness, crustal velocity, etc.), **m** represents the final model, **ma** represents the initial model, and **d** represents the measured travel times. Damping was applied to the inversion to minimize the difference between the final velocity model and the background velocity model. The

damping was applied by multiplying the square of a damping factor (γ) by the square of the difference between the final and background models.

In order to determine the optimal parameters, parameter space was searched and it was determined that using damping to regularize the solution yielded the best results in terms of preserving resolution. The tradeoff curve in Figure 3-9 shows damping versus the RMS data misfit for a range of damping values. A damping value of 1200 is a compromise between minimizing the error while maintaining stability. Moreover, the lateral resolution of the inversion is an important factor when interpreting the tomographic images. The study area was divided into 0.5° and 1.0° grids, and inversions were performed for each grid. The number of travel times greatly exceeds the number of blocks. For the 0.5° grid, a hit count (travel time distance in km per grid) of 250 km was selected as a reasonable threshold for determining which grids to include in the inversion.

3.4 Results

In the final model (Figure 3-12), velocities are shown for those grid cells with at least 250 km total length of ray paths passing through them and containing ray paths from at least seven events. Pn velocity variations are indicated by a color scale, with blue and red representing high and low Pn velocity, respectively. To assess the uncertainty in the model, errors in traveltimes from the earthquake location algorithm were propagated through the inversion (Menke and Abbott, 1990) to obtain a map of standard deviation in the Pn velocities (fig. 3-10). The standard deviation values across the study area are small and well resolved, not exceeding 0.05 to 0.1 km/s in most of the areas. Cells with variances $\geq$ 0.3 km/s were considered to be poorly resolved. Most of them located around the edges of the study area.

Pn velocities range between 8.3 and 8.4 km/s across the central part of the Tanzania Craton and into the Kibaran Belt. Pn velocity ranges between 8.2 and 8.3 km/s in northern Tanzania along the eastern side of the Mozambique Belt where the Eastern Branch of the EARS impinges on the Craton. Pn velocities range between

8.1 and 8.2 km/s beneath most of the Western Branch of the EARS, including beneath the Virunga/Kivu volcanic province. The lowest Pn velocities of 8.0 to 8.1 km/s are found in southern Tanzania where the Eastern and Western Branches of the EARS may join. This region encompasses the Rungwe volcanic province, the northern part of Lake Malawi and the region of Cenozoic and Karoo rifts extending to the NE of the Rungwe volcanic province along the southern edge of the Tanzania Craton. To the south of this region towards the Mozambique border, the Pn velocities increase from 8.1 to 8.2 km/s.

3.5 Discussion

In this section we compare our results to previous studies of uppermost mantle velocity structure in East Africa and address the two questions raised in the introduction: 1) To what extent does the cold, thick lithosphere of the Tanzania Craton extend beneath the Proterozoic mobile belts that surround it? 2) Do the thermal anomalies in the deeper mantle previously imaged beneath the Cenozoic volcanic provinces in the Western Rift extend upward to the base of the crust?

The fast Pn velocities beneath the Tanzania Craton are consistent with the velocities previously reported by Brazier et al. (2000) and Nyblade and Brazier (2002), as well as the Pn velocity of 8.3 km/s from the KRISP refraction profile (fig. 3-10) (Prodehl et al. 1994; Fuchs et al. 1997 and references therein). The high Pn velocities are consistent with the presence of old, cold and chemically depleted cratonic lithosphere. The fast Pn velocities of the Tanzania Craton are also consistent with studies of similar cratonic regions elsewhere in the world (Christensen and Mooney, 1995).

The extension of the fast Pn velocities to the west beneath the Kibaran Belt and to the east beneath the Mozambique Belt indicates the presence of cratonic lithosphere beneath these mobile belts. The presence of cratonic lithosphere beneath the Mozambique Belt was suggested previously by Brazier et al. (2000) and Nyblade and Brazier (2002) from Pn velocities and by Adams et al. (2012) and O'Donnell et al. (2013) from fast upper mantle shear wave velocities. Further support for cratonic

lithosphere beneath the Mozambique Belt comes from xenolith studies indicating Archean lithospheric mantle beneath the mobile belt in northern Tanzania (Chesley et al., 1999; Aulbach et al., 2008; Mana et al., 2012). The seismic and geochemical observations clearly indicate that the development of the Eastern Branch of the EARS within the TDZ is strongly affected by the presence of cratonic lithosphere beneath the Mozambique Belt, as has been suggested before (e.g., Tesha et al., 1997; Hetzel and Strecker, 1994; Nyblade and Brazier 2002; Ebinger et al., 1997; Foster et al., 1997).

To the west of the mapped craton boundary, our results indicate a similar structural configuration with the Kibaran Belt thrust over the margin of the Tanzania Craton. Nyblade and Brazier (2002) also suggested that strong cratonic lithosphere extended beneath the Kibaran Belt and may have influenced where the Western Branch developed (i.e., just to the west of the cratonic margin at depth). Our results show craton-like fast Pn velocities beneath much of the Kibaran Belt, thus supporting the interpretation that the Western Branch of the EARS has developed in weaker mobile belt lithosphere just to the west of the craton edge (Nyblade and Brazier, 2002).

Regarding the southern extent of the craton, (figure 3-10) shows fast velocities under the northern part of the Ubendian Belt, but not the southern part around Lake Rukwa or under the Usagaran Belt. Thus, to the south of the craton it does not appear that mobile belt crust has been thrust over the cratonic lithosphere. Overall, our results indicate that the craton extends about 950 km West to East, from about longitude 30° to 38 ° at its widest point. The extension of cratonic lithosphere to the north is not constrained in our model. However, the shear velocity models from Adams et al. (2012) and O' Donnell et al. (2013) show the presence of fast velocities beneath the Rwenzori Belt and Uganda Basement Complex. Thus, it appears that in a south-north direction, the craton is about 1200 km long, extending from latitude -8° in the south to latitude 2.5° in the north.

The Pn map shows slightly lower velocities beneath the Virunga/Kivu volcanic province in the Western Rift to the west of the Tanzania Craton. However, the Pn velocities are not significantly lower than elsewhere along the Western Rift

where there is no volcanism. Therefore, assuming that the velocity variations reflect first order temperature variations, we find little evidence for regional heating of the uppermost mantle beneath the Virunga/Kivu province. This finding is consistent with fast Pn and Sn velocities beneath this region of the Western Rift reported by Nolet and Mueller (1982) from modeling waveforms from regional earthquakes.

The region of somewhat lower Pn velocities (8.0 to 8.1 km/s) beneath the Rungwe volcanic province can be similarly interpreted. The velocities found beneath the province are similar to those extending to the NE along the craton margin where there are no volcanic rocks, and therefore there appears to be little regional heating of uppermost mantle related to the volcanic province. Moreover, these lowest uppermost mantle velocities extend continuously and underlie the SE flank of the craton, beneath the Usagaran belt. This trend has been recently supported by Mulibo (2012), who mapped a zone of seismicity extending from the southeastern margin of the Tanzanian Craton towards the ocean. Although the timing and extent of extension and present day deformation is unknown, this feature may indicate the onset of rifting.

In contrast to our Pn velocities beneath the Virunga/Kivu and Rungwe volcanic provinces indicating little regional heating of the uppermost mantle, deeper mantle structure beneath the volcanic province is clearly perturbed, as described in section 3.2.2. Surface and body wave tomography images show low velocity anomalies at depths of ~ 70 km and deeper in the mantle (Adams et al., 2012; O'Donnell et al., 2013; Mulibo and Nyblade, 2013). Outlines of the regions of lower shear velocities at ~70 km depth from O'Donnell et al. (2013) are shown in Figure 3-10. The P wave tomography model of Mulibo and Nyblade (2013) shows relative velocity reductions of 3 % at 200 km depth, while our model shows virtually no reduction compared to non-volcanic regions of the Western Rift. Generally partial melt in mantle materials begins to occur when mantle velocities drop by about 6% from the normal value (Sato et al., 1989), which is not the found in our model. This comparison indicates that the thermally perturbed mantle beneath the volcanic provinces at depth has not broadly affected the thermal structure of the upper mantle just below the Moho.

3.6 Summary and conclusions

In this study, Pn traveltimes of local and regional earthquakes were inverted using a standard singular value decomposition algorithm assuming an isotropic medium (Wiggins, 1972; Menke, 1989) to obtain uppermost mantle velocity variations across East Africa. Our results reveal fast Pn velocities beneath the Tanzania Craton, the extension of these fast velocities beneath the Mozambique Belt to the east of the craton, the Kibaran Belt west of the craton, and beneath the northern half of the Ubendian Belt to the southwest of the craton. We can conclude that the width of the craton (west to east) at its widest point is ~ 950 km and its length from south to north is ~1200 km. Therefore, the areal extent of the cratonic lithosphere is much larger than is indicated by the mapped boundaries of the craton (fig. 3-1).

Pn velocities beneath the volcanic provinces along the Western Branch are not anomalously slow, indicating little, if any, perturbation to the uppermost mantle beneath them. This is in contrast to upper mantle structure at depths $\geq$ 70 km beneath the volcanic regions which is clearly perturbed. The fast Pn velocities beneath the Western Branch everywhere contrast with the slow Pn velocities of 7.5-7.8 km/s beneath the Eastern Branch in Kenya, showing that the upper mantle beneath the Eastern Branch has been altered much more than beneath the Western Branch.

References

Adams, A., Nyblade, A. and Weeraratne, D. (2012), Upper mantle shear wave velocity structure beneath the East African plateau: evidence for a deep, plateau wide low velocity anomaly, Geophysical Journal International, 189(1), 123–142.

Aulbach, S., Rudnick, R.L. and McDonough, W. F. (2008), Li-Sr-Nd isotope signatures of the plume and cratonic lithospheric mantle beneath the margin of the rifted Tanzanian Craton (Labait), Contributions to Mineralogy and Petrology 155: 79-92, doi 10.1007/s00410-007-0226-4.

Bellon, H. and Pouclet, A. (1980), Datation K-Ar de quelques laves du rift ouest I'Afrique Centrale; implications sur l'evolution magmatique et structurale. Geological Rundsch, 69: 59.

Begg, G., Griffin, W., Natapov, L., O'Reilly, S., Grand, S., O'Neill, C., Hronsky, J., Djomani, Y., Swain, C,. Deen, T. and Bowden P. (2009), The lithosphere architecture of Africa: Seismic tomography, mantle petrology, and tectonic evolution, Geosphere, 5, 23-50.

Båth, M. (1975), Seismicity of the Tanzania region, Tectonophysics, 27(4), 353–379.

Brazier, R.A., Nyblade, A.A. and Langston, C.A. (2000), Pn wave velocities beneath the Tanzania Craton and adjacent rifted mobile belts, East Africa, Geophysical Research Letters, 27(16), 2365–2368.

Brazier, A. R, Nyblade, A. A. and Florentin, J. (2005), Focal mechanisms and the stress regime in NE and SW Tanzania, East Africa, Geophysical Research Letters, doi:10.1029/2005GL023156.

Cahen, L., Snelling, N., Delhal, J. and Vail, J. (1984), The geochronology and evolution of Africa, Oxford, United Kingdom, Clarendon Press.

Chesley, J., Rudnick, R. and Lee, C. (1999), Re–Os systematics of mantle xenoliths from the East African rift: age, structure and history of the Tanzania craton, Geochimica Cosmochimica Acta, 63, 1203–1217.

Chorowicz, J. (2005), The East African Rift System, Journal of Africa Earth Sciences, 43, 379-410.

Christensen, N.I. and Mooney W.D. (1995), Seismic velocity structure and composition of the continental crust: A global view, Journal of Geophysical Research, 100, 9761-9788.

Dawson, J. (1992), Neogene tectonics and volcanicity in the North Tanzania sector of the Gregory Rift Valley: contrasts with the Kenya sector, Tectonophysics, 204, 81–92.

De Bremaecker, J.Cl. (1959), Seismicity of the West African Rift Valley, Journal of Geophysical Research, 64, 1961-1966.

Ebinger, C., Djomani, Y., Mbede, Y., Foster, F. and Dawson, J. (1997), Rifting Archean lithosphere: the Eyasi–Manyara–Natron rifts, East Africa, Journal of the Geological Society of London, 154, 947–960.

Ebinger, C.J. (1989), Tectonic development of the western branch of the East African rift system, Geological Society of America Bulletin, 101, 788–791.

Fairhead, J.D. and Girdler, R.W. (1971), The seismicity of Africa, 24, 271–301.

Foster, A., Ebinger, C. and Rex, E.M.D. (1997), Tectonic development of the northern Tanzanian sector of the East African Rift System, Journal of the Geological Society of London, 154(4), 689–700.

Foster, A.N. and Jackson, J. A. (1998), Source parameters of large African earthquakes: implications for crustal rheology and regional kinematics, Geophysical Journal International, 134 (2), 422-448.

Fritz, H., Tenczer, V., Hauzenberger, C.A., Wallbrecher, E., Hoinkes, G., Muhongo, S. and Mogessie, A. (2005), Central Tanzanian tectonic map: A step forward to decipher Proterozoic structural events in the East African Orogen, Tectonics, 24, TC6013, doi:10.1029/2005TC001796.

Fuchs, K., Altherr, R., Muller, B. and Prodehl, C. (1997), Structure and dynamic processes in the lithosphere of the Afro-Arabian Rift system, Tectonophysics, 278, 1-352.

Hearn, T. M. (1984). Pn travel times in southern California, Journal of Geophysical Research, 89, 1843-1855.

Hetzel, R. and Strecker, M.R. (1994), Late Mozambique Belt structures in western Kenya and their influence on the evolution of the Cenozoic Kenya Rift, Journal of Structural Geology, 16(2), 189-20

Huerta, A., Nyblade, A. and Reusch, A. (2009), Mantle transition zone structure beneath Kenya and Tanzania: more evidence for a deep-seated thermal upwelling in the mantle, Geophysical Journal International, 177, 1249–1255.

Julià, J., Ammon, C.J. and Nyblade, A.A. (2005), Evidence for mafic lower crust in Tanzania, East Africa, from joint inversion of receiver functions and Rayleigh wave dispersion velocities, Geophysical Journal International, 162, 555-569.

Kampunzu, A.B., Bonhomme, M.G. and Kanika, M. (1998), Geochronology of volcanic rocks and evolution of the Cenozoic Western Branch of the East African

Rift System, Journal of Africa Earth Sciences, 26 (3), 441–461.

Kebede, F., and Kulhanek, O. (1991), Recent seismicity of the East African Rift System and its implications, Physics Earth and Planetary International, 68, 259-273.

Key, R., Charsley, T., Hackman, B., Wilkinson, A. and Rundle, C. (1989), Superimposed upper Proterozoic collision-controlled orogenies in the Mozambique orogenic belt of Kenya, Precambrian Research, 44, 197-225.

Kim, D., Nyblade, A. A. and Begg, G. (2009), Crustal velocity structure of the Rukwa Rift in the Western Branch of the East African Rift System, South African Journal of Geology, 112, 251-260.

King, D. W., and Calcagnile (1976), P wave velocities in the upper mantle beneath Fennoscandia and western Russia, Geophysical Journal of the Royal Astronomical Society, 46 407-432.

Lubala, R.T. and Rafoni, A. (1987), Pétrologie et signification géodynamique du volcanisme alcalin mio-pliocène de la région du lac Natron (Rift ext-africain, Tanzanie), Sciences Géologiques 40 (1-2), 41–55 (Strasbourg).

Langston, C.A., Nyblade, A. A. and Owens, T. J. (2002), Regional wave propagation in Tanzania, East Africa, Journal of Geophysical Research, 107 (B1), doi:10.1029/ 2001JB000167.

Lahr, J. C. (1999), HYPOELLIPSE Y2K: A computer program for determining local earthquake hypocentral parameters, magnitude, and first-motion pattern, U.S., Geological Survey Open-File Report 99-23, 112 p.

Last, R.J., Nyblade, A.A., Langston, C.A. and Owens, T.J. (1997), Crustal structure of the East African Plateau from receiver functions and Rayleigh wave phase velocities, Journal of Geophysical Research 102, 24469–24483.

Lenoir, J.L., Liegeois, J.P., Theunissen, K. and Klerkx, J. (1994), The palaeoproterozoic Ubendian shear belt in Tanzania; geochronology and structure, Journal of African Earth Sciences, 19, 160-184.

LeFevre, L. and Helmberger, D.V. (1989), Upper mantle P velocity structure of the Canadian Shield, Journal of Geophysics Research, 94, 17749-17765.

Mana, S., Furman, T., Carr, M.J., Mollel, G.F., Mortlock, R.A., Feigenson, M.D., Turrin, B.D. and Swisher, C.C., III (2012), Geochronology and geochemistry of the Essimingor volcano: melting of metasomatized lithospheric mantle beneath the North Tanzanian Divergence zone (East African Rift), Lithos, 155, 310–325.

McKenzie, D. P., Davies, D. and Molnar, P. (1970), Plate tectonics of the Red Sea and East Africa, Nature, 226, 234-248.

Menke, W. (1989), Geophysical Data Analysis: Discrete Inverse Theory, International Geophysics Series, 45.

Menke, W., and Abbott, D. (1990), Geophysical theory: New York, Columbia University Press, 458 pp.

Möller, A., Appel, P., Mezger, K. and Schenk, V. (1995), Evidence for a 2 Ga subduction zone; eclogites in the Usagaran Belt of Tanzania. Geology, 23, 1067–1070.

Mougenot, D., Recq, M., Virlogeux, P. and Lepvrier, C. (1986), Seaward extension of the East-African Rift, Nature, 321, 599–603.

Mulibo, G.D. (2012), Investigation of mantle structure beneath Eastern Africa: implications for the origin of the Cenozoic tectonism and propagation of the rift system, PhD thesis, The Pennsylvania State University.

Mulibo, G.D.and Nyblade, A.A. (2013), The P and S wave velocity structure of the mantle beneath eastern Africa and the African superplume anomaly, Geochemistry Geophysics Geosystems.

Nolet, G., and Mueller, S. (1982), A model for the deep structure of the East Africa rift system from simultaneous inversion of teleseismic data, Tectonophysics, 84, 151-178.

Nyblade, A.A. and Langston, C.A. (1995), East African earthquakes below 20 km depth and their implications for crustal structure, Geophysical Journal International, 121, 49–62.

Nyblade, A.A. and Brazier, R.A. (2002), Precambrian lithospheric controls on the development of the East African rift system, Geology, 30, 755–758.

Nyblade, A.A. and Robinson, S.W. (1994), The African superswell, Geophysical Research Letters, 21, 765–768

Nyblade, A.A., Langston, C.A., Last, R.J., Birt, C. and Owens, T.J. (1996), Seismic experiment reveals rifting of craton in Tanzania, EOS, Transactions, American, Geophysical, Union, 77(51), 517–521.

O'Donnell, J., Adams, A., Nyblade, A., Mulibo, G., Tugume, F. and Weeraratne, D. (2013), The uppermost mantle shear wave velocity structure of eastern Africa from Rayleigh wave tomography: Constraints on rift evolution, Geophysical Journal International, 194, 961-978.

Park, Y. and Nyblade, A.A. (2006), P-wave tomography reveals a westward dipping low velocity zone beneath the Kenya Rift, Geophysical Research Letters, 33(4), doi:10.1029/2005GL025605.

Pasteels, P., Villeneuve, M., Paepe, P.D. and Klerkx, J. (1989), Timing of the volcanism of the southern Kivu province: implications for the evolution of the western branch of the East African Rift system, Earth and Planetary Science Letters., 94(3–4), 353–363.

Ritsema, J., Nyblade, A.A., Owens, T.J., Langston, C.A. and VanDecar, J.C. (1998), Upper mantle seismic velocity structure beneath Tanzania, east Africa: implications for the stability of cratonic lithosphere, Journal of Geophysical Research, 103, 21201–21213.

Prodehl, C., Keller, G.R. and Khan, M.A. (Eds.) (1994), Crustal and Upper Mantle Structure of the Kenya Rift, Tectonophysics, 236, 483 pp.

Roberts, E., N. Stevens, P. O'Connor, P. Dirks, M. Gottfried, W. Clyde, R. Armstrong, A. Kemp, and S. Hemming (2012), Initiation of the western branch of the East African Rift coeval with the eastern branch, Nature Geosciences, 5, 289–294.

Sato, H., Sacks, I.S., Murase, T., Muncill, G. and Fukuyama, H. (1989), Qp-melting temperature relation in peridoite at high pressure and temperature: attenuation mechanism and implications for the mechanical properties of the upper mantle. Journal of Geophysical Research 94: doi: 10.1029/89JB00738. issn: 0148-0227.

Schlüter, T. (1997). Geology of East Africa, Berlin; Stuttgart; Borntraeger, Germany, Druckereizu Altenburg GmbH.

Simon, R. E., C. Wright, E. M. Kgaswane and M. T. O. Kwadiba (2002), The P wave speed structure below and around the Kaapvaal Craton to depths of 800 km, from traveltimes and waveforms of local and regional earthquakes and mining induced tremors, Geophysical Journal International, 151, 132-145, doi:10.1046/j. 1365-246X.2002.0175.x.

Smith, M. and Mosley, R (1993), Crustal heterogeneity and basement influence on the development of the Kenya rift, East Africa. Tectonics 12, 591-606.

Tesha, A. L., Nyblade, A. A., Keller, G. R. and Doser, D. I. (1997), Rift localization in suture-thickened crust: evidence for Bouguer gravity anomalies in northeastern Tanzania, East Africa, Tectonophysics, 278, 315–328.

Tugume, F., Nyblade, A. and Julià, J. (2012), Moho depths and Poisson's ratios of Precambrian crust in East Africa: evidence for similarities in Archean and Proterozoic crustal structure, Earth and Planetary Science Letters, 355–356, 73–81.

Tugume, F., Nyblade, A., Julià, J., Meijde M. (2013), Precambrian crustal structure in Africa and Arabia: Evidence lacking for secular variation, Tectonophysics, 609, 250-266.

Verniers, J., Jourdan, P. P., Paulis, R.V., Frascaspada L. and Debock, F.R. (1989), The Karroo Graben of Metangula Northern Mozambique, Journal of African Earth Sciences, 9.1, 137-58.

Weeraratne, D., Forsyth, D., Fischer K. and Nyblade, A. (2003), Evidence for an upper mantle plume beneath the Tanzanian craton from Rayleigh wave tomography, Journal of Geophysical Research, B., 108, 1-17.

Wiggins, R. (1972), The general linear inverse problem: Implications of surface waves and free oscillations for Earth structure, Reviews of Geophysical and Space Physics, 10, 251-285.

Wohlenberg, J. (1969), Remarks on the seismicity of east Africa between 42N-12S and 23E-40E, Tectonophysics, 8(4–6), 567–577.

Table 3-1: Velocity model used for event relocation from Langston et al. (2002)

Layer thickness (km)	P-wave vel. (km/s)	S-wave vel. (km/s)	Density (g/cm^3)
10	5.84	3.38	2.33
10	6.26	3.62	2.50
10	6.68	3.83	2.67
7	7.09	4.10	2.84
Half space	8.28	4.74	3.31

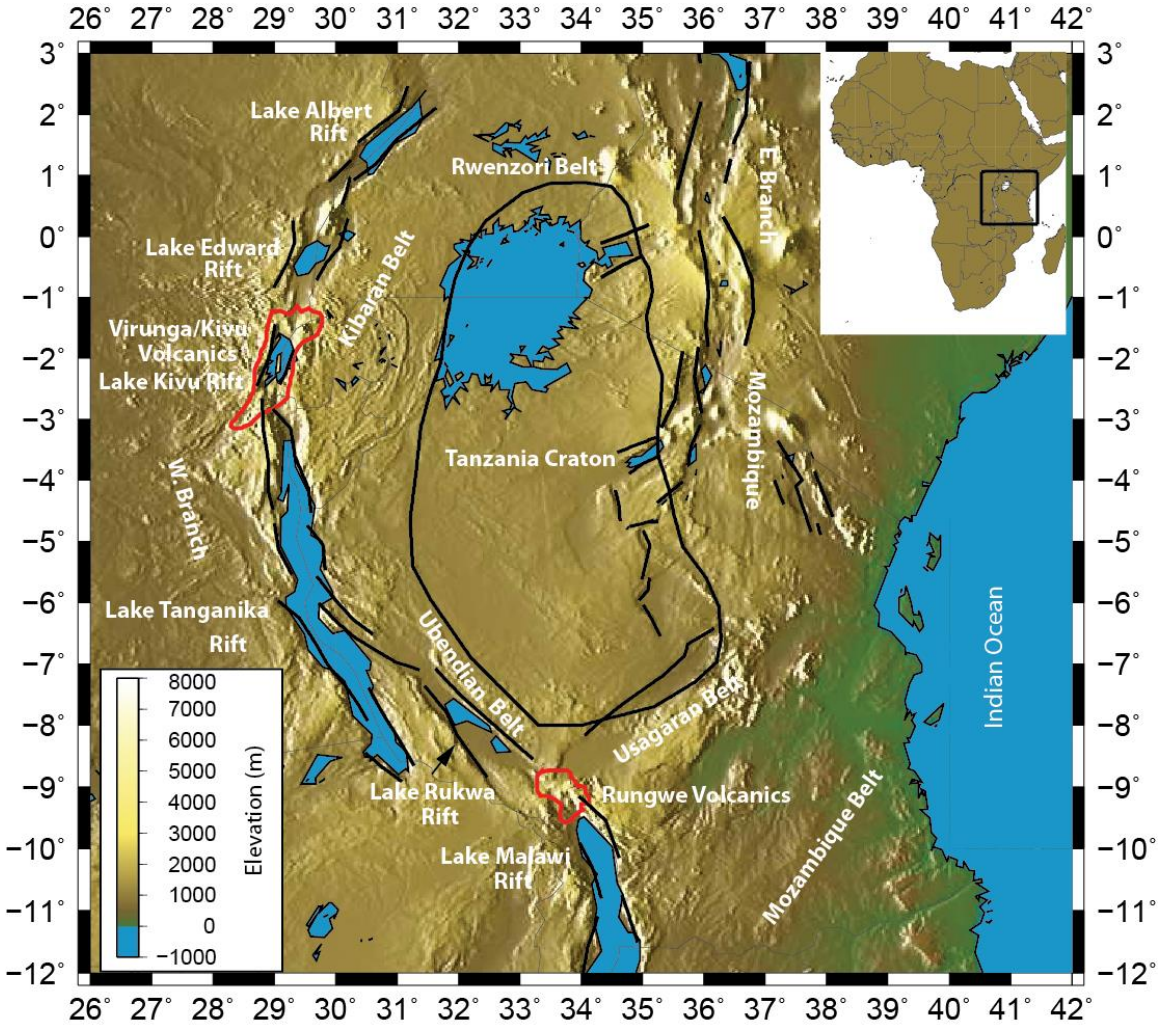

Figure 3-1. Elevation map of East Africa illustrating the locations of geological provinces. Solid red line shows the volcanic provinces in the Western Branch of the EARS. Cenozoic rift faults and the Tanzania Craton are shown in solid black lines.

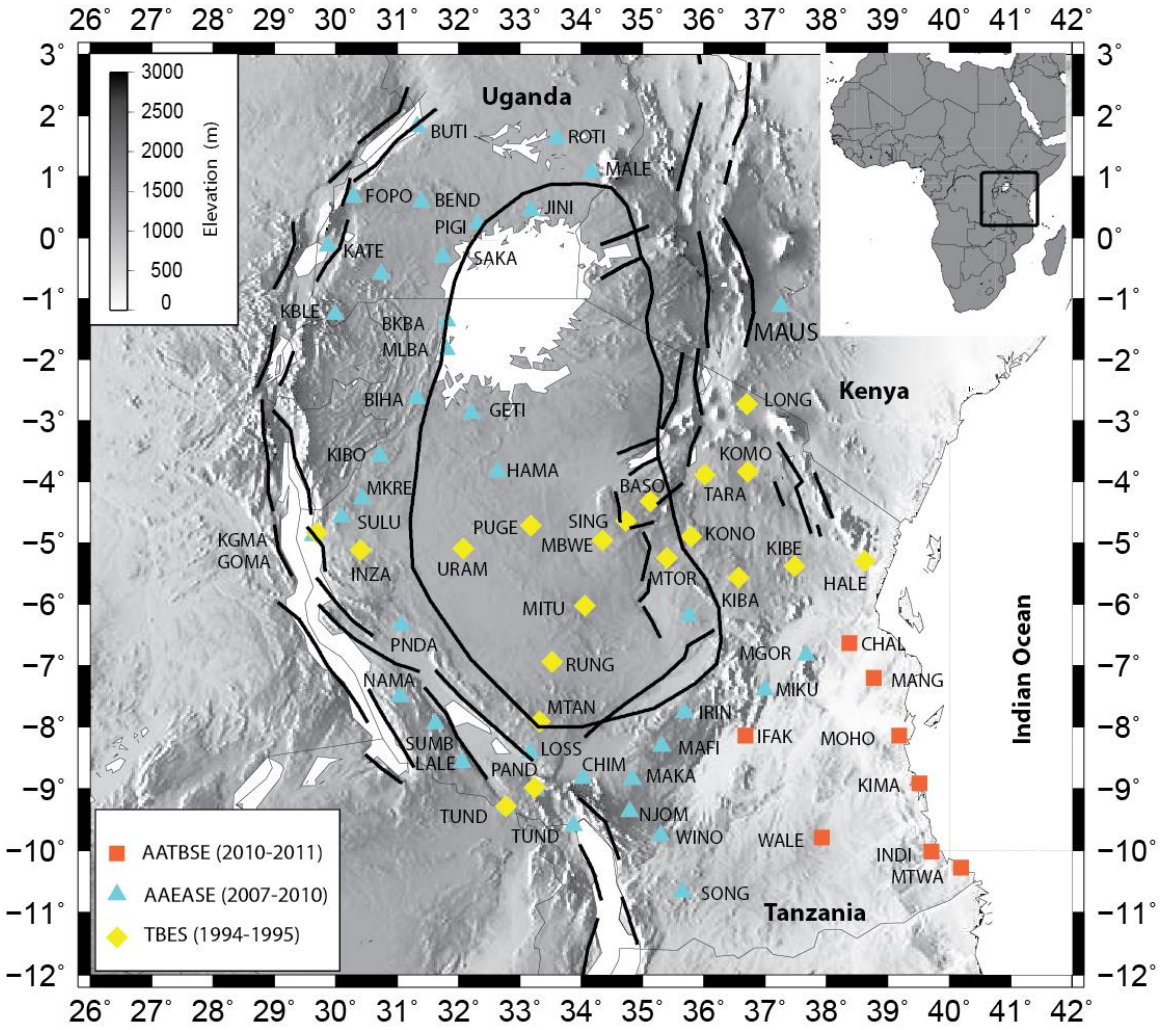

Figure 3-2. Locations of seismic stations used in this study. Yellow rhombuses are stations from the 1994-1995 Tanzania Broadband Seismic Experiments (TBSE). Blue triangles are stations from the 2007-2010 AfricaArray East African Seismic Experiment (AAEASE). Red squares are stations from the 2010-2011 AfricaArray Tanzania Broadband Seismic Experiments (AATBSE). Rifts, faults and the craton boundary are illustrated as solid black lines.

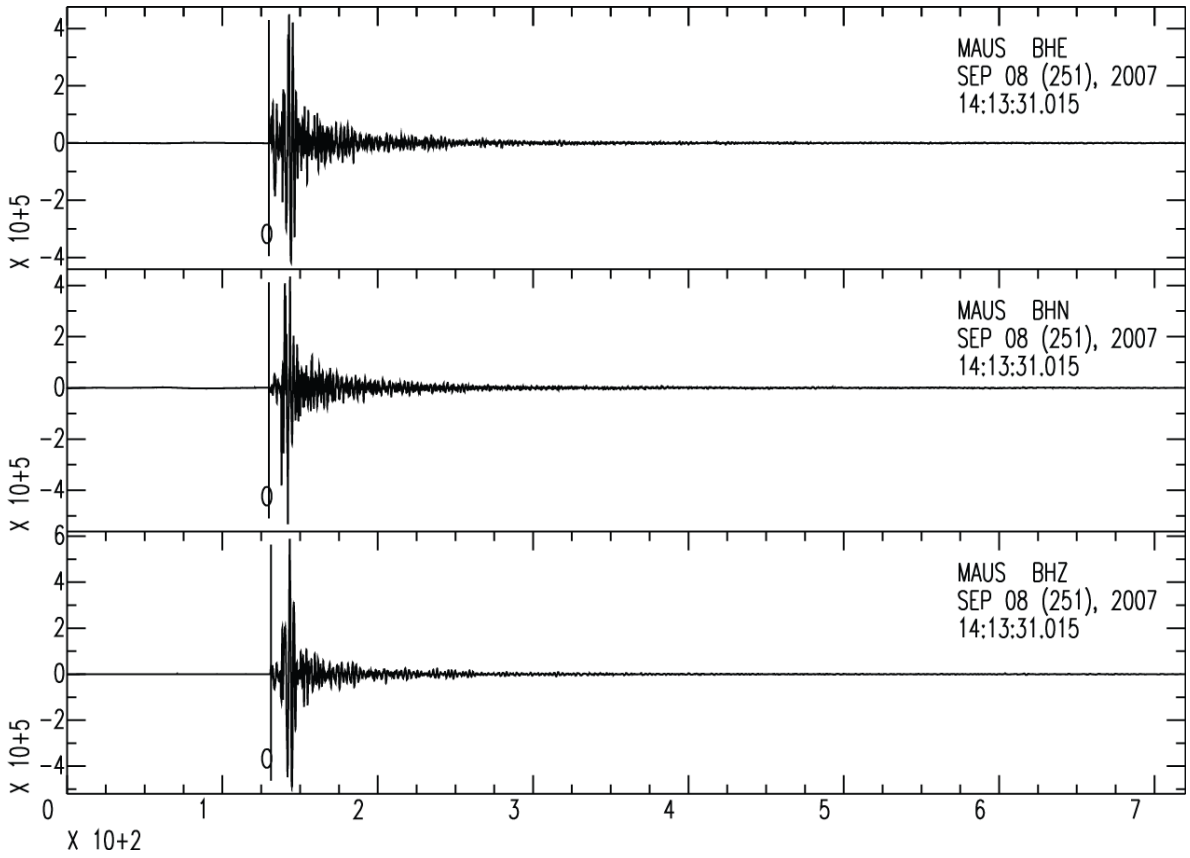

Figure 3-3. Example of an earthquake used in this study recorded on station MAUS.

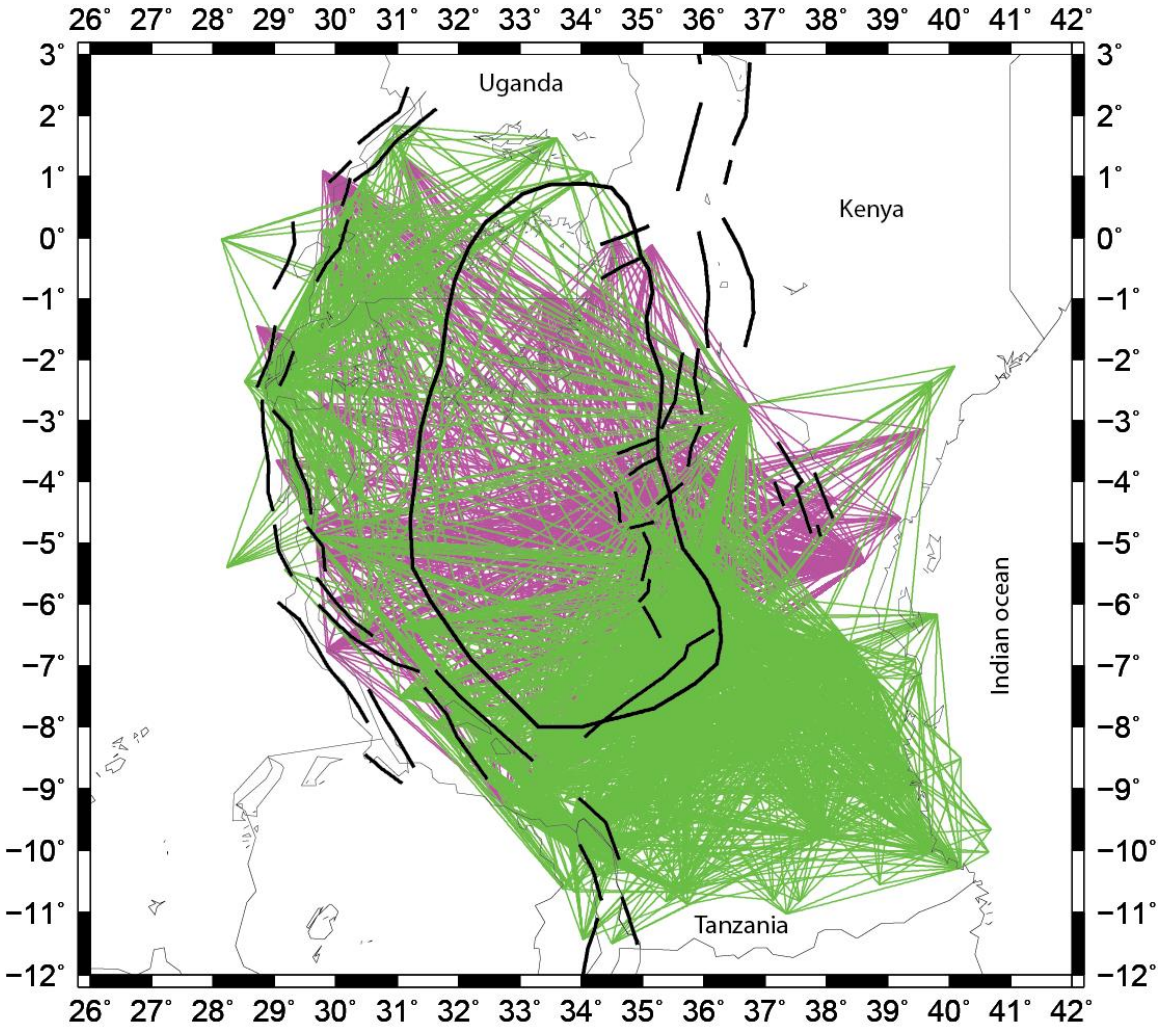

Figure 3-4. Map showing seismic ray coverage. Magenta color lines show path coverage from previous studies (Brazier et al. 2000 and Nyblade and Brazier, 2002). Green lines show path coverage for events picked in this study. Rifts and craton are shown in solid black lines.

.

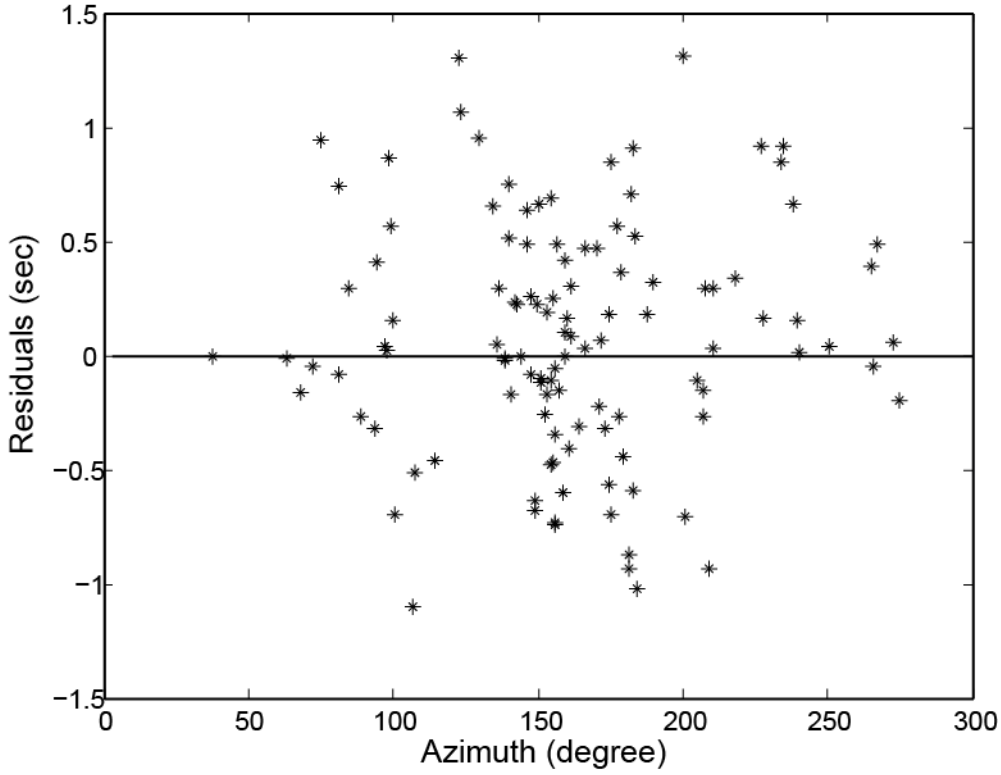

Figure 3-5. Plot showing Pn travel time residuals vs azimuth for station MGOR, indicating no azimuthal anisotropy.

.

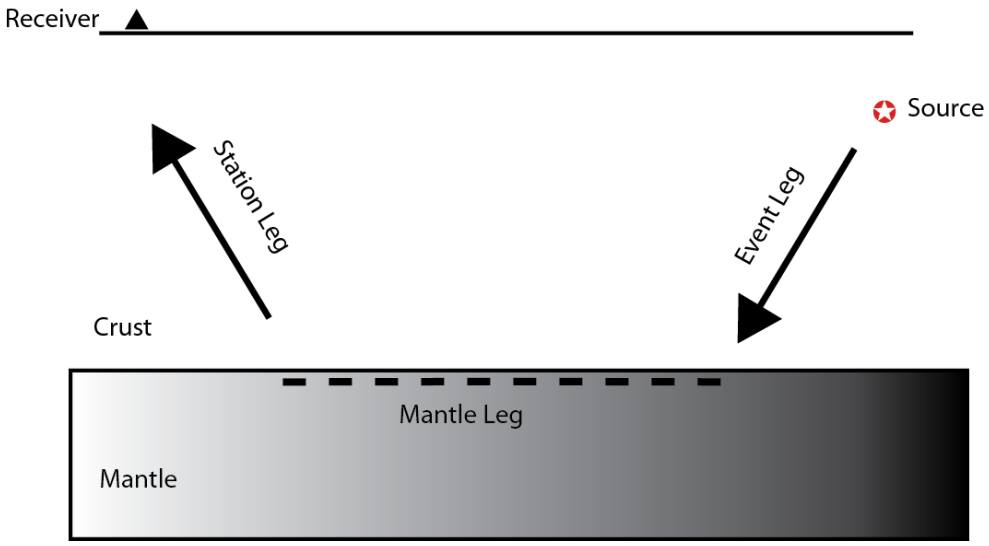

Figure 3-6. Ray path geometry utilized in the generalized inversion method.

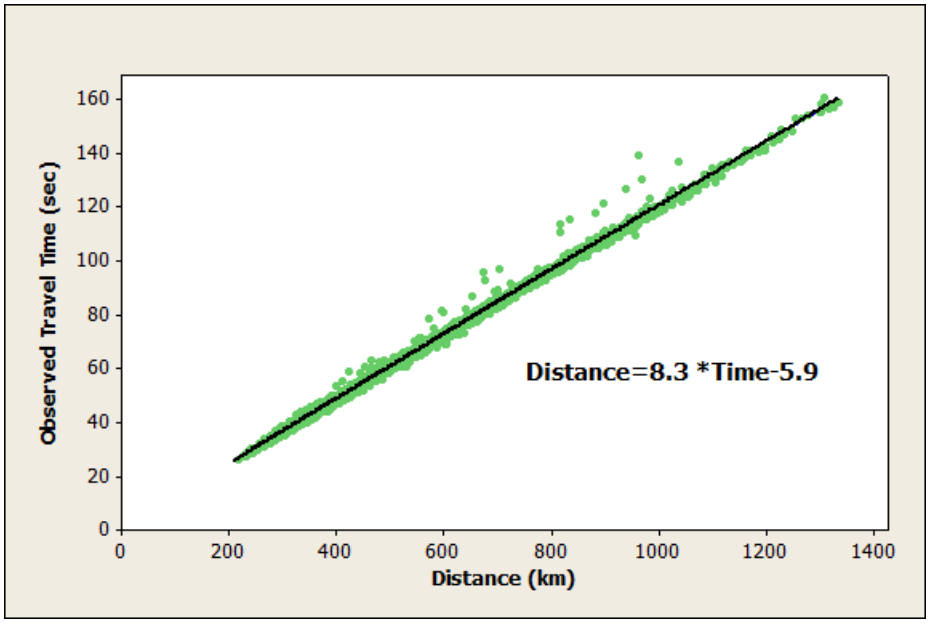

Figure 3-7. Plot of travel time vs distances in mantle. A regression line (black) yields an average Pn velocity of 8.3 km/s.

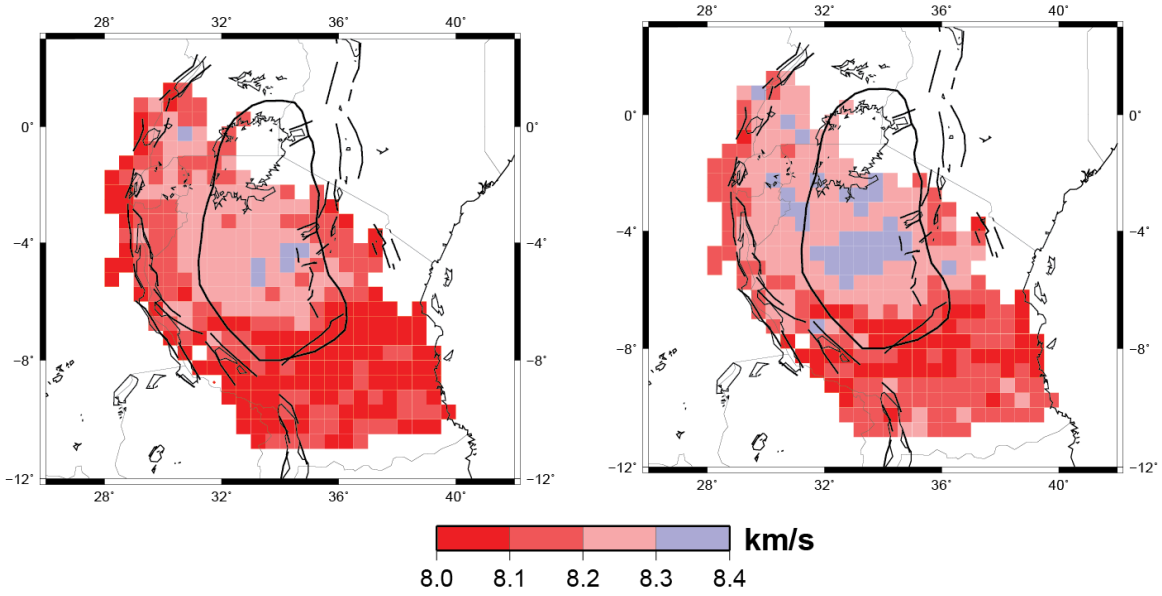

(a) (b)

.

Figure 3-8. Pn velocity results from using starting models of (a) 8.1 km/s and (b) 8.2 km/s.

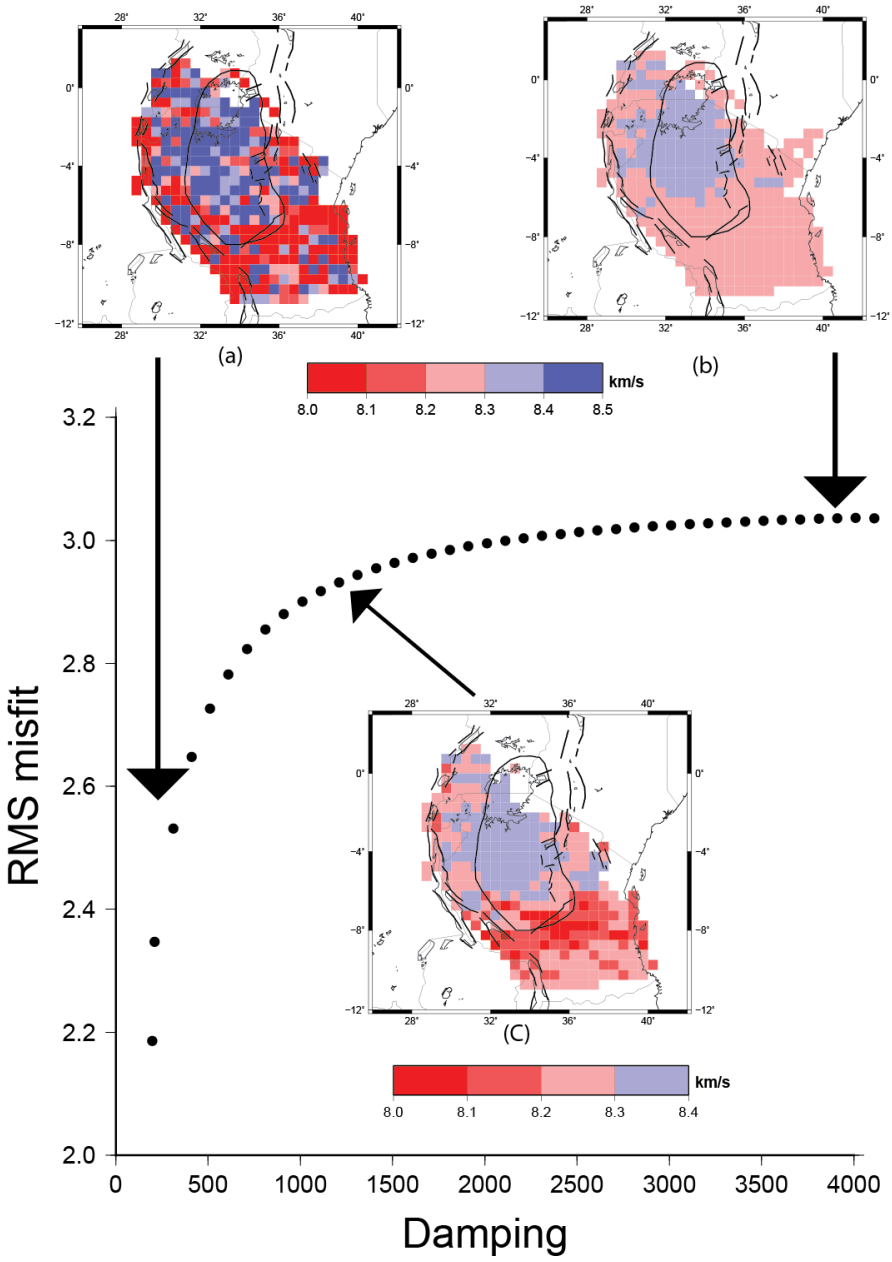

Figure 3-9. Trade-off curve showing the balance between model roughness and root-mean square (rms) error at constant hitcount. Model (a) at damping 300 shows an elevated error, while model (b) at damping 3500 shows as only smooth model. The selected model (c) from the knee of the trade-off curve has a damping value of 1200, which minimizes the error while maintaining the stability.

.

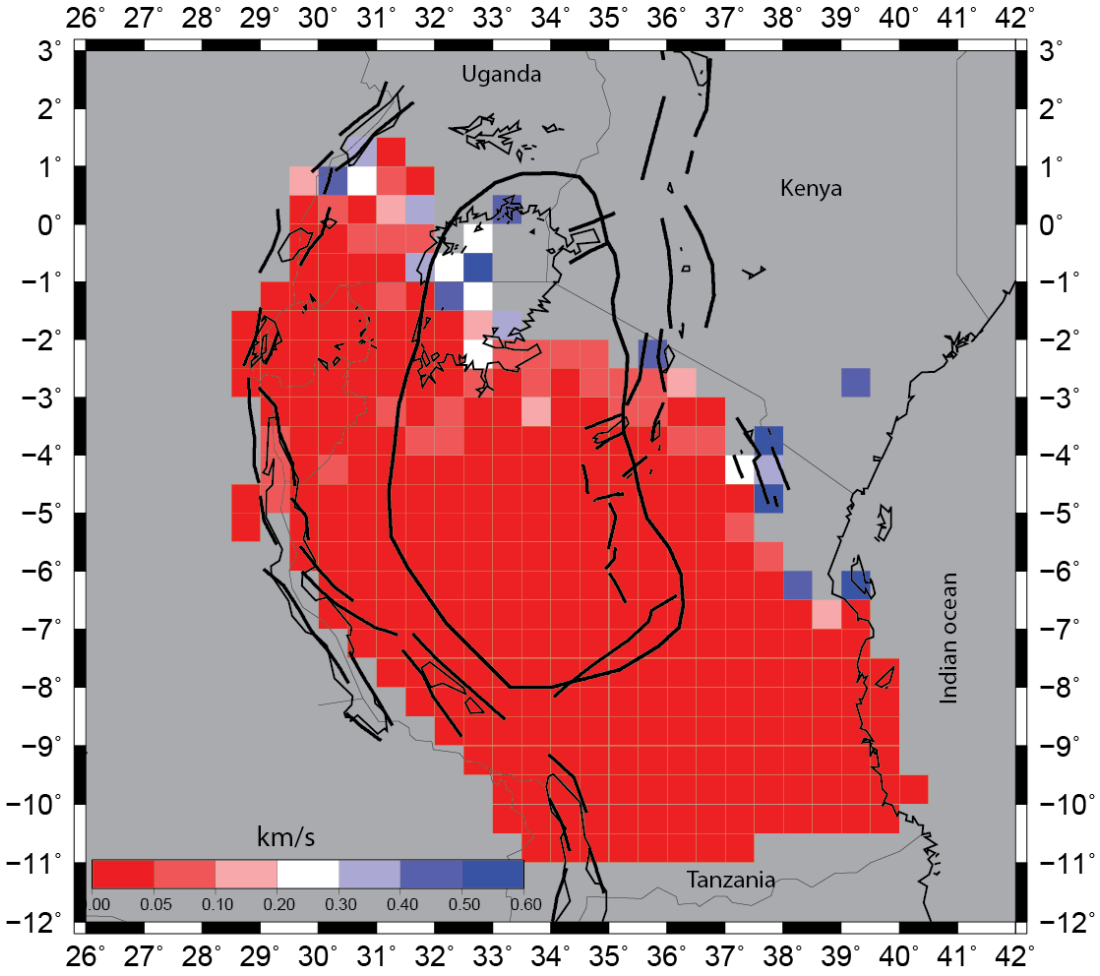

Figure 3-10. Map shows the standard deviation results from the inversion of Pn travel times.

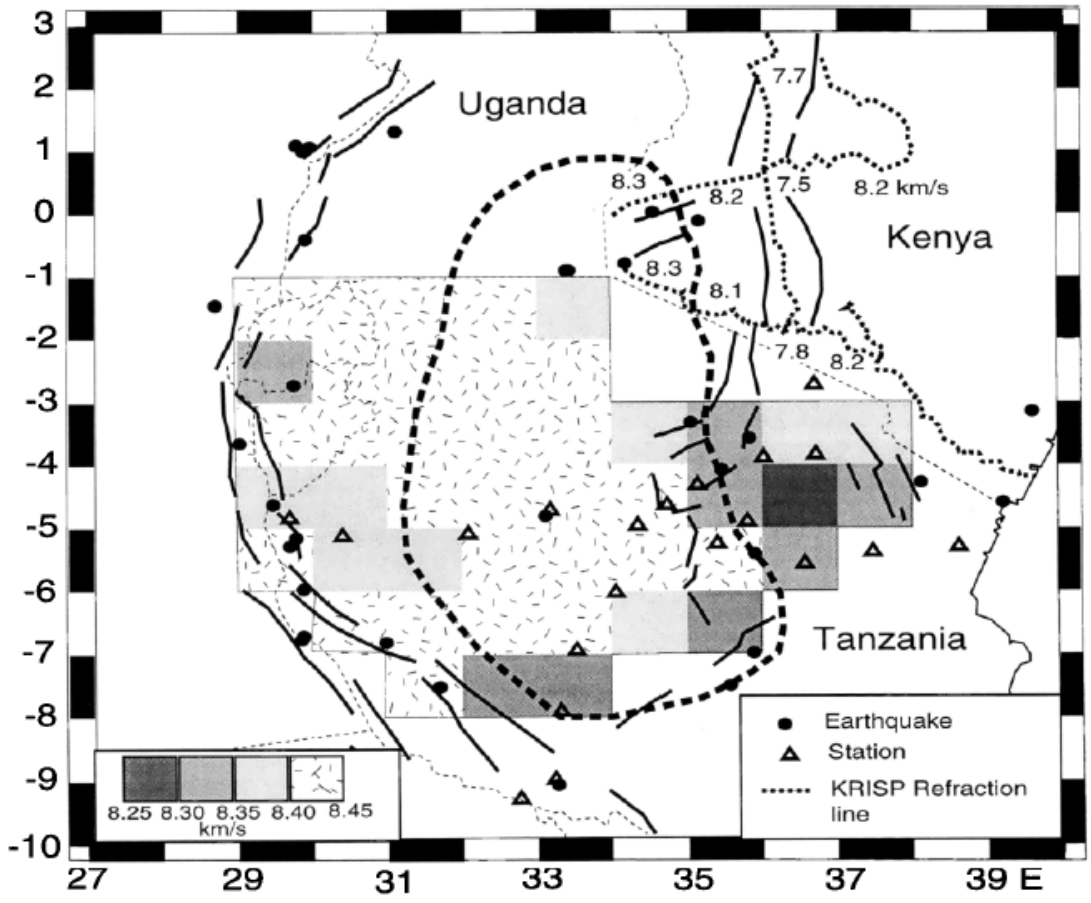

Figure 3-11. Map of Pn velocities across Tanzania obtained by Brazier et al. (2000).

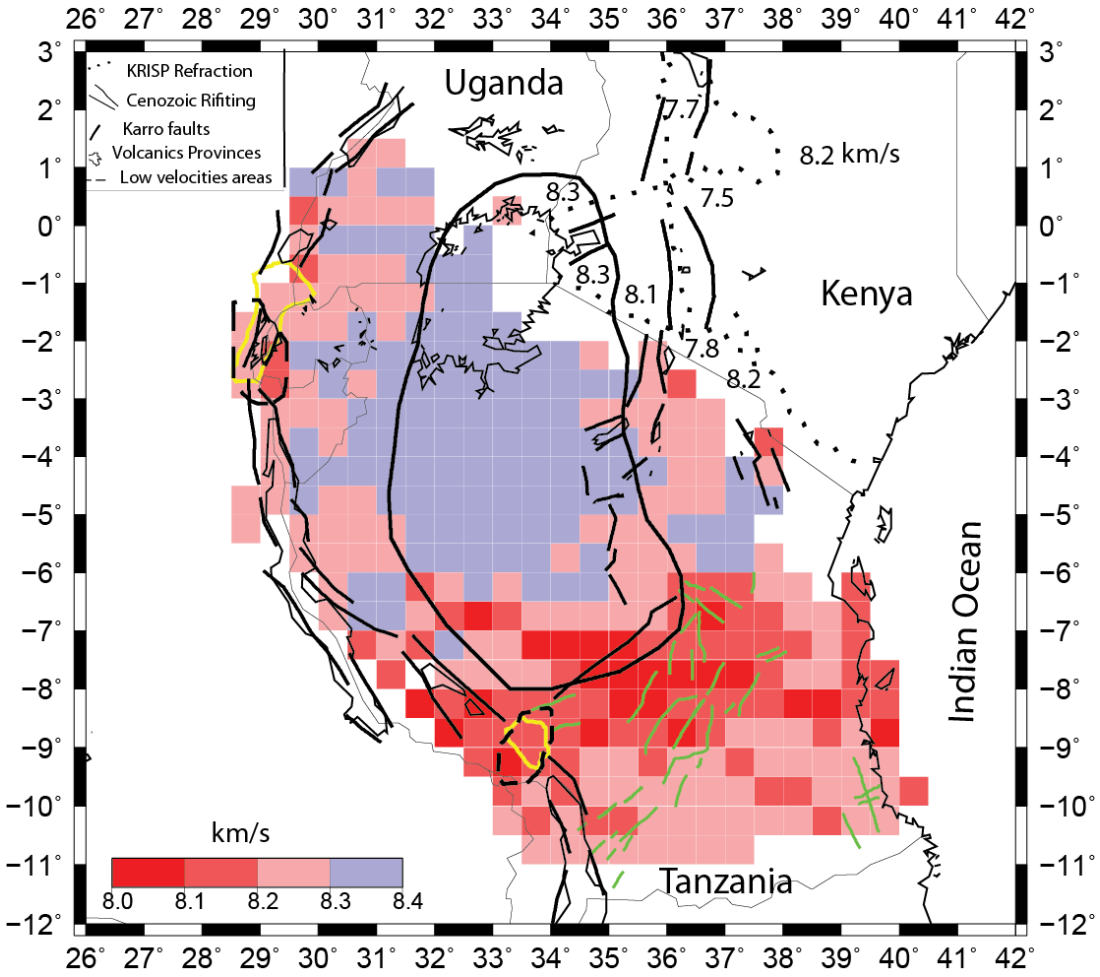

Figure 3-12. Map showing Pn velocities across Tanzania and velocities in (km/s) in Kenya obtained from KRISP refraction profiles (dotted lines). Solid lines represent the craton perimeter, rift faults. The dashed lines mark areas where the shear velocity is ≤ 4.3 km/s at 68 km depth (O'Donnell et al., 2013). Geological and volcanic provinces are the same as figure 3-1.

4 CRUSTAL STRUCTURE OF THE UBENDIAN AND USAGARAN BELTS, EAST AFRICA FROM MODELING REGIONAL SEISMOGRAMS USING A NON-DOMINATED SORTING GENETIC ALGORITHM

4.1 Introduction

There has been a long standing debate about secular variation in Precambrian crustal structure, as recently reviewed in Tugume et al. (2012, 2013), Arndt and Davaille (2013) and Abbott et al. (2013). Whether or not Proterozoic crust is thicker than Archaean crust is at the core of this debate. In this study, we contribute to this debate by examining crustal structure in two Paleoproterozoic terranes in East Africa, the Ubendian and Usagaran Belts, and comparing the thickness of the crust beneath these terranes to average Precambrian crustal structure across East Africa.

To estimate crustal thickness beneath these terranes, we model seismograms from two earthquakes that occurred in the Lake Malawi rift recorded at regional distances on several broadband seismic stations located in these terranes. Through a comparison of our results with previously published estimates of crustal thickness in East Africa, we are able to evaluate the extent to which the crust beneath these terranes has been thickened.

4.2 Background

4.2.1 Geology and tectonics

The Paleoproterozoic Ubendian and Usagaran Belts in southern Tanzania, together with the Bangweulu block in northern Zambia, formed between ~2.05 to ~ 1.8 Ga (Cahen et al., 1984) (fig. 4-1). The Ubendian Belt trends NW-SE and is flanked by the Archaean Tanzania Craton to the northeast, the Bangweulu block to the south, the Usagaran Belt to the east, and the Mesoproterozoic Kibaran Belt to the northwest (fig. 4-1). The belt is composed of several terranes bounded by shear

zones (McConnell, 1972; Daly, 1998; Daly et al., 1989). The main rock types are granulites, gneisses and amphibolites deformed during the Ubendian orogeny (Lenoir et al., 1994; Theunissen et al., 1992), which includes strike-slip deformation along the southwestern side of the Tanzania Craton (Daly et al., 1985; Daly et al., 1989; Lenoir et al., 1994). The Ubendian Belt subsequently experienced repeated orogenic cycles between 1890 and 1860 Ma (Boniface et al., 2012) and 590 and 520 Ma (Boniface and Schenk, 2012) which were associated with the opening of small ocean basins and the subduction of oceanic lithosphere in between the Bangweulu block and the Tanzania Craton.

The Usagaran Belt trends NE-SW to E-W along the southeastern margin of the Tanzania Craton (fig. 4-1). Compared to the Ubendian Belt, the Usagaran Belt resulted from collision and accretion against the Tanzanian Craton with less strike-slip deformation (Lenoir et al., 1994). Similar to the Ubendian Belt, parts of the Usagaran Belt were reworked and modified during the Pan-African orogenic events associated with the formation of the Neoproterozoic Mozambique Belt (Reddy et al., 2004). The Usagaran Belt contains thick successions of supracrustal rocks, strongly deformed gneisses and undeformed granitoids (Cahen et al., 1984; Sommer et al., 2005a). The northwestern part of the Belt is strongly deformed with high grade metamorphic rocks, whereas the southeastern part consists of undeformed, weakly foliated granitoid bodies overlain by supracrustal rocks.

The Ubendian Belt has been divided into several smaller blocks or sub-terranes, (Upangwa, Mbozi, Lupa, Ufipa, Nyika, Katuma, Ubende and Wakole; Daly et al. 1985) (fig. 4-2). These sub-terranes are bounded by shear zones comprised of ductile and brittle faults rocks (Daly, 1988). The Usagaran Belt has not been divided similarly into sub-terranes.

4.2.2 Previous studies of crustal structure

Crustal structure in the Ubendian and Usagaran belts and neighboring terrains has been investigated previously using waveform modelling of seismograms from regional events and teleseismic P-wave receiver functions. Modelling regional

seismograms has been done by Kim et al. (2009) and Langston et al. (2002). Kim et al. (2009) investigated the crustal structure of Cenozoic Rukwa Rift by modeling the seismogram from the 1994 Mw 5.9 Rukwa earthquake recorded on station PANDA (fig. 4-1). The Rukwa Rift lies within the Ubendian Belt. They obtained a velocity model with a Moho at 38 km depth and 4.5 km of low velocity rock in the upper crust, which they interpreted as rift basin sediments. A Moho depth of 42 km beneath the Rukwa Rift was previously reported by Camelbeek and Iranga (1994) from modelling the travel times of PmP waves generated by regional earthquakes and recorded on a local seismic network around the Rukwa Rift.

Langston et al. (2002) also investigated the crustal structure beneath Tanzania by modeling waveforms and phase travel times from the 1994 Mw 5.9 Rukwa earthquake recorded at the 1994-1995 Tanzania Broadband Seismic Experiment (TBSE) stations. They modeled the waveforms using a wave number integration algorithm and phase time inversion technique. Using the waveforms from stations in the Tanzania Craton and Mozambique Belt, they obtained three velocity models, one for the Craton, one for the Mozambique Belt and an integrated model for both terranes. The models are all similar and show that the crustal structure in the Tanzania Craton and Mozambique Belt is simple and laterally homogenous. The combined crustal model has a linear velocity gradient of 0.004/s through the crust, with a top layer P velocity of 5.84 km/s and a bottom layer P velocity of 7.0 km/s. The model has a fixed Poisson's ratio of 0.25 and a Moho at 40.4 km depth.

P wave receiver functions have been used to investigate the crustal structure within the study region by Last et al. (1997), Julià et al. (2005) and Tugume et al. (2012, 2013). Last et al. (1997) and Juliá et al. (2005) used data from the Tanzania Broadband Seismic Experiment (TBSE), while Tugume et al. (2012, 2013) used data from the Africa Array East African Seismic Experiment (AAEASE). Last et al. (1997), using a slant stacking method, reported Moho depths of 37 to 42 km for the Tanzania Craton, 36 to 39 km for the Mozambique Belt, and 40 to 45 km for the Ubendian Belt.

Julià et al. (2005) investigated crustal structure by jointly inverting receiver functions and surface wave dispersion measurements. They obtained Moho depths

for stations in the Mozambique Belt of 36 to 40 km, 38 to 42 km in the Tanzania Craton, and between 38 and 42 km in the Ubendian Belt. In addition, they found evidence for mafic lithologies in the bottom of the crust ~5 to 8 km at most stations.

Tugume et al. (2012, 2013) used two different methods, H-k stacking and the joint inversion of receiver functions with surface wave dispersion measurements, to characterize the crustal structure in East Africa. Tugume et al. (2012) found a crustal thickness of 42 to 48 km for stations in the Ubendian Belt and between 37 and 39 km for stations in the Usagaran Belt, suggesting that the Ubendian Belt has thicker crust than the Usagaran Belt, as well as the Tanzania Craton and Mozambique Belt.

4.3 Data and method

4.3.1 Data

For modelling crustal structure, we used regional seismograms from the earthquakes that occurred on the 6th of December 2009 near Karonga, Malawi (Mw 5.9 and 6.0, respectively), recorded on the Africa Array East African Seismic Experiment (AAEASE) stations (fig. 4-1). The network was operated from December 2008 to June 2010. All the stations were equipped with broadband seismometers (Guralp CMG-3T, Guralp EPS, or STS-2), 24 bit data loggers and Global Position System (GPS) clocks. Data were recorded continuously at 40 samples per second.

We modelled the whole waveform, which at the frequencies of interest is comprised mainly of Rayleigh and Pnl waves (fig. 3). The Pnl phase is a long-period waveform recorded at regional distances primarily composed of two portions. The first portion is the upper mantle phase (Pn), which is comprised of P wave interactions with the uppermost mantle, for instance the headwave along the Moho and turning waves within the lid. Following the Pn phase is the PL phase, a long-period wavetrain (fig.3) that propagates as partially trapped P-SV reverberations in the crust (Oliver and Majoe, 1960; Wallace and Helmberger, 1982).

Raw velocity seismograms were processed for modeling. First, the instrument response was removed from the recorded seismograms by deconvolution and then integrated to produce a displacement seismogram. The seismograms were rotated from vertical, radial and transverse components. A Butterworth filter was the applied with a pass band between 10 s and 50 s. The cutoff frequencies were chosen to remove long period signals and high frequency features produced by lateral variations in Earth structure.

The focal parameters for the two events used were taken from the Global CMT Catalog. We have utilized the strike, dip and rake parameters from the catalog to calculate the moment tensor using a unity scalar moment M (Aki and Richards, 1980).

4.3.2 Method

To model the crustal structure, we used the Non-Dominated Sorting Genetic Algorithm (NSGA-II, Deb et al. 2002) together with a velocity model parameterization that consists of 6 crustal layers and a half space mantle with variable P wave velocity. We tested the effect of different layer velocities, thickness and Poisson's ratio. We found that the shallow waveforms were affected by the lower crust and are insensitive to the uppermost mantle velocity. As we used a fixed Vp/Vs ratio, changing P-wave velocities will also change the S-wave velocities. Changing layer thickness will trade off with velocities in the fitting process. In the model, the bottom two crustal layers have variable thicknesses (Table 4-1), and the Vp/Vs ratio in each layer was held constant at 1.75.

Internal to the genetic algorithm, synthetic seismograms are computed using the reflection-matrix method (Kennett, 1983). In this method, focal mechanisms and source characteristics for the earthquake and a velocity model are required to generate a synthetic seismogram. For the computations, frequency and slowness bands and tapers are fixed, as described in Table 4-2.

4.3.2.1 Non-Dominated Sorting Genetic Algorithm (NSGA-II)

The Non-Dominated Sorting Genetic Algorithm (NSGA-II, Deb et al. 2002) is a specific version of a general genetic algorithm. In general, genetic algorithms are iterative stochastic searching mechanisms that evaluate progressively improved mathematical models using a learning mechanism to improve the efficiency and accuracy of the search mechanism (Deb et al. 2002). The learning mechanism involves at each iteration an evaluation of the quality of the current proposed velocity models and the previous velocity models. The best models are kept and the lesser quality models are discarded. In NSGA–II the solution to a multi-objective problem is a set of solutions which are better than the rest of the solutions in all dimensions of the search space. A solution is called dominant if each objective value is smaller than its counterpart. The best solutions are known as non-dominated solutions or Pareto-optimal solutions (fig. 4-4) (Deb et al. 2002). As all non-dominated solutions are good ones, any single solution from the non-dominated solutions is satisfactory and acceptable (Deb et al. 2002). The process of sorting solutions is based on their degree of non-dominance in population, referred to as ranking or fitness function. Each solution is assigned a fitness or rank equal to its non-dominated level (1 is the best level, 2 is the next best level, and so on). Rank 1 solutions are non-dominated if Rank 1 solutions are removed from the dataset, then Rank 2 solutions are the non-dominated set of the remainder. The ranking continues until all data points are ranked (fig. 4-5).

The first step in the NSGA-II procedure is to generate an initial population, in our case a group of velocity models P°. Each initial model $X_i^{(t)}, i = 1, \dots, \mu$ is then utilized to produce synthetic waveforms. These are compared to the observed seismograms using a fitness or objective function as shown in equation 4-1 below

$$f_k\left(X_i^{(t)}\right) = \sum \left| g\left(X_i^{(t)}\right) - g(Y^{obs}) \right|, \quad k = 1, \dots . n, i = 1, \dots, n, \dots\dots \text{(4-1)}$$

Where $f_k\left(X_i^{(t)}\right)$ is fitness objective, $g\left(X_i^{(t)}\right)$ is the synthetic waveform, $g(Y^{obs})$ is the observed waveform and n is the total number of objectives, which for this study is 4. The initial population is a set of random velocity models. Each

iteration (or generation) within this genetic algorithm begins with a population of velocity models or generation. Each velocity model in each generation is evaluated to assess how closely it corresponds to the observed seismogram through the fitness function. Then fitness values are compared and sorted using the Pareto optimal solution approach, where the best velocity models are non-dominated.

These models are then utilized to obtain the next iteration of velocity models through the process of recombination and mutation. The recombination process involves the random selection of a proportion (P_c) of pairs of models to produce the next generation, through weighted averages biased toward the better solutions. For instance at iteration t, consider two velocity models; $X_i^{(t)} and\ X_{i'}^{(t)}$. If x^{ij} is a velocity at the j^{th} layer on the i^{th} model, then through recombination, two new velocity models are calculated from the models and the velocity at each layer is estimated by equations 4-2 and 4-3,

$$x_{ij}^{(t+1)} = \frac{\left(x_{ij}^{(t)} + x_{i'j}^{(t)}\right)}{2} + \alpha^{\beta} \quad \text{..... (4-2)}$$

$$x_{i'j}^{(t+1)} = \frac{\left(x_{ij}^{(t)} + x_{i'j}^{(t)}\right)}{2} - \alpha^{\beta} \quad \text{..... (4-3)}$$

where α^{β} is a random weighted distance from the closest range end point. The obtained result is a model in the range of the two models and is considered a weighted average of the prior models.

A mutation is a process of perturbing the new generation models to avoid becoming trapped in local minima, and at the same time helps to find new regions in the model space. A proportion of models (P_m) are chosen to be mutated. Each layer in the selected model has a perturbed velocity. At this point all models from adjacent generations are evaluated and sorted, and the best used to initiate the next generation.

Part of the evaluation performed during the iteration is to check the models against geological constraints. We have applied constraints to improve the modelling in terms of reducing the trade-off between number of model parameters, and lessening the probability of converging to a local minima and raising the convergence rate by considering only part of the model space. To account for and

decrease these effects, we allowed variation in model parameters within prescribed limits. Although these trade-offs can give rise to several local minima, the genetic algorithm is capable of identifying the global minimum. We constrained errors in modelled Pn arrival times to less than one second, and the average crustal velocity to values between between 6.4 and 6.8 km/s. We also only permitted models where velocity increased with depth. The algorithm is considered to have converged when all models passed to the next generation are rank 1 and meet the constraints for multiple generations.

We apply the NSGA-II to solve four objectives functions, matching the whole radial and vertical component seismograms and the Pnl wavetrain in both radial and vertical components. The four objectives functions are used because the whole waveform is dominated by the large amplitude Rayleigh wave, but important information on crustal structure is also contained in the smaller amplitude Pnl wavetrain (fig. 4-3). We ran the NSGA-II for 100 generations using a population size of 30. In addition, the probability of recombination (P_c) was set to be 0.9, and the probabilities of mutation (P_m) set to 0.05. These numbers are chosen to allow convergence while preventing being caught in local minima. A range of both values were tested. The values we attained are similar to other seismological studies (Boomer and Brazier, 2009).

4.3.2.2 Uncertainties

The solution set of velocity models follows a Boltzman distribution (Deb et al., 2002). We use an unbiased estimator for the Boltzman distribution to calculate the 95% confidence intervals for our selected model. The confidence interval for each layer is computed and plotted together with the final model (figs 4-6 to 4-13).

4.4 Results

We have selected the best fitting model for each station from the Pareto front plot and visually compared the synthetic seismogram for this model with the data. An example of the Pareto front for station KGMA is shown in Figure 4-5. In Figures 4-6 to 4-13, we show the synthetic seismograms from this study together with that obtained from the Langston et al. (2002) combined crustal model (i.e. Tanzania Craton and Mozambique Belt) and the Moho depths from Tugume et al. (2012, 2013). In this section, we discuss what differences appear if we generate the waveform using the combined crustal model from Langston et al. (2002), while in case of Tugume et al. (2012, 2013) we only compare the difference in the crustal thickness.

4.4.1 Ubendian Belt

4.4.1.1 Station KGMA

Station KGMA is located 740 km from the earthquake epicenter at the northwestern corner of the Ubendian Belt (fig. 4-2). We obtained a good match in the arrival times and wave shapes between the synthetic waveform and the data for all 4 objectives (radial and vertical components for both full waveforms and Pnl wave trains (See Figure 4-6). The crustal velocity model shows Moho at 39 km depth, in agreement with results reported by Tugume et al. (2012, 2013) and Langston et al. (2002). Seismograms from the Langston et al. (2002) model also show a good match to data, but the Rayleigh wave arrives slightly late. Our model has faster mid-crustal layers which produce a better match to the timing of the Rayleigh wave.

4.4.1.2 Station PNDA

Station PNDA is located 548 km from the epicenter (fig. 4-2). There is a reasonable match between the full waveform synthetic and data and a good fit between the synthetic Pnl wave trains and the data, as can be seen by alignment of the phases in Figure 4-7. The crustal velocity model has Moho at 39 km depth, in agreement with results from Tugume et al. (2012, 2013). The Langston et al. (2002) model gives a delayed Rayleigh wave compared to the data, which results from an overall slower crustal model compared to our model.

4.4.1.3 Station NAMA

Station NAMA is located 422 km from the epicenter (fig. 4-2). The match between the synthetic full waveform and data is satisfactory but not as good compared to the two previous stations, and the same can be said about the Pnl wavetrain match (fig. 4-8). The velocity model has Moho at 42 km depth, in agreement with Langston et al. (2002), but about 5 km thinner than Tugume et al. (2012, 2013). The Rayleigh wave in the synthetic for the Langston et al. (2002) model arrives significantly late, which results from the much slower crustal velocities in the Langston et al. (2002) model compared to our model.

4.4.1.4 Station SUMB

Station SUMB is located 341 km from the epicenter (fig. 4-2). The observed full waveform is complicated and a poor match is obtained for the full waveform (fig. 4-9). However, a good match is observed for the synthetic Pnl wave train compared to the data. Similar waveforms fit are found for the Langston et al. (2002) model. Our velocity model has Moho at 41 km depth, in agreement with Langston et

al. (2002), but 5 km thinner than Tugume et al. (2012, 2013). Our model has much slower mid-crustal layers than the Langston et al. (2002) model.

4.4.1.5 Station LALE

Station LALE is located 260 km from the epicenter (fig. 4-2). The observed full waveform is complicated and a poor match is obtained for the full waveform. However, a good match is observed for the Pnl wavetrain, and similar waveform fits are found for the Langston et al. (2002) model (fig. 4-10). Our velocity model has Moho depth at 45 km depth, in agreement with Tugume et al. (2012, 2013), but 5 km thicker than in the Langston et al. (2002) model. Our crustal model has a somewhat slower lower crust than the Langston et al. (2002) model.

4.4.2 Usagaran Belt

4.4.2.1 Station MGOR

Station MGOR is located 542 km from the epicenter in the Mozambique Belts (fig. 4-2), but roughly 70% of the travel path lies within the Usagaran Belt. The radial full wave component is not well matched but a reasonable match is obtained for the vertical component full waveform, and a good fit is obtained for the Pnl wave train (fig. 4-11). Similar waveform matches were observed for the Langston et al. (2002) model. Our velocity model has Moho depth at 41 km, in agreement with Langston et al. (2002) and 6 km deeper than Tugume et al. (2012, 2013). Our velocity model has similar velocities to the Langston et al. (2002) model.

4.4.2.2 Station MIKU

Station MIKU is located 444 km from the epicenter in the Mozambique Belts (fig. 4-2), but roughly 75% of the travel path lies within the Usagaran Belt. A reasonable match is obtained for the full waveforms and for the radial component of the Pnl wavetrain (fig. 4-12). On the vertical component, the Pl phase in the synthetic arrived earlier compared to the observed data. The synthetic waveforms from the Langston et al. (2002) model do not provide a better match to the data. Our velocity model has a Moho at 42 km depth, slightly thicker than the Langston et al. (2002) model and 7 km thicker than Tugume et al. (2012, 2013). Our velocity model has similar velocities to the Langston et al. (2002) model.

4.4.2.3 Station MAFI

Station MAFI is located 243 from the epicenter within the Usagaran Belt (fig. 4-13). A good match between the synthetic full waveform and data for both crustal models is observed, but not for the Pnl wavetrain (fig. 4-13). For both models, the Pl phase arrives early compared to the data. Our velocity model has a Moho at 35 km, which is 3 km thinner than with crustal thickness reported by Tugume et al. (2012, 2013) and 5 km thinner than the Langston et al. (2002) model. Our model shows faster velocities in the mid and lower crust compared to the Langston et al. (2002) model.

4.5 Discussion

In this section we use our results to further examine the thickness of the Ubendian and Usagaran Belts relative to the average crustal thickness for East Africa as represented by the combined Langston et al. (2002) crustal model. As reviewed in section 4.1.1.2, crustal thickness estimates from Tugume et al. (2012, 2013) for stations NAMA, SUMB and LALE in the Ubendian Belt suggest overall

thicker crust compared to elsewhere in East Africa. Specifically, we discuss whether or not the crust beneath the entire Ubendian and Usagaran Belts is thicker than average for East Africa, or if the areas of thickened crust are localized beneath only part of the mobile belts.

For comparison, estimates of crustal thickness from our results and Tugume et al. (2012, 2013) are shown in Table 4-3. Recall that in the Langston et al. (2002) combined model the Moho is at a depth of 40 km. For the Usagaran Belt, our results show little evidence for crustal thickening. We obtained a Moho depth of 35 km for station MAFI, which is 5 km thinner than the crust in the Langston et al. (2002) model. The thin crust beneath station MAFI could be related to the younger magmatic event at 1820 Ma in the Usagaran Belt (Sommer et al., 2005b). Crustal thickness at MGOR and MIKU is 41 and 42 km respectively, similar to the Langston et al. (2002) crustal thickness. These estimates of crustal thickness are greater than Tugume et al. (2012, 2013) because the MGOR and MIKU stations are located in the Mozambique Belt. The receiver functions estimate of crustal thickness give a local estimate (Tugume et al. 2013) while our estimates average structure over the entire ray path, much of which lies (70-75%) in the Usagaran Belt.

For the Ubendian Belt, crustal stations KGMA and PNDA indicate that the crustal thickness is not anomalous with Moho depths at 39 km. These Moho depths are similar to the Langston et al. (2002) model and the results for Tugume et al. (2012, 2013). However, the crust at stations NAMA, LALE and SUMB are significantly thicker in agreement with the result from Tugume et al. (2012, 2013). These three stations are all located in the Ufipa sub-terrane (fig. 4-2), while stations PNDA and KGMA located in the Wakole sub-terrane (fig. 4-2). This result suggests that the entire Ubendian Belt does not have thickened crust, as inferred by Tugume et al. (2012, 2013), but rather that just the Ufipa sub-terrane has thickened crust. The average thickness for the Ufipa sub-terrane from our result is 43 km, while from Tugume et al. (2012, 2013) is 45 km, in close agreement and a few km thicker than the crust in the Langston et al. (2002) model.

The geological history of the area during the amalgamation of Gondwana provides some insights as to why the Ufipa sub-terrane crust has been thickened.

Boniface and Schenk (2012) present geochemical evidence that a small ocean basin existed between the Tanzania Craton and Bangweulu block just prior to the assembly of Gondwana during the Pan-African tectonothermal event. We suggest that the Ufipa crust was thickened during the final stage of the closing of the ocean basin. The Ufipa sub-terrane accommodated most of the crustal shortening during this collisional event, resulting in thickened crust compared to the other less deformed sub-terranes within the Ubendian Belt.

Our results do not indicate similar crustal thickening beneath the Usagaran Belt during the Pan-African event, even though there was significant tectonism outboard of the Usagaran Belt during the formation of the Mozambique Belt.

Lastly, our results do not indicate any systematic differences in crustal thicknesses between the Archean and Proterozoic. The Usagaran Belt and much of the Ubendian Belt have similar crustal thickness to the Tanzania Craton.

4.6 Conclusion and summary

We have investigated the crustal structure of Ubendian and Usagaran Belts by modelling regional seismograms from the Karonga, Malawi earthquakes using the Non-Dominated Genetic Algorithm method. This method allows us to search the parameters efficiently to model regional broadband seismograms for crustal structure. This technique is based on the NSGA-II procedure that generates random models consistent with an allowable set of parameter values. Using accurate estimates of the focal mechanism and location, these models are used to compute synthetic seismograms that are then compared with the recorded data, and the best fitting model is estimated. Using this technique, one-dimensional average crustal structures for each source-receiver pair along the Usagaran and Ubendian Belts were obtained, while the methods used by Tugume et al. (2012, 2013) produced one-dimensional models beneath each station.

In the Usagaran belt we obtained average Moho depths of 35 km for station MAFI and of 41 and 42 km for stations MOGR and MIKU, respectively. These results, in comparison to average Precambrian crustal thickness in East Africa, provide no evidence for crustal thickening. In the Ubendian Belt, we obtained an average Moho depth of 43 km beneath the Ufipa sub-terrane compared to 39 km for Wakole sub-terrane. These results indicate localized thickening in the Ufipa sub-terrane but not beneath the entire Ubendian Belt. There is no clear evidence in our result to indicate that Paleoproterozoic crust in East Africa is substantially thicker than Archean crust, while secular variations that arise from crustal genesis processes might be possible, as suggested in previous studies (Tugume et al., 2013).

References

Abbott, H., Mooney, W.D. and VanTongeren, A. (2013), The character of the Moho and lower crust within Archean cratons and the tectonic implications, Tectonophysics, 609, 690-705.

Arndt, N. and Davaille, A. (2013), Episodic Earth evolution, Tectonophysics, 609, 661-674.

Aki, K. and Richards, P.G. (1980), Quantitative Seismology, Freeman and Co., New York, 37, 121.

Boniface, N. and Schenk, V. (2012), Neoproterozoic eclogites in the Paleoproterozoic Ubendian Belt of Tanzania: evidence for a Pan-African suture between the Bangweulu Block and the Tanzania Craton, Precambrian Research, 208–211, 72–89.

Boniface, N., Schenk, V. and Appel, P. (2012), Paleoproterozoic eclogites of MORB-type chemistry and three Proterozoic orogenic cycles in the Ubendian Belt (Tanzania): evidence from monazite and zircon geochronology, and geochemistry, Precambrian Research, 192–195, 16–33.

Boomer, K and Brazier R. (2009), Stochastic Modelling of the Velocity Structure: Beyond Joint Inversion Methods. The 11th Biennial SAGA Conference and Exhibition (vol. 1), South African Geophysical Association.

Cahen, L., Snelling, N., Delhal, J. and Vail, J. (1984), The geochronology and evolution of Africa, Oxford, United Kingdom, Clarendon Press.

Camelbeeck, T. and Iranga, M.D. (1996), Deep crustal earthquakes and active faults along the Rukwa trough, eastern Africa, Geophysical Journal International, 124, 612-630.

Daly, M.C. (1988), Crustal shear zones in central Africa: a kinematic approach to Proterozoic tectonics, Episodes 11, 5-11.

Daly, M.C., Klerkx, J. and Nanyaro, J.T. (1985), Proterozoic exotic terranes and strike-slip accretion in the Ubendian belt of south-west Tanzania. Terra Cognita 5, 257.

Daly, M.C., Chorowicz, J. and Fairhead, J.D. (1989), Rift basin evolution in Africa: the influence of reactivated steep basement shear zones. In: Inversion tectonics (Edited by Cooper, M.A. and Williams,G.D.) Geological Society of London Special Publication 44, 309-334.

Deb K., Agrawl, A., Pratap, A. and Meyarivan, T. (2002). A fast elitist non-dominated sorting genetic algorithm for multi-objective optimization: NSGA-II, IEEE Transactions on Evolutionary Computation, 6, 182-197.

Julià, J., Ammon, C.J. and Nyblade, A.A. (2005), Evidence for mafic lower crust in Tanzania, East Africa, from joint inversion of receiver functions and Rayleigh wave dispersion velocities, Geophysical Journal International, 162, 555-569.

Kennett, B.L.N. (1983), Seismic Wave Propagation in Stratified Media, Cambridge University Press, Cambridge.

Kim, S., Nyblade, A.A. and Baag, C-E. (2009), Crustal Velocity Structure of the Rukwa Rift in the Western Branch of the East African Rift System, South African Journal of Geology, 112, 251-260.

Langston, C. A., Nyblade, A. A. and Owens, T. J. (2002), Regional wave propagation in Tanzania, East Africa, Journal of Geophysical Research, 107 (B1), doi:10.1029/ 2001JB000167.

Last, R.J., Nyblade, A.A., Langston, C.A. and Owens, T.J. (1997), Crustal structure of the East African Plateau from receiver functions and Rayleigh wave phase velocities, Journal of Geophysical Research, 102, 24469–24483.

Lenoir, J., Liégeois, J-P., Theunissen, K. and Klerkx, J. (1994), Origin and regional significance of late Precambrian and early Palaeozoic granitoids in the Pan-African belt of Somalia, Geologische Rundschau, 83, 624–641.

McConnell, R.B. (1972), Geological development of the rift system of eastern Africa, Bulletin of the Geological Society of America, 83, 2549-2572.

Oliver, J., and Major, M. (1960), Leaking modes and the PL phase, Bulletin of the Geological Society of America, 50, 165– 180.

Reddy, S.M., Collins, A.S., Buchan, C. and Mruma, A.H. (2004), Heterogeneous excess argon and Neoproterozoic heating in the Usagaran Orogen, Tanzania, revealed by single grain 40Ar/39Ar thermochronology, Journal of African Earth Sciences, 39, 165–176.

Sommer, H., Kröner, A., Muhongo, S. and Hauzenberger, C. (2005a), SHRIMP zircon ages for post-Usagaran granitoid and rhyolitic rocks from the Palaeoproterozoic terrain of southwestern Tanzania, South African Journal of Geology, 108, 247-256.

Sommer, H., Kröner, A., Hauzenberger, C. and Muhongo, S. (2005b), Reworking of Archaean and Palaeoproterozoic crust in the Mozambique belt of central Tanzania as

documented by SHRIMP zircon geochronology, Journal of African Earth Sciences, 43, 447-463.

Theunissen., K., Lenoir., J. I., Liegeois., J. P. Delvaux, D. and Mnrma., A. (1992), Major Pan-African imprint in the Ubendian belt of SW Tanzania: U-Pb on zircon geochronology and structural context. Comptes rendus Academie Sciences Paris 314 (II), 1355-1362.

Tugume, F., Nyblade, A., Julia, J. (2012), Moho depths and Poisson's ratios of Precambrian in East Africa: evidence for similarities in Archean and Proterozoic Crustal structure, Earth and Planetary Science Letters, 355–356, 73–81.

Tugume, F., Nyblade, A., Julià, J., Meijde M. (2013), Precambrian crustal structure Arabia: Evidence lacking for secular variation, Tectonophysics, 609, 250-266.

Wallace, T. C., and D. V. Helmberger (1982), Derermination of seismic parameters of moderate size earthquake from regional waveforms, Physics of the Earth and Planetary Interiors, 30, 185-196

Table 4-1: Random starting model used in the NSGA-II

Thickness (km)	Vp (km/s)
5.0	5.2 - 7.2
5.0	5.2 - 7.2
6.0	5.2 - 7.2
6.0	5.2 - 7.2
4.0-10.0	5.2 - 7.2
4.0-10.0	5.2 - 7.2
Half space	7.8-8.6

Table 4-2: Parameters used to calculate synthetic seismograms for station KGMA

Parameter	Value
Slowness for full waveform	0.01 0.2 0.3 0.4 (range of low slowness to higher slowness)
P factor	1
Frequency	0.00 1.0 1.0 (low freq., upper freq. and Nyquist freq.)
Number of points	2048
Distance	740.4 km
Azimuth	320.4 degree
Number of sources	1
Source depth	12.0
Receiver depth	0.0
Components of moment tensor	0.1897 0.3852 0.1271 0.7800 0.2075 -0.9697

Table 4-3: Results from this study (NSGA-II) and Tugume et al. (2012, 2013).

Vs, Vp and σ are S wave velocity, P wave velocity and Poisson's ratio, respectively. (JI) signifies the Moho depth determined by joint inversion of receiver functions and surface wave dispersion measurements, while (H-K) stands for using stacking, both by Tugume et al. (2012, 2013). NSGA signifies the Moho depth determined in this study.

Terrane	Station	Averg. Vs (Tugume et al. 2012, 2013) (km/s)	σ	Averg. Vp (km/s)	Moho (JI) (km)	Moho (H-K) (km)	Moho (NSGA) (km)	Averg. Vp (NSGA) (km/s)
	KGMA	3.7	0.28	6.7	41	39.6	39	6.6
	PNDA	3.6	0.28	6.6	38	40.9	39	6.6
Ubendian	NAMA	3.8	0.24	6.5	46	47 .5	42	6.8
Belt	SUMB	3.6	0.28	6.5	46	44.6	41	6.3
	LALE	3.7	0.24	6.4	43	46.7	45	6.4
Average		**3.7**	**0.26**	**6.5**	**43**	**42**	**41**	**6.5**
Mozambique	MGOR	3.5	0.26	6.2	33	36.1		
Belt	MIKU	3.6	0.26	6.3	33	37.1		
	MGOR	-	-	-	-	-	41	6.4
	MIKU	-	-	-	-	-	42	6.4
Usagaran	MAFI	3.6	0.25	6.3	36	38.8	35	6.5
Belt	IRIN	3.7	0.25	6.4	36	39.4	-	-
	MAKA	3.6	0.28	6.5	41	39.1	-	-
Average		**3.6**	**0.26**	**6.3**	**37**	**38**	**39**	**6.5**

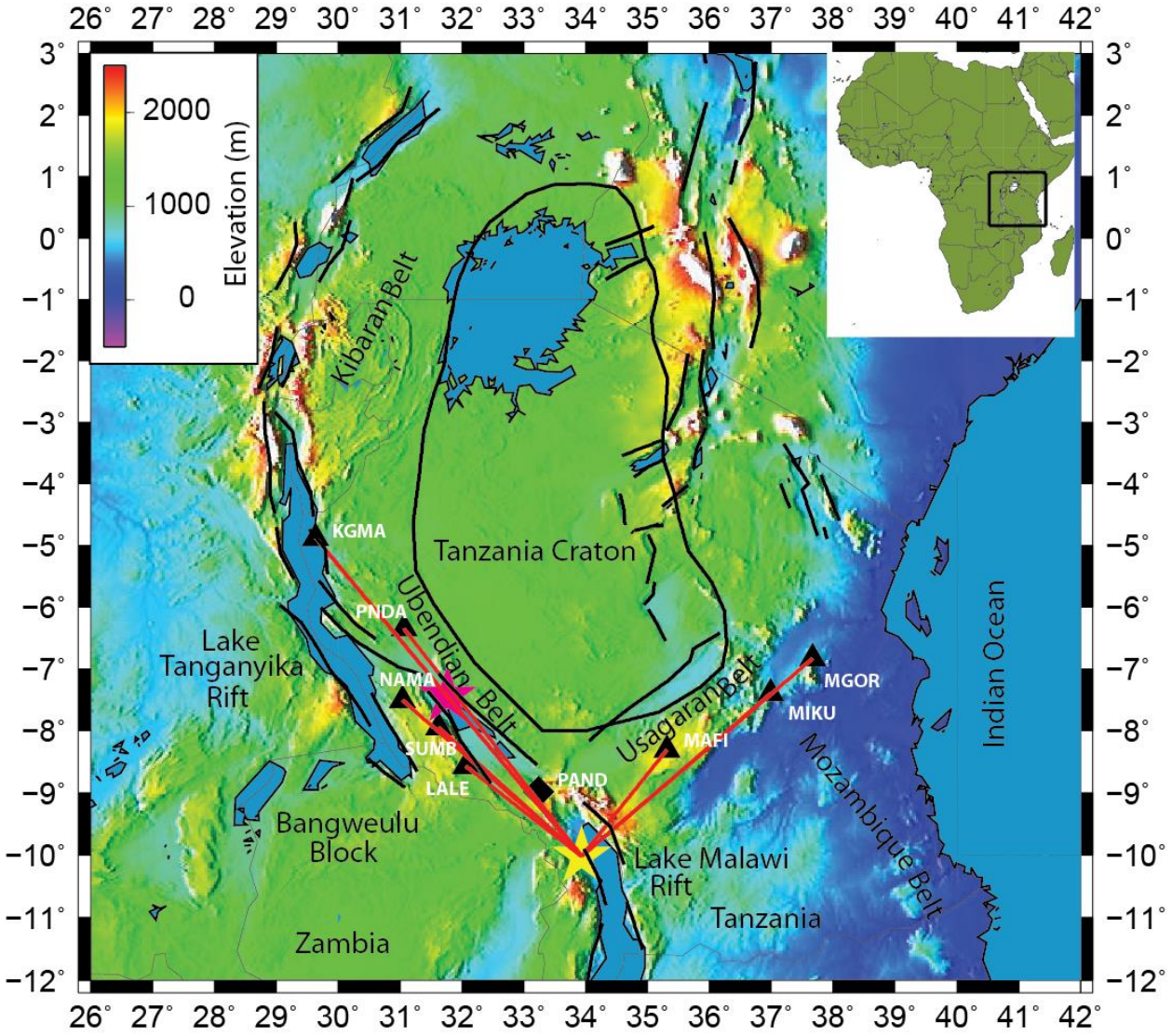

Figure 4-1. Elevation map of East Africa illustrating the locations of geological provinces, earthquake epicenters and seismic stations. The yellow and magenta stars are the epicenters of the Karonga and Rukwa earthquakes, respectively. Black triangles represent AAEASE stations and the black diamond represents a station from the TBSE deployment. Solid red lines show the ray path between stations and the earthquake epicenter.

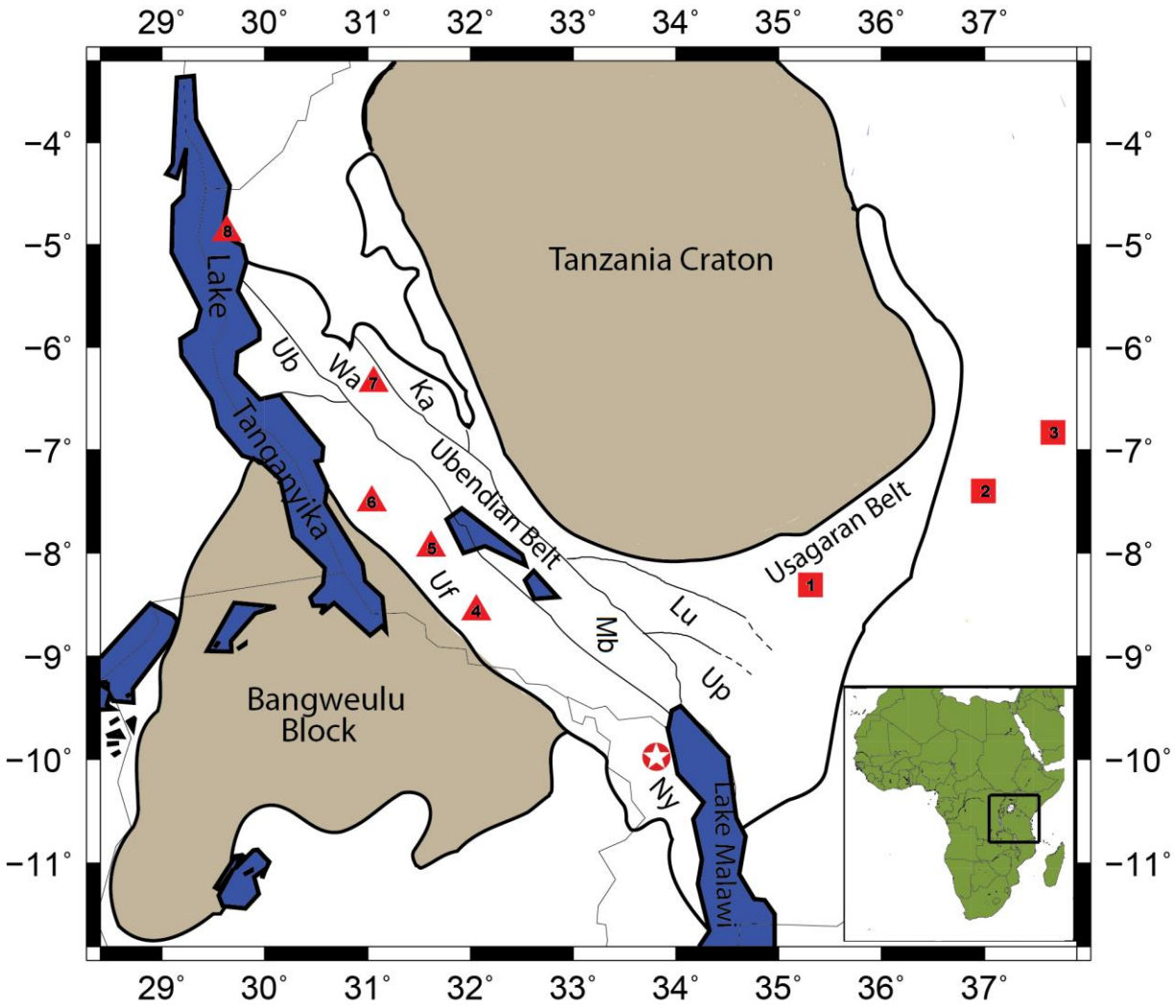

Figure 4-2. Geological map of showing location of the Ubendian and Usagaran Belts the Tanzania Craton and the Bangweulu Block. Sub-terranes shown in the Ubendian Belt are Ubende (Ub), Wakole (Wa), Katuma (Ka), Ufipa (Uf) , Mbozi (Mb), Lupa (Lu), Upangwa (Up) and Nyika (Ny). The epicenter of the Karonga earthquake is shown with the white star and stations are shown in red triangles and squares: 1-MAFI, 2-MIKU, 3-MGOR, 4-LALE, 5-SUMB, 6-NAMA, 7-PNDA, 8-KGMA.

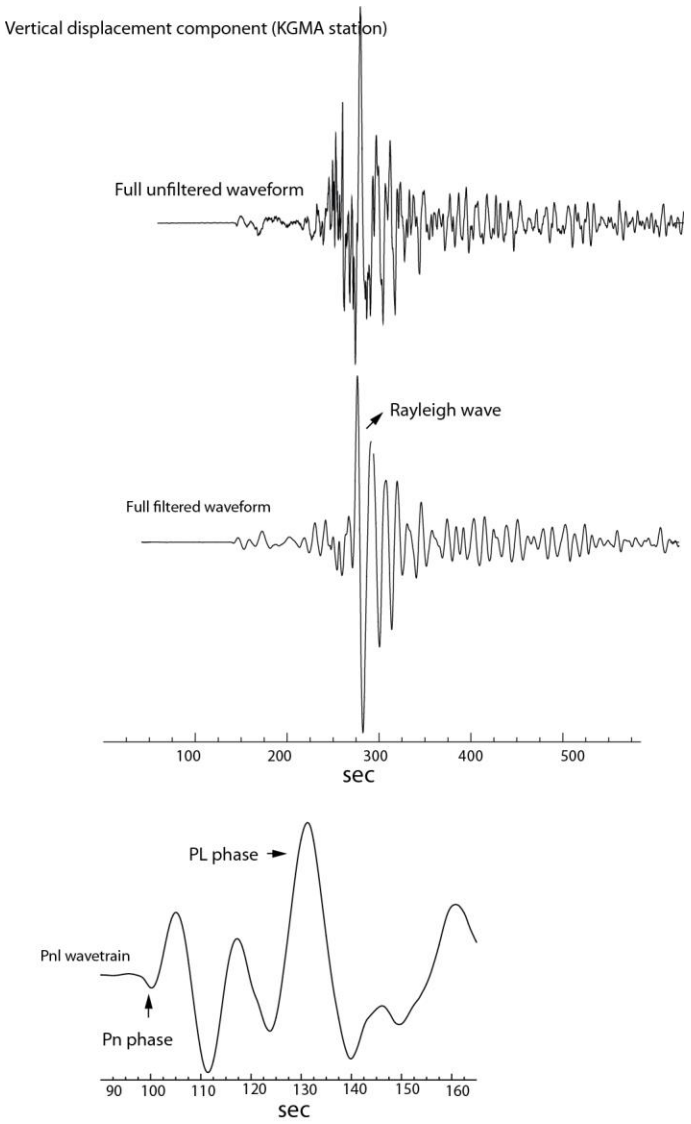

Figure 4-3. Vertical component displacement seismogram from the Karonga earthquake recorded at station KGMA. Top trace is the full unfiltered seismogram, middle trace is the full filtered seismogram and bottom is the Pnl wavetrain together with identified phases.

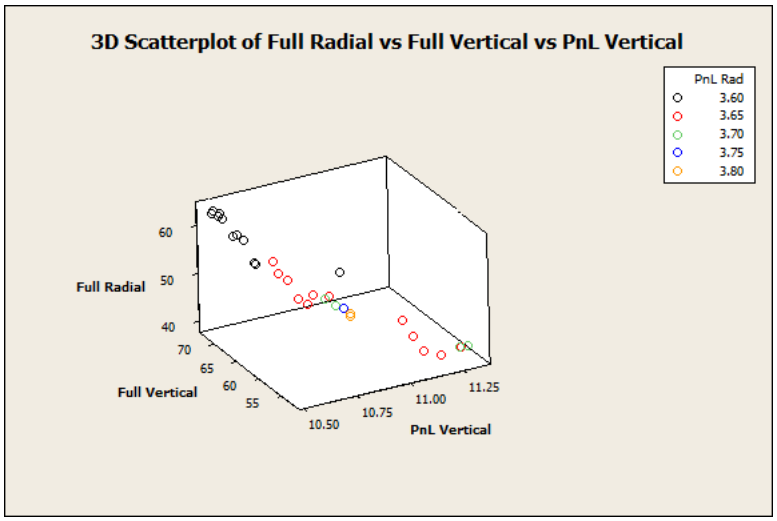

Figure 4-4. Pareto optimal front for the four objectives used in this study for station KGMA.

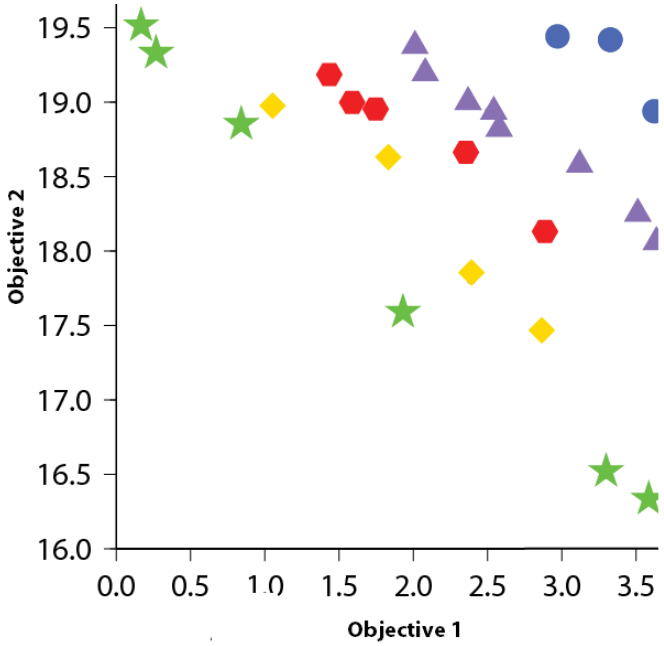

Figure 4-5. Example of the Rank strategy. Green stars are the Pareto optimal set and have Rank 1. If the green stars are removed, then yellow diamonds are optimal and have Rank 2. Red hexagons have Rank 3.

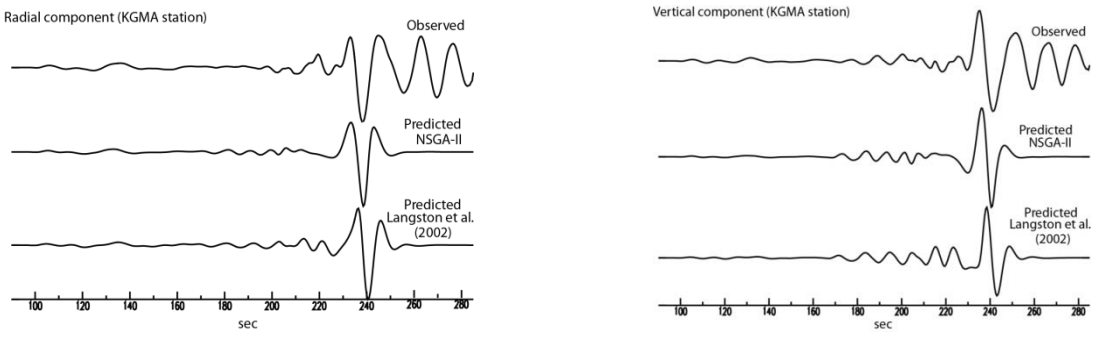

(a)

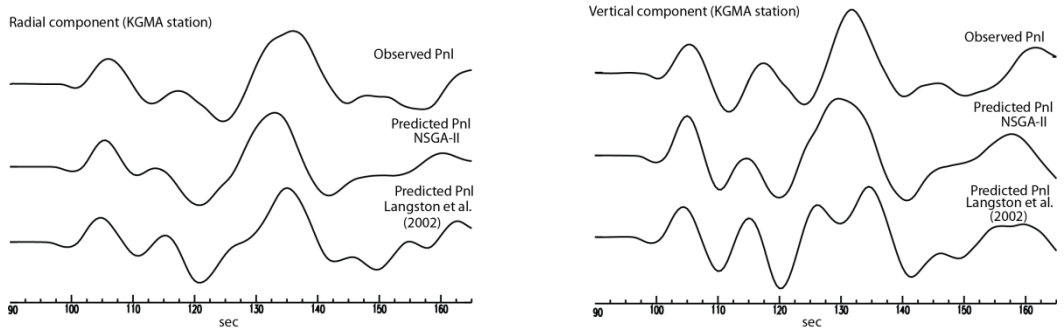

(b)

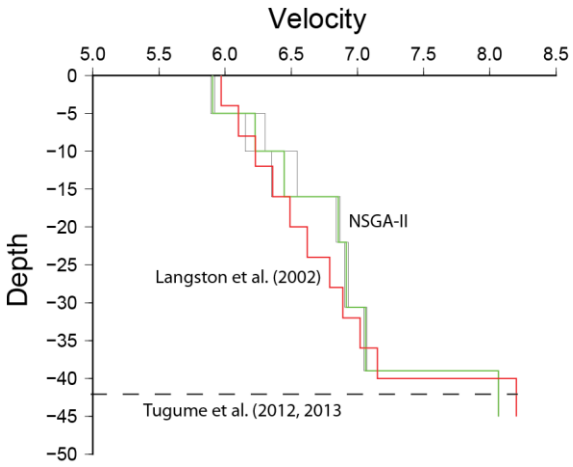

(c)

Figure 4-6. Station KGMA. Velocity models derived using the Non-dominated Sorting Genetic Algorithm. (a) top left and right are the whole waveforms; (b) Pnl wave trains; (c) Velocity models from the NSGA-II (green solid line) and from Langston et al. (2002) (red solid lines), and Moho depth from Tugume et al. (2012, 2013). Uncertainties in the velocity models are shown with thin black line. Depth in y axis is in km and velocity in x axis is in km/s.

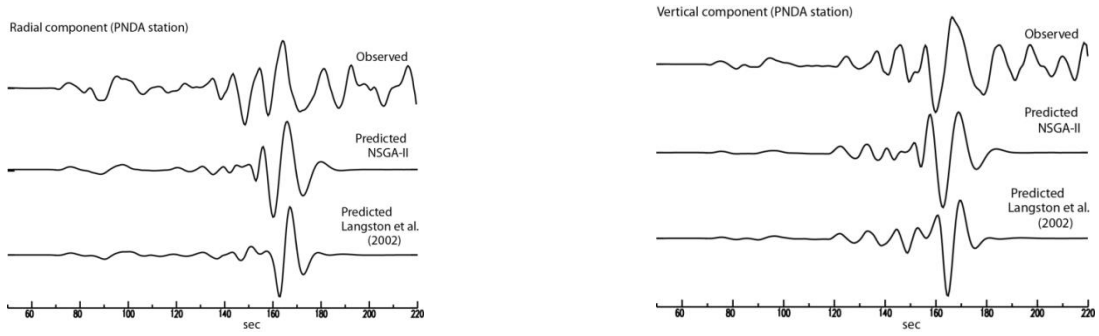

(a)

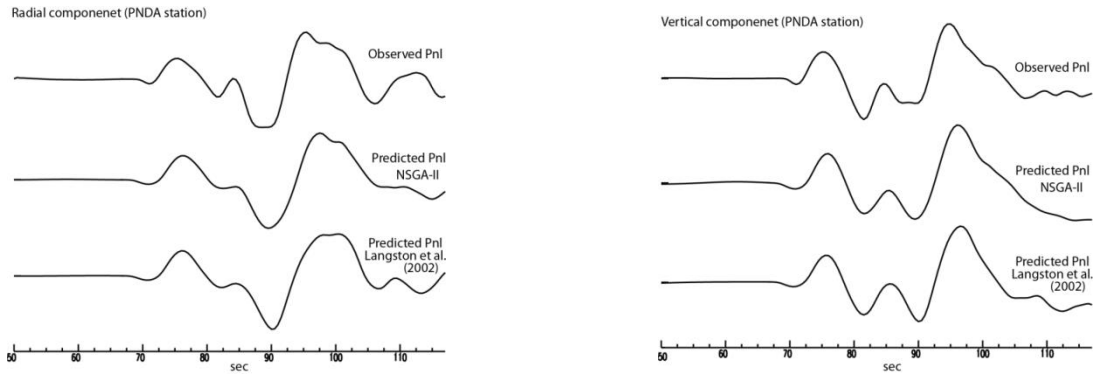

(b)

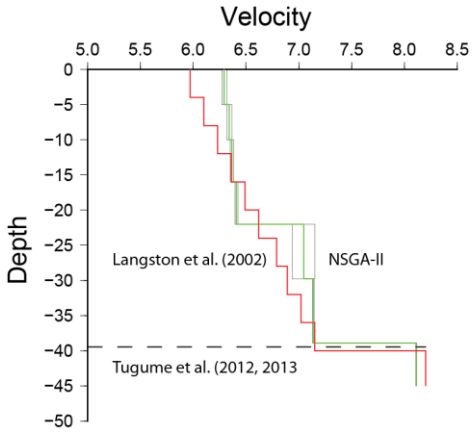

(c)

Figure 4-7. Station PNDA. Velocity models derived using the Non-dominated Sorting Genetic Algorithm. (a) top left and right are the whole waveforms; (b) Pnl wave trains; (c) Velocity models from the NSGA-II (green solid line) and from Langston et al. (2002) (red solid lines), and Moho depth from Tugume et al. (2012, 2013). Uncertainties in the velocity models are shown with thin black line.

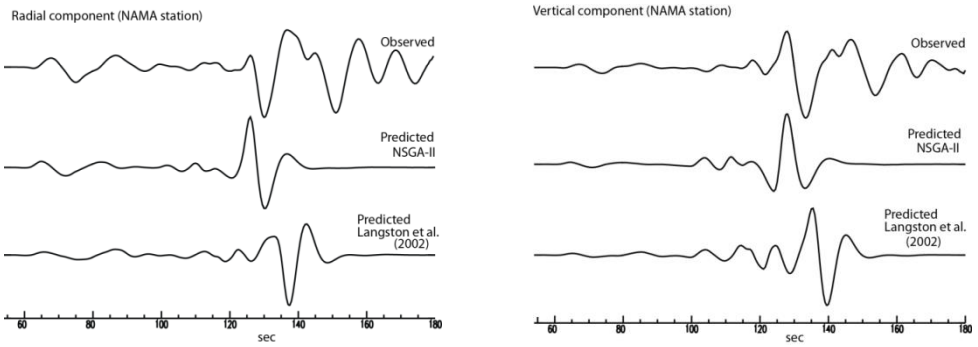

(a)

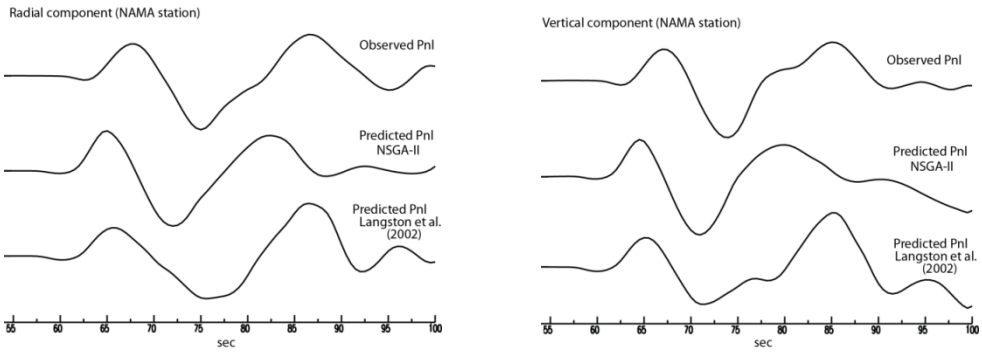

(b)

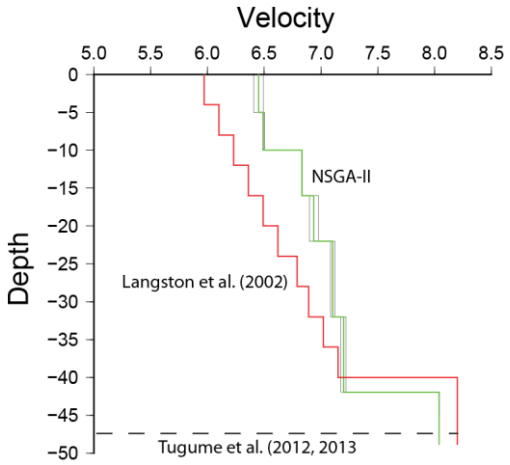

(c)

Figure 4-8. Station NAMA. Velocity models derived using the Non-dominated Sorting Genetic Algorithm. (a) top left and right are the whole waveforms; (b) Pnl wave trains; (c) Velocity models from the NSGA-II (green solid line) and from Langston et al. (2002) (red solid lines), and Moho depth from Tugume et al. (2012, 2013). Uncertainties in the velocity models are shown with thin black line.

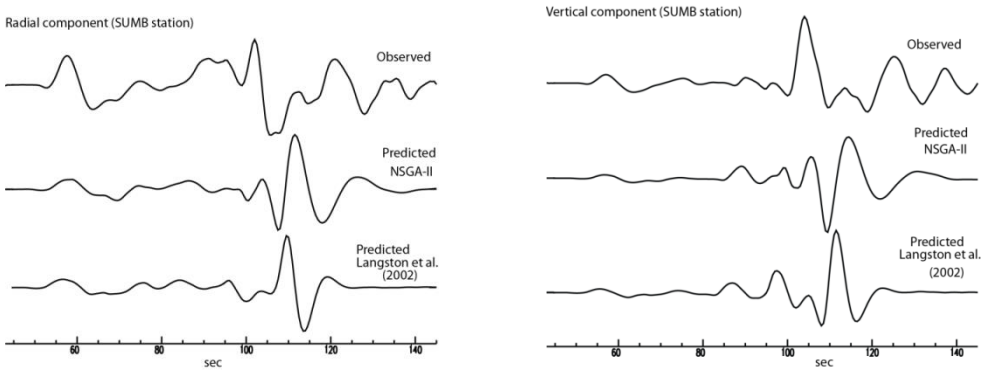

(a)

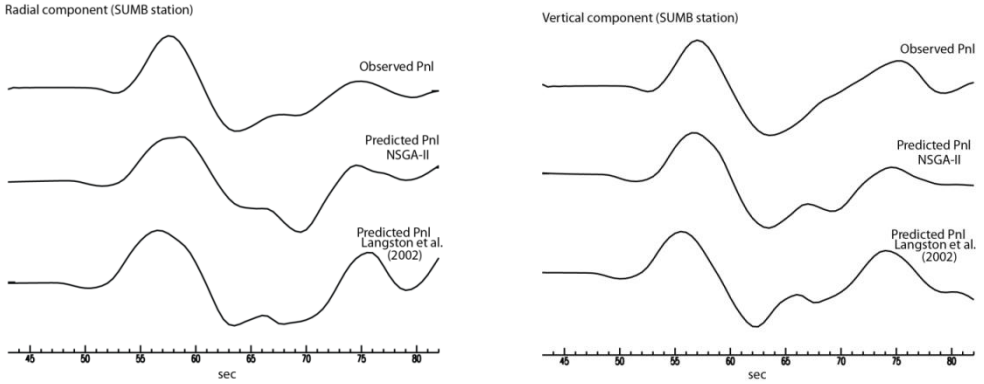

(b)

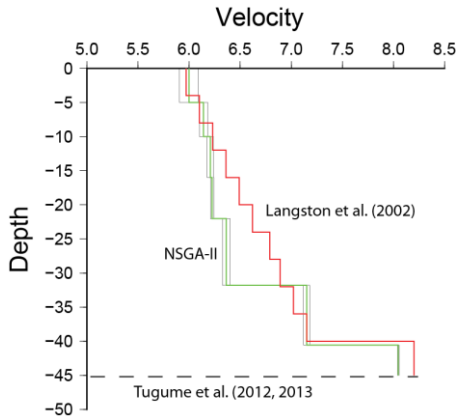

(c)

Figure 4-9. Station SUMB. Velocity models derived using the Non-dominated Sorting Genetic Algorithm. (a) top left and right are the whole waveforms; (b) Pnl wave trains; (c) Velocity models from the NSGA-II (green solid line) and from Langston et al. (2002) (red solid lines), and Moho depth from Tugume et al. (2012, 2013). Uncertainties in the velocity models are shown with thin black line.

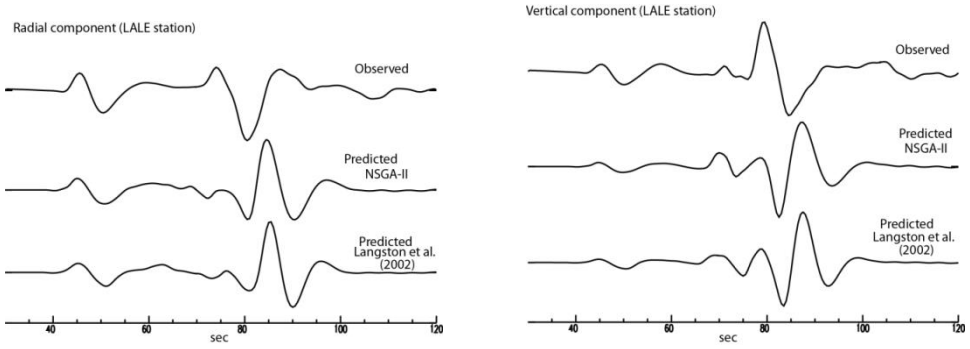

(a)

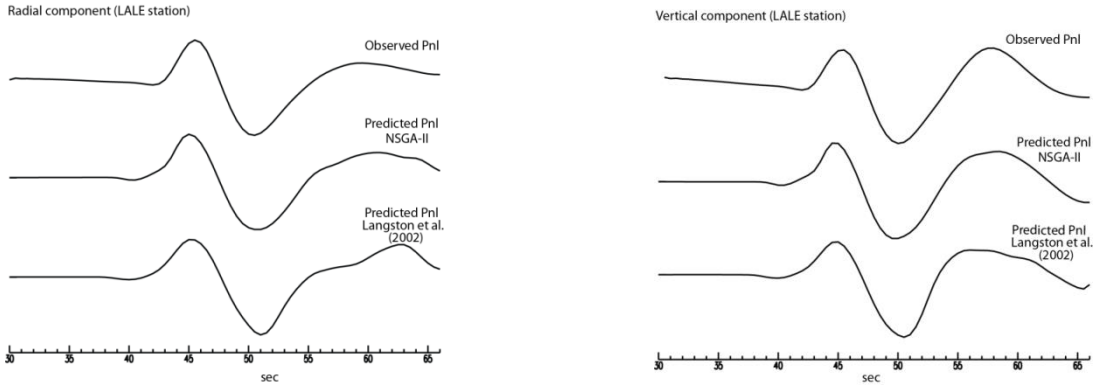

(b)

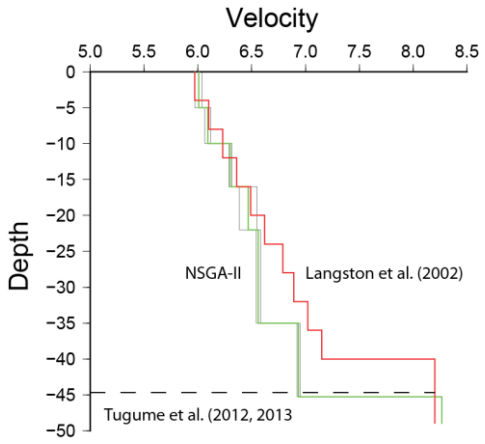

(c)

Figure 4-10. Station LALE. Velocity models derived using the Non-dominated Sorting Genetic Algorithm. (a) top left and right are the whole waveforms; (b) Pnl wave trains; (c) Velocity models from the NSGA-II (green solid line) and from Langston et al. (2002) (red solid lines), and Moho depth from Tugume et al. (2012, 2013). Uncertainties in the velocity models are shown with thin black line.

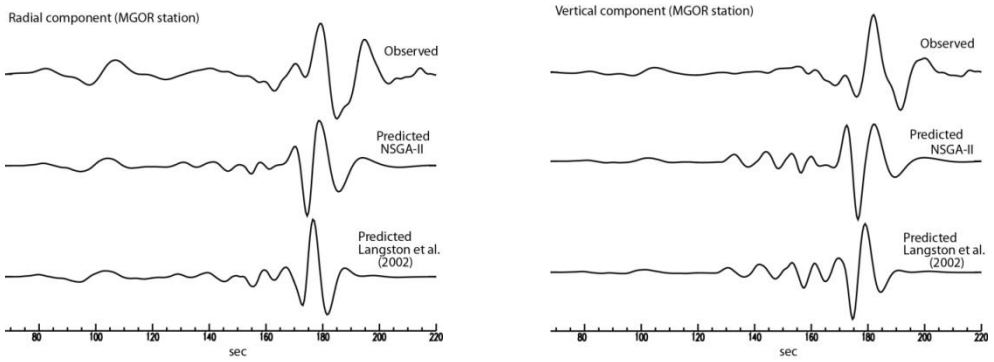

(a)

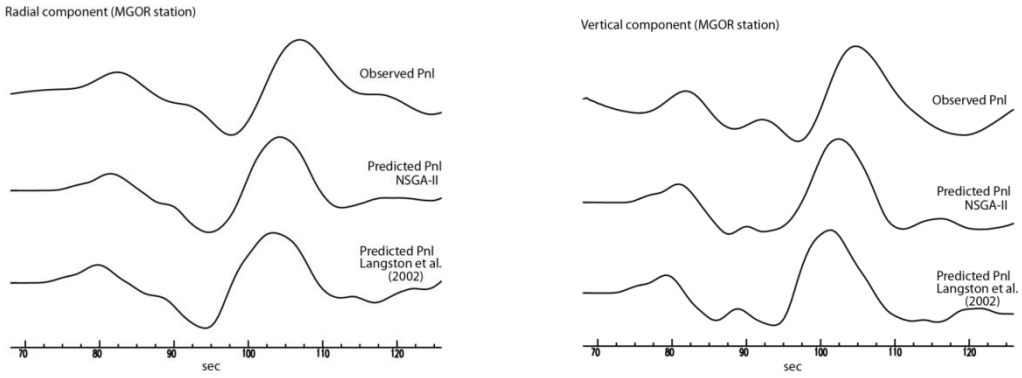

(b)

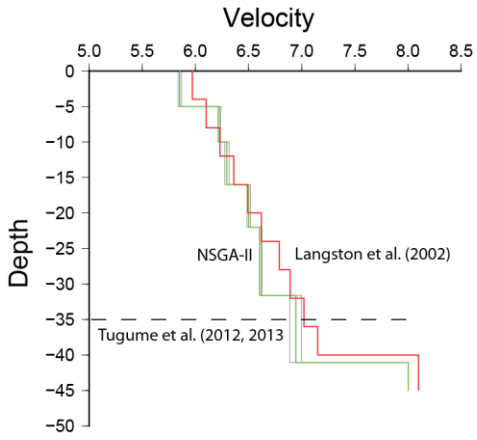

(c)

Figure 4-11. Station MGOR. Velocity models derived using the Non-dominated Sorting Genetic Algorithm. (a) top left and right are the whole waveforms; (b) Pnl wave trains; (c) Velocity models from the NSGA-II (green solid line) and from Langston et al. (2002) (red solid lines), and Moho depth from Tugume et al. (2012, 2013). Uncertainties in the velocity models are shown with thin black line.

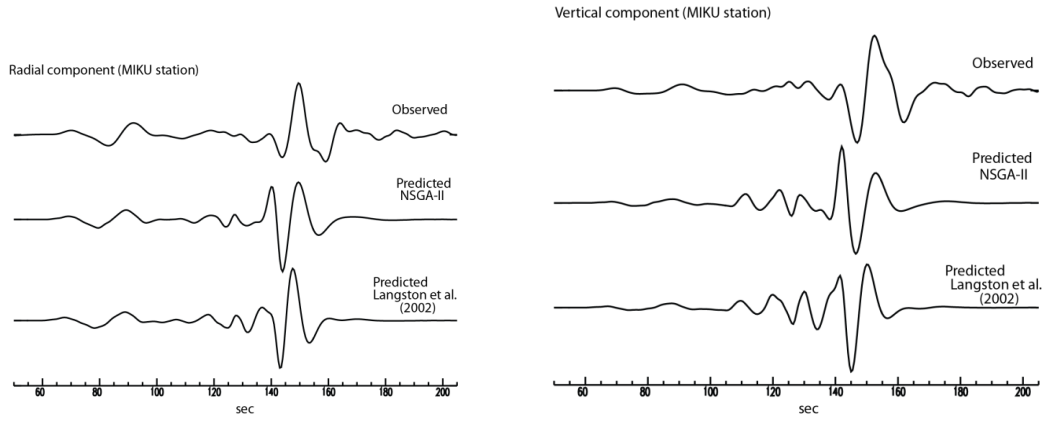

(a)

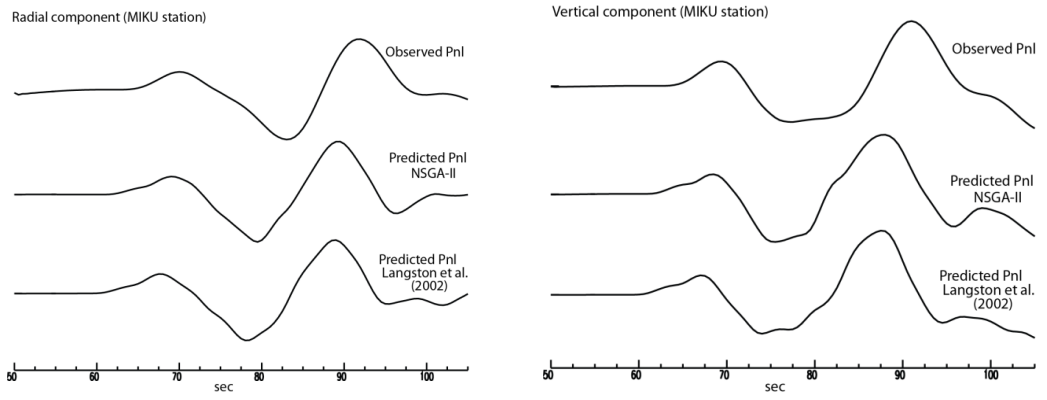

(b)

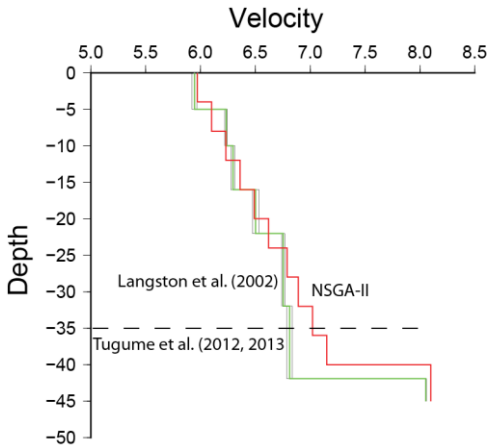

(c)

Figure 4-12. Station MIKU. Velocity models derived using the Non-dominated Sorting Genetic Algorithm. (a) top left and right are the whole waveforms; (b) Pnl wave trains; (c) Velocity models from the NSGA-II (green solid line) and from Langston et al. (2002) (red solid lines), and Moho depth from Tugume et al. (2012, 2013). Uncertainties in the velocity models are shown with thin black line.

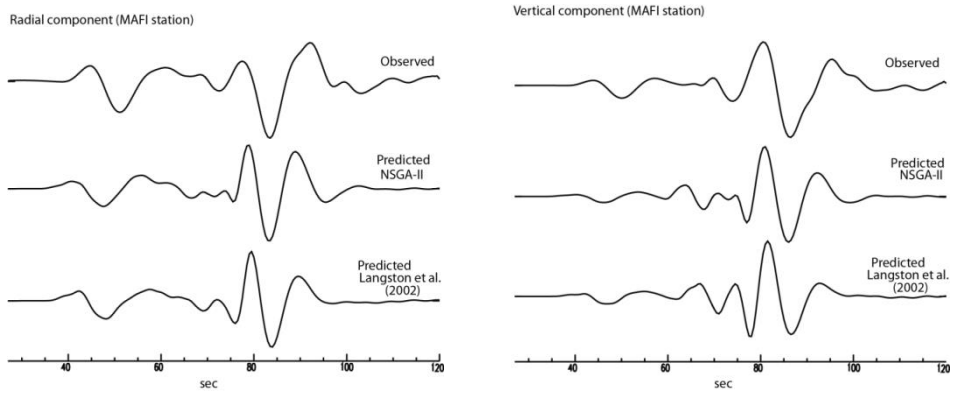

(a)

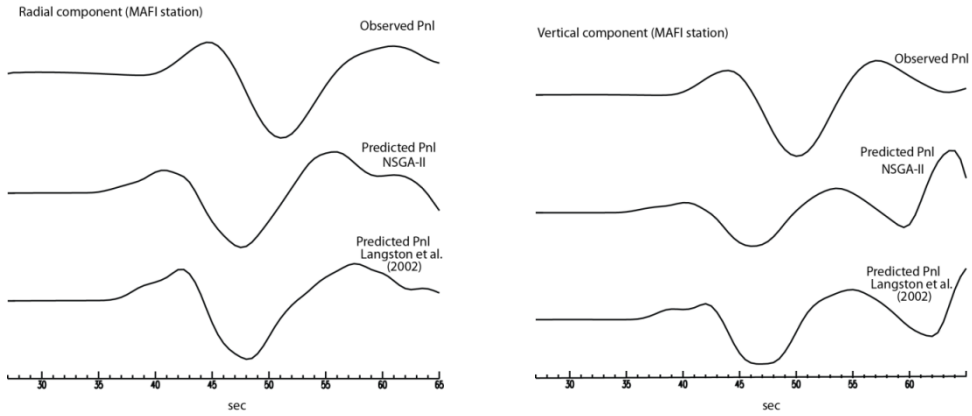

(b)

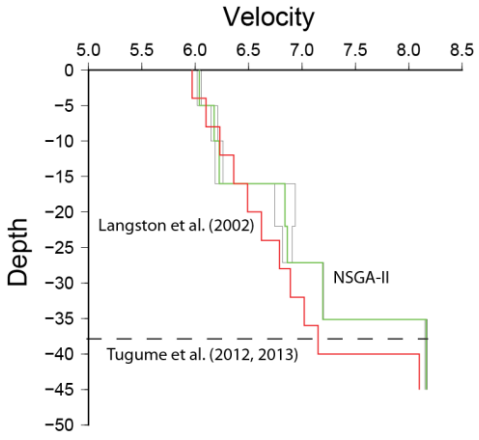

(c)

Figure 4-13. Station MAFI. Velocity models derived using the Non-dominated Sorting Genetic Algorithm. (a) top left and right are the whole waveforms; (b) Pnl wave trains; (c) Velocity models from the NSGA-II (green solid line) and from Langston et al. (2002) (red solid lines), and Moho depth from Tugume et al. (2012, 2013). Uncertainties in the velocity models are shown with thin black line.

5 CONCLUSION

Several different seismic methods have been used to investigate the structure of the crust and uppermost mantle, locally beneath the Khartoum Basin in Sudan and regionally beneath East Africa, to advance knowledge of the tectonic evolution and volcanism of the region.

In the first part of the thesis, a study of the crustal structure beneath the Khartoum basin is presented. H-k stacking indicates that the crustal thickness beneath the Khartoum basin ranges from 33 to 37 km, with an average of 35 km, and that the crustal Vp/Vs ratio ranges from 1.74 to 1.81, with an average of 1.78. Furthermore, joint inversion of receiver functions and Rayleigh wave group velocities yield similar results for the depth of the Moho, as well as an average shear wave velocity of 3.7 km/s for the crust.

These results are the first seismic estimates of Moho depth for a basin in Sudan. The results are compatible with Moho depths determined by a number of gravity studies in Sudan (Browne et al., 1985; Mohamed et al., 2001) and central Sudan (Jorgensen and Bosworth, 1989; Tedla et al., 2011). These results indicate that the crust and lithosphere under the Sudanese basins have not been thinned to any significant extent, which has important implications for understanding Cenozoic volcanism in central Africa. The model proposed by Pèrez-Gussinye et al. (2009) and Ebinger and Sleep (1998) suggested that thinned lithosphere beneath the Sudan basins created a channel at the lithosphere-asthenosphere boundary for magma from the Afar/Ethiopia region to migrate to the west, reaching as far as the Cameroon Volcanic Line. Results showing little crustal thinning, integrated with the elastic thickness (Te) estimates from Pèrez-Gussinye et al. (2009), indicate that there may be insufficient topography on the lithosphere-asthenosphere boundary, at least beneath the basins, to create a channel for the migration of plume material. Consequently, Cenozoic volcanism in regions like the Darfur and the Cameroon Volcanic Line might not be the result of plume material migrating from the Ethiopia/Afar region to the west beneath thinned lithosphere.

In the second part of the thesis, the uppermost mantle P-wave velocities (Pn) beneath most of East Africa were derived in order to determine how they vary across the area. The P-wave travel times were obtained from regional events recorded by three networks: the 1994-1995 Tanzania Broadband Seismic Experiment (TBSE), the AfricaArray East African Seismic Experiment (AAEASE) network, and the AfricaArray Tanzania Basin Seismic Experiment (AATBSE) network. Traveltimes were inverted using a standard singular value decomposition algorithm assuming an isotropic medium (Wiggins, 1972; Menke, 1989). Results show high Pn velocities beneath the Tanzania Craton that are consistent with the presence of old, cold and chemically depleted cratonic lithosphere (Christensen and Mooney, 1995). These fast velocities continue beneath the Mozambique Belt to the east of the craton, the Kibaran Belt west of the craton, and beneath the northern half of the Ubendian Belt to the southwest of the craton. We conclude that craton reaches a maximum width of about 950 km in the east-west direction and a maximum length of about 1200 km in the north-south direction. Therefore, the areal extent of the cratonic lithosphere is much larger than is indicated by the boundaries of the craton mapped at the surface.

The Pn velocities beneath the volcanic provinces along the Western Branch are not anomalously slow, indicating little, if any, perturbation to the uppermost mantle beneath them. These velocities imply that the crust and upper mantle has not been significantly modified by rifting processes of the East African Rift System. This is in contrast to the upper mantle structure at depths $\geq$ 70 km beneath the volcanic regions, which clearly is perturbed. The fast Pn velocities beneath the Western Branch contrast with the slow Pn velocities of 7.5-7.8 km/s beneath the Eastern Branch in Kenya, showing that the upper mantle beneath the Eastern Branch has been altered much more than beneath the Western Branch.

In the third part of the thesis, the crustal structure of the Ubendian and Usagaran Belts was investigated by modeling regional seismograms from the Karonga, Malawi earthquakes using the Non-Dominated Genetic Algorithm method (Deb et al., 2002). In the Usagaran belt, the average Moho depth was found to be 35 km for station MAFI, and 41 km and 42 km for stations MOGR and MIKU, respectively. These results are similar to the average Precambrian crustal thickness

in East Africa, and provide no evidence for crustal thickening. In the Ubendian Belt, the average Moho depth beneath the Ufipa sub-terrane was found to be 43 km, compared to 39 km for Wakole sub-terrane. These results indicate localized thickening in the Ufipa sub-terrane, but not beneath the entire Ubendian Belt. There is no clear evidence that Paleoproterozoic crust in East Africa is substantially thicker than Archaean crust.

In order to test the conclusions of the study in Chapter Two, it would be useful to obtain heat flow measurements from both the northeast and southwest basins of Sudan. Heat flow data could be used to confirm if there is a substantial difference in the surface heat flow between these basins. To better understand the lithosphere in different areas across Sudan, it would be advantageous to conduct a broadband seismic experiment covering the area around Dafour hotspot, the Red Sea, and the Central African Shear Zone in Sudan to determine detailed lithospheric structure. Such an experiment would be important to determine whether or not the lithosphere under these regions has been perturbed similarly to the Afar hotspot.

My investigations have shed substantial light on the crustal structure and evolution of eastern Africa. However, the relationship between the crust and upper mantle during extension, and the role that magmatism plays in the evolution in the volcanically active continental rifts, still remain subjects of debate.

References

Browne, S.E., Fairhead, J.D. and Mohamed, I.I. (1985), Gravity study of the White Nile Rift, Sudan and its regional tectonic setting, Tectonophysics, 113:123-137.

Christensen, N.I. and Mooney, W.D. (1995), Seismic velocity structure and composition of the continental crust: A global view, Journal of Geophysical Research, 100:9761– 9788.

Deb K., Agrawl, A., Pratap, A. and Meyarivan, T. (2002). A fast elitist non-dominated sorting genetic algorithm for multi-objective optimization: NSGA-II, IEEE Transactions on Evolutionary Computation, 6, 182-197.

Ebinger, C.J. and Sleep, N.H. (1998), Cenozoic magmatism throughout east Africa resulting from impact of a single plume, Nature, 395:788-971.

Jorgensen, G.J and Bosworth, B. (1989), Gravity modelling in the central Africa Rifts System, Sudan: rift geometries and tectonic significance, Journal of Africa Earth Sciences, 8:283-306.

Menke, W. (1989), Geophysical Data Analysis: Discrete Inverse Theory, International Geophysics series, 45.

Mohamed, A.Y., Ashcroft, W.A. and Whiteman, A. (2001), Structure development and crustal stretching in the Muglad basin, southern Sudan, Journal of Africa Earth Sciences, 32:179-191.

Pèrez-Gussinye, M., Metois, M., Fernandez, M., Verges, J., Fullea, J. and Lowry, A. (2009), Effective elastic thickness of Africa and its relationship to other proxies for lithospheric structure and surface tectonics, Earth and Planetary Science Letters, 287:152-167.

Tedla, G.E., Meijde, M.V., Nyblade, A.A. and Meer, F.D. (2011), A crustal thickness map of Africa derived from a global gravity field model using Euler deconvolution, Geophysical Journal International, 187:1-9, doi: 10.1111/j. 1365-246X. 2011.05140.x.

Wiggins, R. (1972), The general linear inverse problem: Implications of surfacewaves and free oscillations for Earth structure, Reviews of Geophysical and Space Physics, 10:251-285.

Appendix A: H–k stacks of receiver functions for the Khartoum basin (Chapter 2)

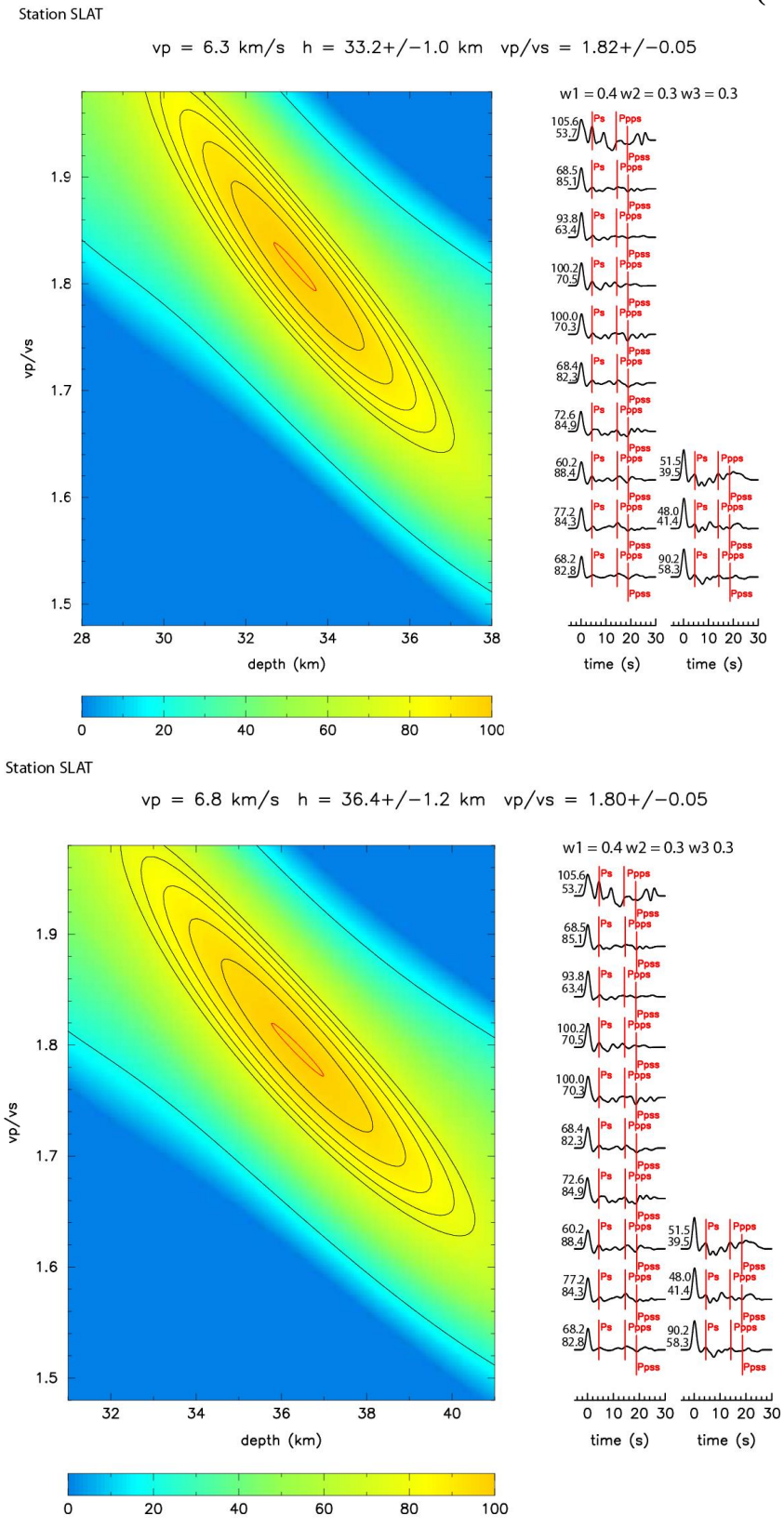

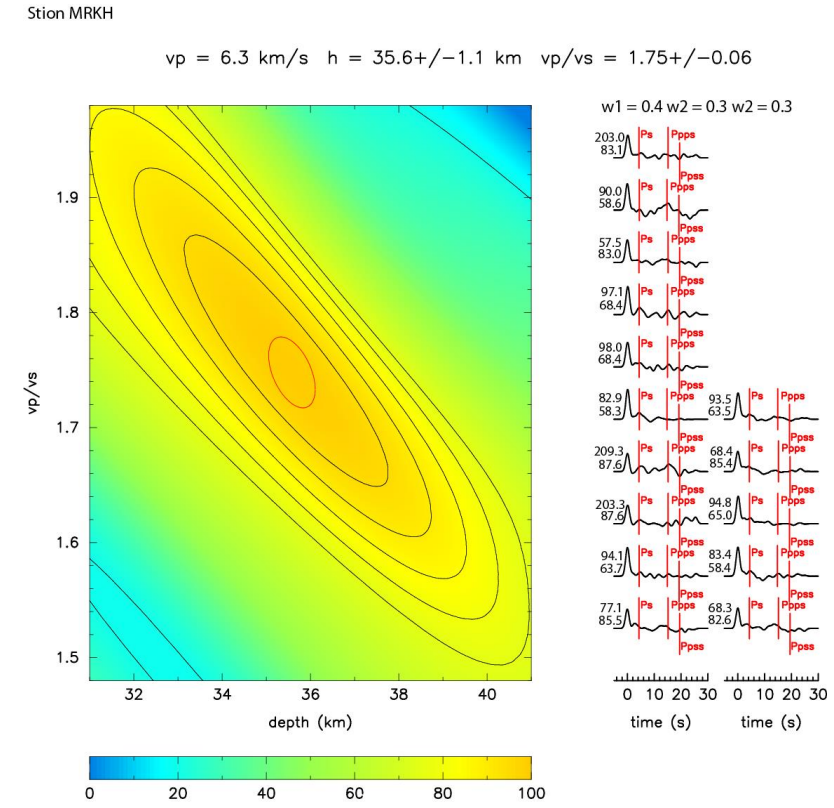
Stion MRKH
vp = 6.3 km/s h = 35.6+/−1.1 km vp/vs = 1.75+/−0.06
w1 = 0.4 w2 = 0.3 w2 = 0.3
vp/vs
depth (km)
time (s)
time (s)
Ps
Ppps
Ppss

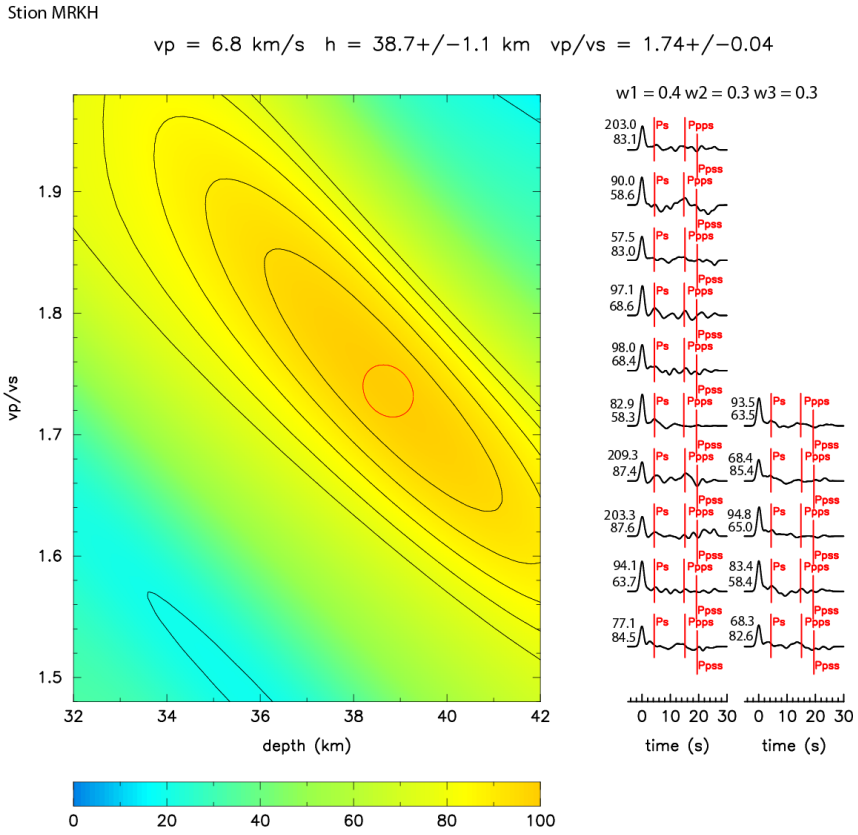
Stion MRKH
vp = 6.8 km/s h = 38.7+/−1.1 km vp/vs = 1.74+/−0.04
w1 = 0.4 w2 = 0.3 w3 = 0.3
vp/vs
depth (km)
time (s)
time (s)
Ps
Ppps
Ppss

staion JAWL

vp = 6.3 km/s h = 31.6+/−1.4 km vp/vs = 1.82+/−0.07

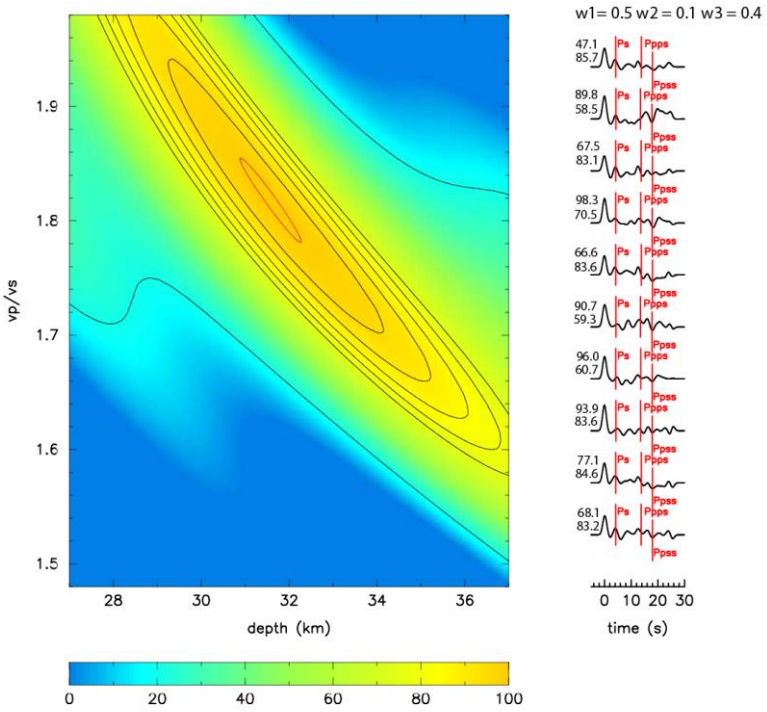

Stion JAWL

vp = 6.8 km/s h = 34.4+/−1.4 km vp/vs = 1.81+/−0.06

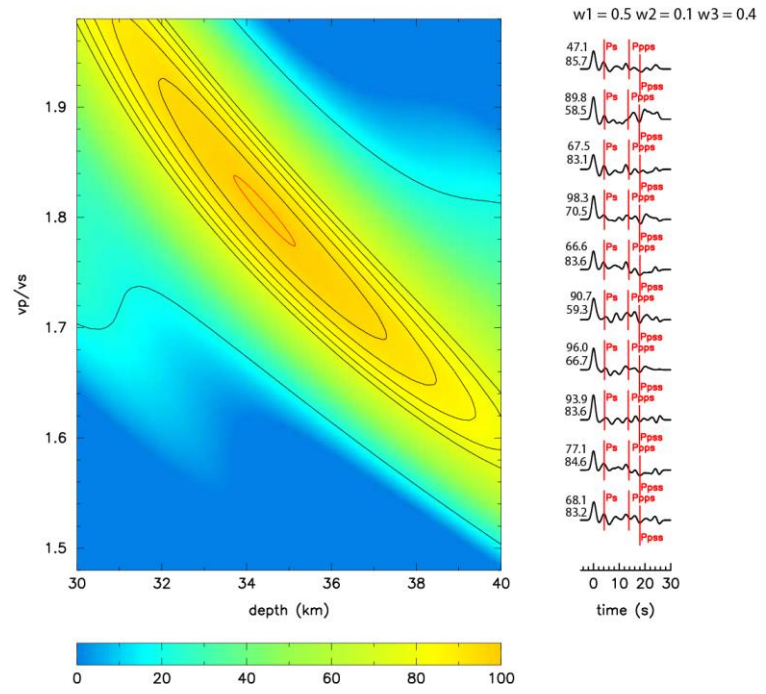

Appendix B: Events used for the Pn tomography study (Chapter 3)

Date	Latitude	Longitude	Depth
Y M D H M S	Degree	Degree	km
2007.09.08.14.15.31.00	-2.94	36.75	12.2
2007.09.10.00.26.21.00	-3.02	36.78	12.2
2007.10.07.21.44.13.00	0.22	30.11	0.02
2007.10.14.07.03.20.00	1.59	30.86	9.5
2007.10.19.01.02.17.00	-0.1	29.84	29.65
2008.02.03.07.34.17.65	-2.49	29.41	12.2
2008.02.03.08.07.56.00	-2.32	29.02	1.43
2008.02.03.10.07.02.00	-2.36	29.06	3.46
2008.02.03.12.51.54.00	-2.36	28.51	12.2
2008.02.03.15.15.09.00	-2.21	28.94	12.2
2008.02.03.23.28.35.00	-2.38	28.76	12.2
2008.02.05.22.54.46.00	-2.33	28.77	12.2
2008.02.08.23.04.43.00	-2.37	28.9	12.2
2008.02.09.01.39.46.00	-2.31	28.84	12.2
2008.02.11.23.59.58.00	-2.3	29.2	16.55
2008.02.12.01.49.00.00	-2.3	29.2	17.2
2008.02.13.09.21.35.00	-0.61	29.92	14.77
2008.02.13.22.05.07.00	-2.4	28.94	12.2
2008.02.15.23.58.29.00	-2.43	28.8	12.2
2008.02.23.10.39.38.00	-2.33	28.56	17.2
2008.02.27.02.07.59.00	-2.33	28.98	12.2
2008.03.06.07.35.29.00	-5.68	36.05	12.2
2008.03.09.01.20.55.00	-2.3	29.14	8.52
2008.03.12.19.07.22.00	4.47	29.78	0
2008.08.26.14.56.59.00	1.83	30.95	25.28
2008.08.31.03.52.54.00	-6.08	35.9	12.2
2008.10.05.00.02.15.00	-1.25	29.46	12.2
2008.10.05.01.03.36.00	-1.01	29.81	6.42
2008.10.06.07.44.35.00	-0.94	29.98	0.06
2008.10.13.02.19.43.00	-5.64	35.95	12.2
2008.10.27.22.02.06.00	-6.6	30.44	12.2
2008.10.30.00.45.47.00	0.08	30.27	0.86
2008.11.13.11.07.11.00	-5.4	28.22	12.2
2008.11.14.01.40.14.00	-0.03	28.14	12.2
2008.11.28.23.22.51.00	-5.07	31.6	12.2

Date	Latitude	Longitude	Depth
Y M D H M S	Degree	Degree	km
2009.02.04.09.25.20.31	-5.44	29.17	9.9
2009.02.15.23.09.31.96	-7.02	37.25	0
2009.06.18.21.53.56.90	-5.39	35.96	14.79
2009.06.19.00.22.0803.16	-5.57	35.98	9.04
2009.06.21.05.43.46.50	-5.64	35.86	19.77
2009.06.21.23.41.56.79	-4.58	34.94	5.56
2009.06.23.02.40.30.26	-5.52	35.76	5.64
2009.06.24.14.39.39.66	-7.3	37.12	10.29
2009.06.25.14.17.19.70	-6.59	35.29	5.12
2009.06.25.15.20.10.04	-6.33	36	0.03
2009.06.25.16.33.28.47	-5.44	36.16	7.31
2009.06.28.02.57.55.09	-7.08	37.22	5.57
2009.06.29.19.49.39.49	-4.74	35.45	15.95
2009.07.01.01.23.20.89	-5.43	35.97	7.39
2009.07.01.02.13.45.45	-5.55	35.88	4.83
2009.07.03.20.59.3.02	-5.94	35.82	19.68
2009.07.05.14.15.5.23	-6.31	35.61	12.06
2009.07.11.13.43.32.63	-5.79	35.89	21.75
2009.07.12.01.30.30.12	-7.04	35.94	32.2
2009.07.15.23.09.35.43	-5.56	35.79	6.21
2009.07.15.23.23.45.54	-5.99	34.8	9.93
2009.07.16.04.30.36.35	-6.24	35.18	0.03
2009.07.16.08.52.56.50	-6.71	35.44	22.15
2009.07.17.03.45.29.19	-6.16	35.28	0.03
2009.07.18.20.45.44.41	-5.81	35.98	19.93
2009.07.20.01.02.33.13	-5.53	35.91	20
2009.07.21.20.20.5.72	-7.03	35.97	0.06
2009.07.23.21.32.31.03	-5.58	35.9	17.1
2009.07.23.21.45.18.72	-5.87	36.43	0
2009.07.23.22.16.30.92	-5.4	35.9	10.27
2009.07.24.03.44.55.79	-5.57	36.05	0.03
2009.07.24.21.48.15.33	-5.75	35.95	17.82
2009.07.26.14.59.4.56	-6.48	35.22	7.23
2009.07.31.00.33.48.25	-5.65	35.89	8.45
2009.07.31.01.33.34.29	-8.4	38	0
2009.07.31.17.07.54.48	-5.87	35.79	24.64
2009.08.01.21.47.49.69	-7.67	38.23	17.61
2009.08.01.22.39.31.21	-6.02	35.86	14.98
2009.08.03.03.22.55.98	-7.74	38.03	0.02
2009.08.10.22.54.48.47	-10.43	34.36	8.05

Date	Latitude	Longitude	Depth
Y M D H M S	Degree	Degree	km
2009.08.14.21.29.30.07	-9.19	33.71	0.06
2009.08.22.09.22.22.15	-7.08	35.44	9.81
2009.09.04.04.53.49.53	-7.1	35.96	1.75
2009.09.04.15.32.53.63	-7.08	35.94	14.74
2009.09.11.09.06.59.24	-6.67	36.17	9.9
2009.09.16.07.17.18.41	-7.37	36.94	7.36
2009.09.23.00.28.29.87	-7.18	35.86	4.06
2009.09.23.19.59.54.10	-7.49	36.31	23.21
2009.10.02.01.21.19.93	-7.04	36.04	27.17
2009.10.07.00.50.32.06	-7	35.96	5.68
2009.10.15.00.24.48.63	-6.44	35.84	144.05
2009.10.19.16.38.16.04	-7.36	36.23	31.34
2009.10.22.19.24.15.43	-7	35.98	0.03
2009.10.23.20.15.56.82	-7	36	0.03
2009.10.23.20.25.50.51	-7.15	35.63	38.12
2009.10.24.21.42.9.46	-6.98	36	0.03
2009.10.26.02.08.57.58	-7.02	35.98	10.08
2009.10.26.19.20.21.27	-6.99	35.98	0.03
2009.11.06.02.08.58.85	-6.16	35.25	35.3
2009.11.06.23.24.3.88	-7.55	37.54	0.03
2009.11.08.04.23.35.13	-7.38	37.42	0.04
2009.11.09.03.37.26.12	-7.31	37.31	0.03
2009.11.12.20.06.34.91	-9.88	33.85	0.03
2009.11.13.20.00.41.53	-6.99	36.02	1.11
2009.11.29.17.21.19.46	-8.31	36.76	23.4
2009.12.06.19.16.53.06	-9.93	33.84	0.03
2009.12.06.19.36.40.44	-9.99	33.89	0.07
2009.12.06.19.58.14.47	-9.88	33.82	0.06
2009.12.06.20.16.52.66	-9.99	33.9	0.05
2009.12.07.03.35.39.17	-10	33.89	0.02
2009.12.07.06.01.30.45	-9.96	33.86	0.04
2009.12.07.08.41.24.18	-10	33.88	0.02
2009.12.07.09.31.43.92	-9.89	33.82	0.05
2009.12.07.17.12.2.28	-9.92	33.85	0.02
2009.12.07.18.09.37.14	-9.91	33.83	0.05
2009.12.07.18.16.31.06	-9.88	33.82	0.06
2009.12.07.18.42.40.93	-9.89	33.82	0.05
2009.12.08.06.10.17.95	-9.88	33.86	6.39
2009.12.08.06.15.10.22	-9.86	33.79	12.92
2009.12.08.06.42.57.55	-9.85	33.86	6.84

Date	Latitude	Longitude	Depth
Y M D H M S	Degree	Degree	km
2009.12.10.07.48.14.00	-9.72	34.01	5.11
2009.12.10.09.02.4.77	-9.69	34.01	13.26
2009.12.11.23.04.2.74	-9.74	33.9	5.71
2009.12.12.00.41.42.84	-9.8	33.78	17.34
2009.12.12.02.27.2.18	-9.77	33.86	9.23
2009.12.14.10.31.53.06	-9.8	33.93	9.72
2009.12.14.23.17.51.32	-9.66	33.83	14.65
2009.12.15.20.18.43.13	-9.75	33.88	8.54
2009.12.18.11.56.26.55	-9.7	33.9	13.36
2009.12.20.07.34.35.20	-9.88	33.91	8.03
2009.12.21.02.22.5.07	-9.8	33.85	9.14
2009.12.22.23.51.28.71	-9.83	33.74	27.71
2009.12.23.03.21.47.89	-9.93	33.83	8.4
2009.12.27.00.30.52.57	-9.9	33.92	5.72
2010.01.02.14.13.10.40	-10.67	33.88	12.2
2010.01.03.16.14.46.14	-6.95	35.78	0
2010.01.03.17.08.35.84	-7	36.1	0.03
2010.01.03.17.36.57.75	-6.9	35.21	0.03
2010.01.04.20.22.14.16	-10.62	33.71	12
2010.01.04.21.00.16.90	-6.64	33.83	12
2010.01.05.21.11.41.93	-7.33	35.41	0.03
2010.01.05.23.27.12.77	-5.67	35.93	0.04
2010.03.01.08.40.28.58	-9.89	33.86	0.05
2010.03.02.03.03.0.49	-7.87	37.21	383.53
2010.03.03.23.04.10.37	-5.9	35.92	30.33
2010.03.04.01.39.51.71	-9.88	33.8	0.03
2010.03.06.01.55.30.88	-5.5	35.75	9.79
2010.03.06.20.00.44.85	-8.55	32.61	0.03
2010.03.18.21.26.15.12	-9.85	33.87	0.03
2010.03.20.23.38.35.31	-6.93	36.55	0.03
2010.04.03.19.04.52.55	-7.96	37.73	3.5
2010.04.03.22.00.51.59	-7.52	37.57	0.05
2010.04.04.21.16.32.91	-7.1	37.35	0.03
2010.04.04.21.51.6.63	-10.82	37.57	12
2010.04.05.10.17.24.33	-11.02	37.35	12
2010.04.07.10.03.10.17	-5.84	36.21	0
2010.04.08.23.57.43.28	-4.26	35.38	12.2
2010.04.16.10.23.41.35	-7.7	37.74	12.79
2010.04.16.10.23.42.28	-7.6	37.6	0.03

Date	Latitude	Longitude	Depth
Y M D H M S	Degree	Degree	km
2010.04.19.22.30.57.43	-10.8	37.14	13.2
2010.04.20.19.34.3.05	-6.17	39.8	0
2010.04.21.01.12.17.23	-9.71	33.8	0
2010.04.21.01.12.32.01	-9.31	34.95	26.93
2010.04.22.12.57.23.64	-9.88	33.87	0.03
2010.04.24.15.46.32.97	-8.54	38.91	17.04
2010.04.24.20.16.42.97	-7.52	37.56	8.96
2010.04.25.21.58.55.46	-7.81	37.76	0.01
2010.04.26.11.54.33.28	-5.32	35.91	5.84
2010.04.27.03.39.41.93	-8.08	37.3	27.68
2010.04.29.22.52.3.98	-6.93	37.99	17.94
2010.05.01.08.37.48.76	-5.55	35.84	15.42
2010.05.01.18.39.57.32	-6.76	35.68	13.63
2010.05.02.21.33.20.31	-7.1	38.38	15.28
2010.05.03.15.07.50.30	-6.74	38.05	67.44
2010.05.04.21.34.12.80	-4.51	36.09	12.2
2010.05.05.00.03.15.73	-5.26	35.88	12.2
2010.05.05.08.11.33.00	-5.52	35.85	12.2
2010.05.05.11.18.42.00	-5.35	35.86	12.2
2010.05.05.18.57.33.99	-9.33	35	21.88
2010.05.06.08.01.21.80	-9.58	35.01	7.42
2010.05.08.17.52.45.16	-6.38	35.21	0.03
2010.05.10.05.38.51.80	-7.53	37.27	16.77
2010.05.16.20.37.18.76	-9.41	34.91	21.61
2010.05.17.05.05.28.97	-6.9	39.45	22.18
2010.05.17.05.25.19.96	-8.79	39.02	5.37
2010.05.18.04.57.10.90	-7.02	37.88	0.03
2010.05.18.05.38.26.94	-7.26	38.08	18.13
2010.05.18.23.09.03.00	0.98	30.45	12.2
2010.05.20.02.22.48.18	-3.65	35.96	0.02
2010.05.21.01.26.32.20	-7.48	37.65	0.02
2010.05.21.10.03.18.68	-6.99	36.58	10.65
2010.05.22.19.08.30.38	-5.83	35.87	6.05
2010.05.22.19.47.47.00	-3.18	29.99	12.2
2010.05.23.04.16.18.30	-8.39	38.63	24.32
2010.05.23.05.27.53.84	-6.18	36	0
2010.05.23.21.45.15.23	-6.69	36.18	16.34
2010.05.23.22.30.41.24	-2.36	39.72	12.2
2010.05.23.22.30.49.00	-2.11	40.09	5.37

Date	Latitude	Longitude	Depth
Y M D H M S	Degree	Degree	km
2010.05.24.15.42.50.50	-5.71	35.84	29.24
2010.05.25.17.12.34.92	-10.87	35.73	12
2010.05.26.17.16.38.87	-6.99	36.29	3.86
2010.06.03.02.34.22.57	-9.83	38.89	11.09
2010.06.03.19.04.27.94	-9.42	34.94	20.4
2010.06.13.22.42.33.04	-10.22	35.11	12.87
2010.06.17.04.00.38.38	-7.05	36.13	34.25
2010.06.17.12.55.8.39	-8.32	36.1	31.06
2010.06.19.09.01.47.09	-7.62	37.7	36.05
2010.06.19.19.29.59.45	-8.93	39.14	39.91
2010.06.19.23.41.5.77	-7.73	37.57	0.02
2010.06.20.00.38.46.50	-8.14	36.43	30.25
2010.06.20.00.38.47.60	-8.17	36.34	18.39
2010.06.29.19.48.29.85	-4.01	34.81	12.2
2010.06.29.20.05.52.85	-3.22	35.38	12.2
2010.06.30.03.25.13.47	-8.65	36.56	15.16
2010.07.01.01.43.42.39	-6.45	36.43	17.96
2010.07.01.13.07.58.68	-7.06	35.82	14.86
2010.07.01.20.13.19.95	-9.65	39.61	7.8
2010.07.03.04.43.29.43	-7.1	36.28	7.98
2010.07.03.14.03.45.14	-9.98	35.84	23.02
2010.07.05.23.33.55.66	-8.36	35.71	360.74
2010.07.06.02.28.41.73	-10.2	36.39	7.67
2010.07.06.18.15.41.00	-9.36	34.92	24.31
2010.07.07.18.48.10.78	-9.62	34.91	24.25
2010.07.09.17.08.53.57	-6.35	35.19	11.59
2010.07.10.14.33.17.32	-8	36.84	25.56
2010.07.10.14.33.24.97	-8.17	36.35	0.03
2010.07.11.23.51.43.15	-6.61	35.1	0.03
2010.07.14.00.54.3.94	-7.8	37.43	12
2010.07.14.01.56.28.70	-7.84	38.85	15.17
2010.07.15.20.38.37.39	-7.29	35.81	31.63
2010.07.24.00.01.28.68	-6.92	37.79	28.77
2010.07.29.02.56.8.27	-6.8	38.15	25.37
2010.08.03.19.42.16.96	-9.41	39.03	38.3
2010.08.08.01.34.2.66	-10.03	40.64	31.94
2010.09.05.02.08.44.46	-9	37.56	14.25
2010.09.07.15.46.21.20	-7.95	36.01	12
2010.09.17.19.29.33.75	-8.11	37.2	40.03

Date	Latitude	Longitude	Depth
Y M D H M S	Degree	Degree	km
2010.09.17.21.51.52.49	-9.09	37.41	23.54
2010.10.20.22.34.51.19	-8.51	40.19	31.88
2010.10.29.22.56.4.94	-9.29	35.21	12
2011.01.19.18.55.50.75	-6.76	36.08	16.35
2011.01.19.20.01.15.64	-8.33	36.65	14.1
2011.01.19.21.00.39.42	-6.41	35.93	12.2
2011.01.21.02.16.25.48	-10.55	38.86	23.74
2011.01.21.21.51.52.15	-8.5	36.74	13.02
2011.02.02.11.00.49.86	-8.14	38.15	234.71
2011.02.03.01.25.55.29	-9.68	39.54	27.78
2011.02.03.14.21.17.95	-6.49	35.94	10.05
2011.02.07.04.29.23.03	-10.39	34.19	13.82
2011.02.07.14.31.55.85	-5.72	35.93	19.81
2011.02.15.09.28.34.95	-7.94	38.61	31.88
2011.02.17.22.31.54.13	-8.18	38.01	17.02
2011.02.21.23.59.32.36	-5.83	36.15	79.11
2011.03.02.00.02.1.70	-7.01	36.12	0
2011.03.05.00.48.59.57	-9.09	38.91	13.04
2011.03.06.14.42.32.58	-10.82	35.38	12.2
2011.03.07.12.09.42.54	-5.56	35.73	0.01
2011.03.08.00.22.3.33	-7.78	37.91	8.07
2011.03.08.03.34.12.89	-7.32	38.06	28.91
2011.03.08.20.31.38.87	-11.5	34.5	12.2
2011.03.09.08.07.0.46	-6.54	35.32	19.44
2011.03.19.19.44.39.00	-8.34	32.91	150.88
2011.03.21.09.57.27.93	-7.61	37.38	172.33
2011.03.22.02.15.54.58	-8.43	33.46	35.71
2011.03.23.08.06.19.09	-7.14	37.85	0.03
2011.03.24.22.51.30.73	-6.32	36.29	25.49
2011.03.25.10.04.40.15	-8.43	39.42	30.75
2011.03.25.19.01.10.39	-6.76	36.54	0.03
2011.04.03.08.32.13.73	-7.07	38.01	0.03
2011.04.03.14.27.26.95	-9.09	36.82	12.2
2011.04.03.15.26.58.32	-9.01	39.25	29.35
2011.04.07.00.34.37.43	-3.91	35.89	12.2
2011.04.11.20.19.7.10	-9.79	38.17	17.28
2011.04.13.08.13.30.34	-6.3	36.57	0.03
2011.04.15.08.49.35.05	-4.31	35.79	12.2
2011.04.19.10.40.24.61	-5.95	35.91	21.88

Date	Latitude	Longitude	Depth
Y M D H M S	Degree	Degree	km
2011.04.19.13.36.35.45	-6.42	36.29	0.03
2011.04.23.21.08.42.73	-8.82	38.43	16.2
2011.04.24.21.23.49.88	-6.27	36.44	11.52
2011.05.03.10.26.33.90	-6.01	36.19	12.28
2011.05.09.14.50.5.43	-7.79	37.85	0
2011.05.25.05.19.53.21	-9.66	40.68	16.77
2011.05.26.03.07.5.23	-6.65	36.12	0.03
2011.05.30.19.10.7.40	-8.45	34.9	12.2
2011.06.01.23.21.50.01	-6.57	35.7	0
2011.06.05.00.19.45.98	-7.18	36.9	12.2
2011.06.05.21.01.18.22	-7.78	37.96	17.54
2011.06.06.00.47.59.19	-7.75	39.09	33.48
2011.06.08.04.27.54.49	-6	36.54	0.02
2011.06.10.08.28.17.98	-7.12	39.52	30.28
2011.06.11.00.10.40.67	-7.22	39.48	47.52
2011.06.11.07.47.2.90	-6.61	35.75	0.05
2011.06.16.23.45.53.92	-4.92	35.65	0
2011.06.24.15.55.17.29	-7.01	35.54	0
2011.06.26.07.28.0.57	-6.56	35.18	0
2011.07.01.14.04.57.32	-10.56	35.49	12.2

Appendix C: Azimuthal anisotropy analysis (Chapter 3)

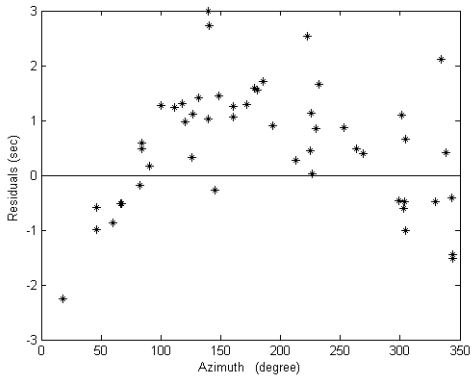

Station TARA

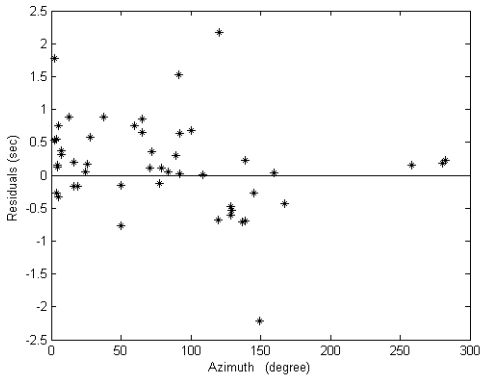

Station SING

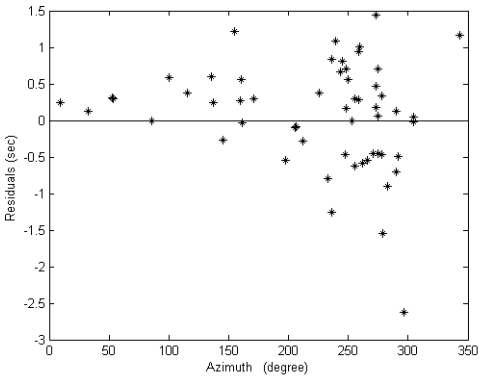

Station MTAN

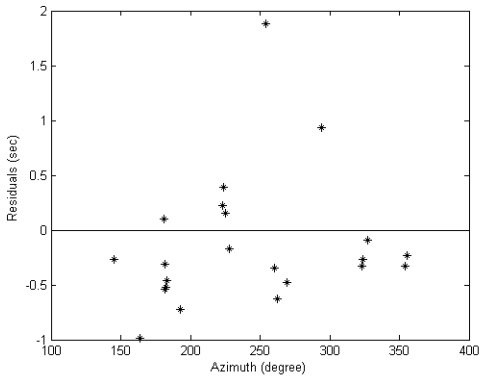

Station KIBA

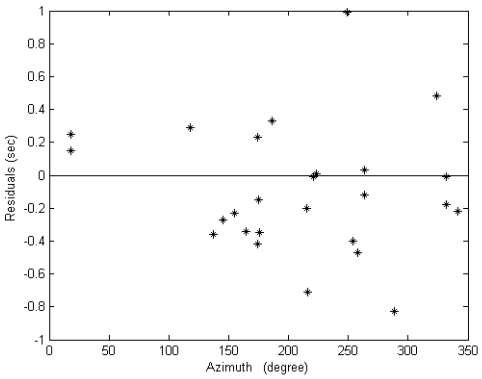

Station LONG

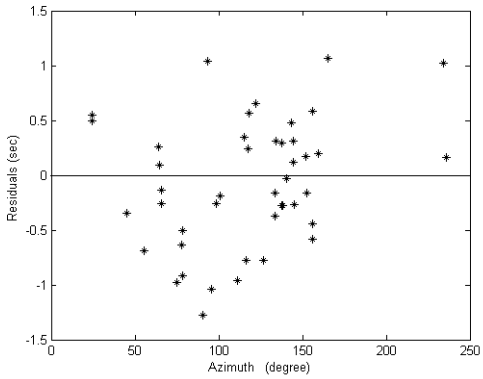

Station HALE

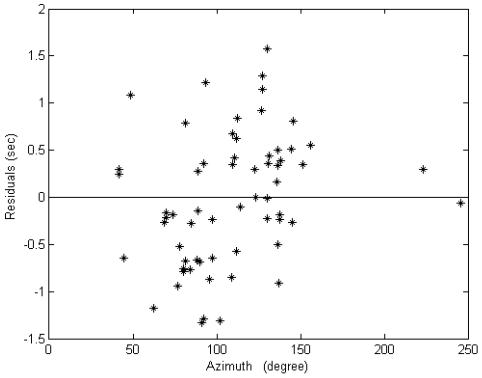

Station RUNG

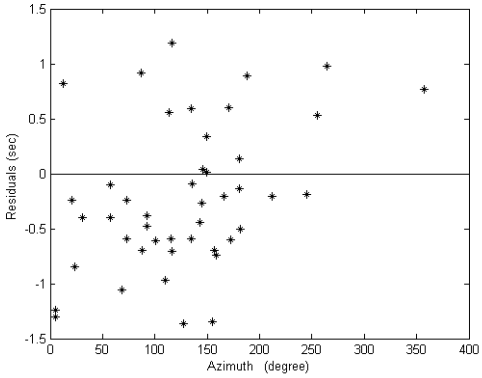

Station KIBE

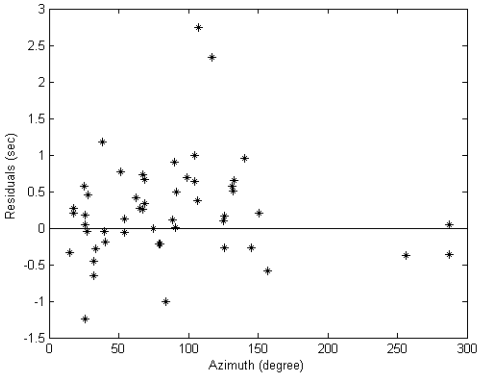

Station KOMO

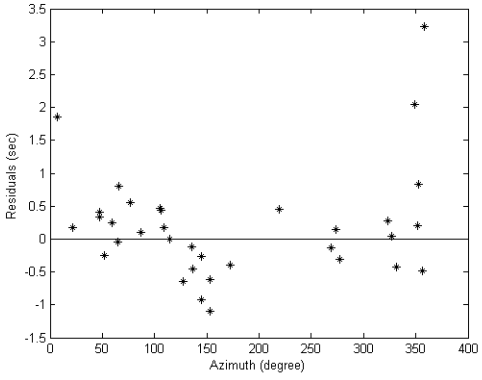

Station INZA

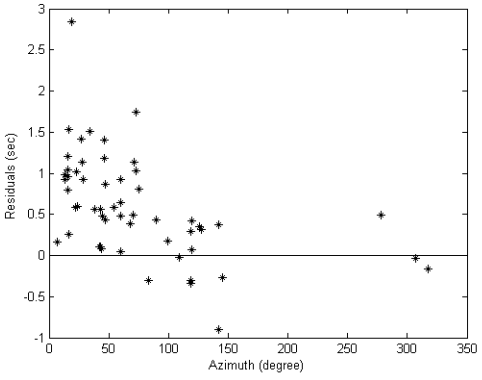

Station URAM

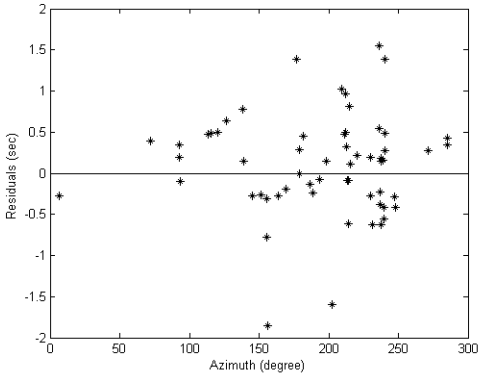

Station PUGE

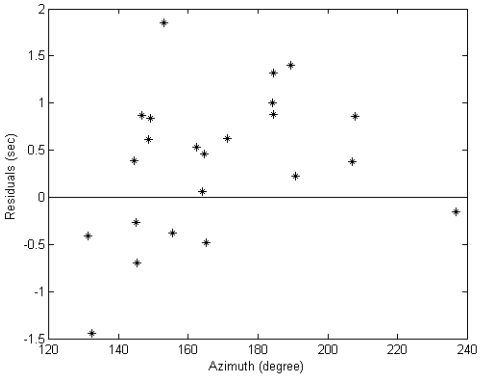

Station GOMA

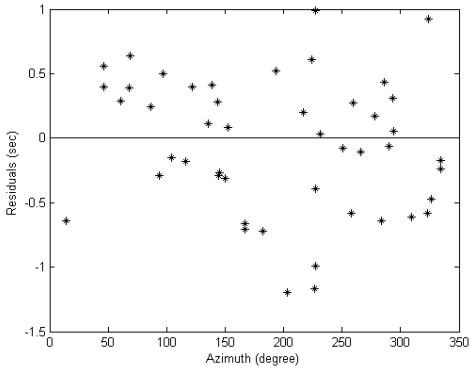

Station MBWE

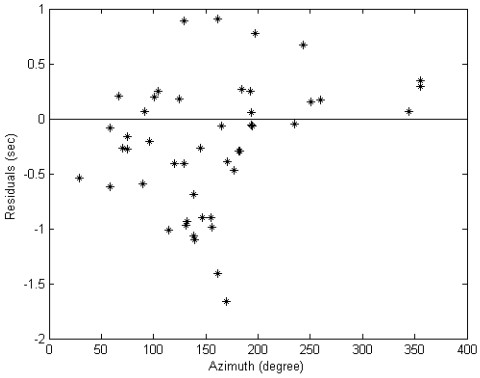

Station MTOR

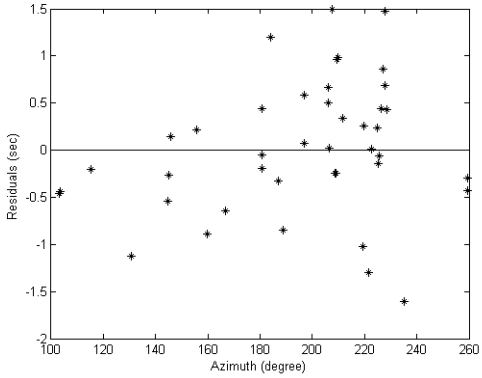

Station MITU

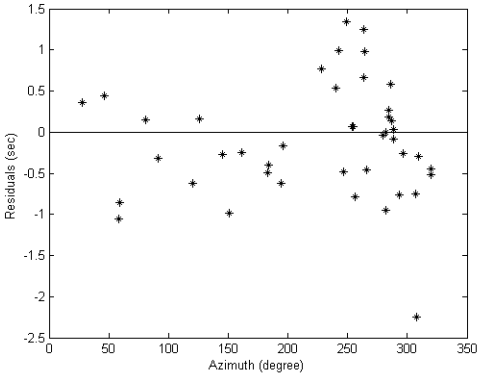

Station TUND

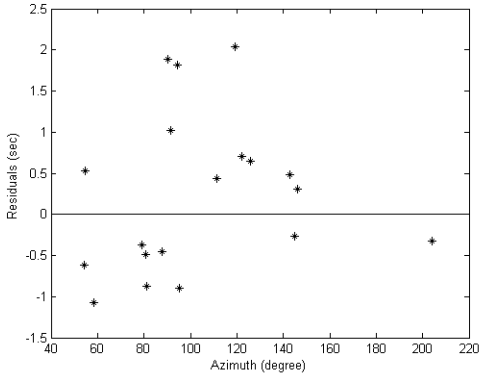

Station BASO

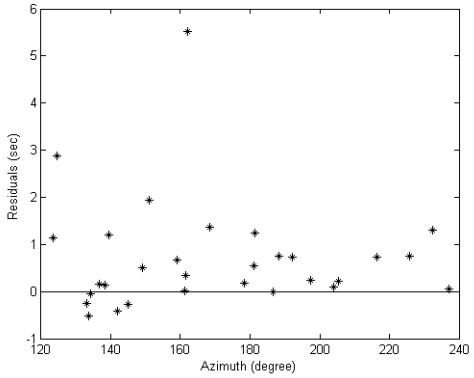

Station PAND

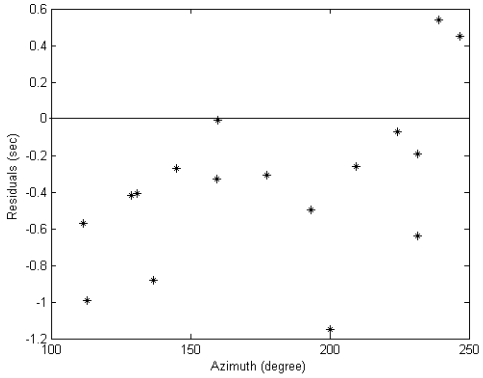

Station KOND

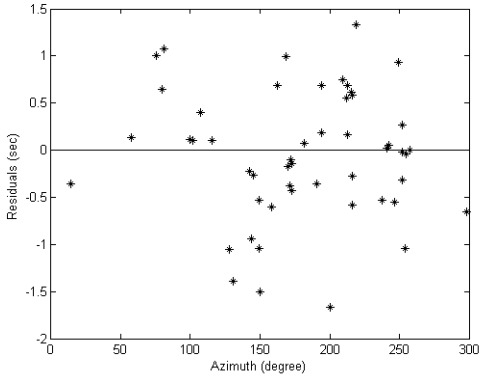

Station KOMO

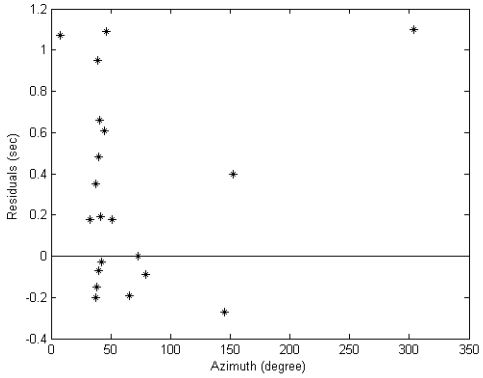

Station BEND

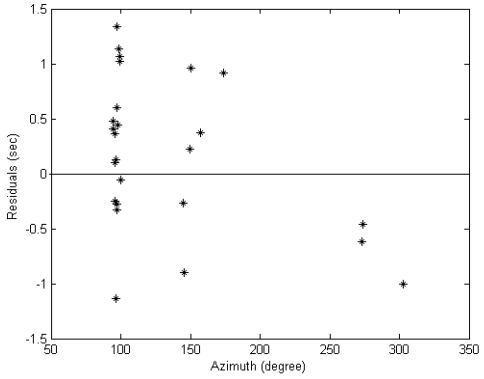

Station BIHA

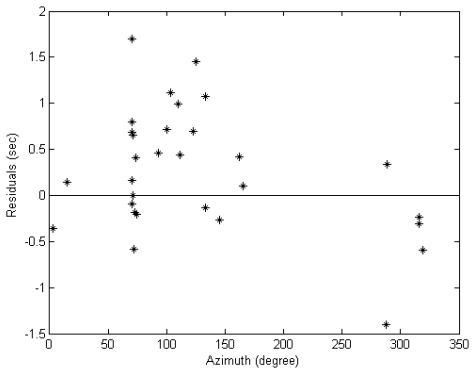

Station BKBA

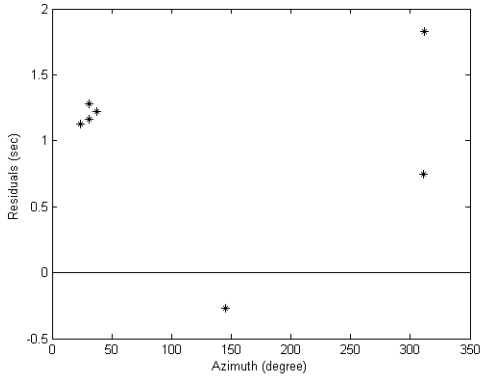

Station BUTI

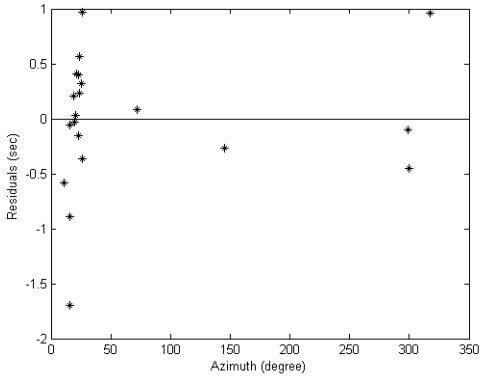

Station FOBO

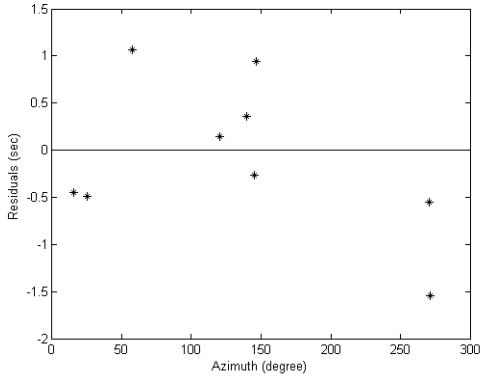

Station GTIT

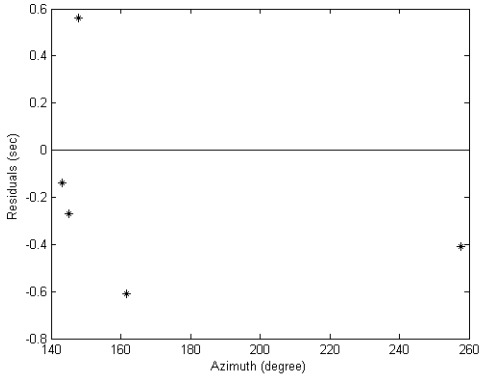

Station HAMA

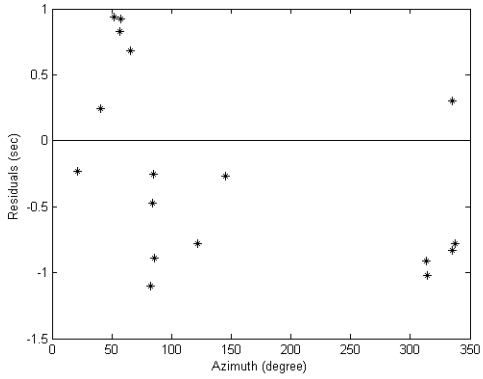

Station JINI

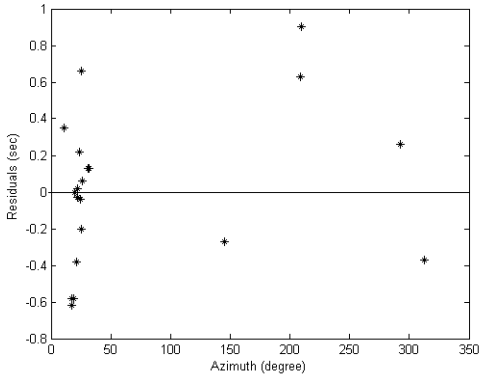

Station KATE

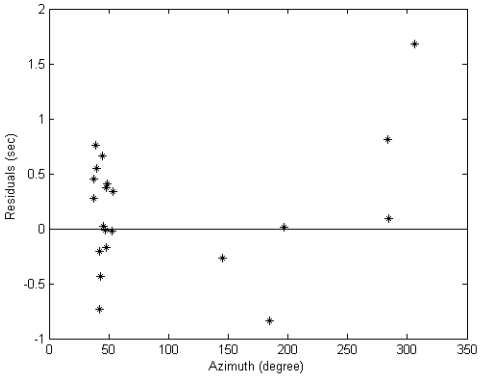

Station KBLE

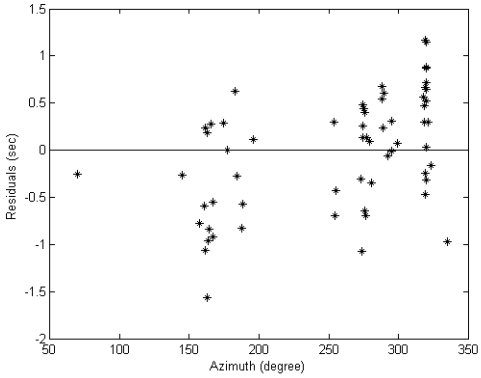

Station KGMA

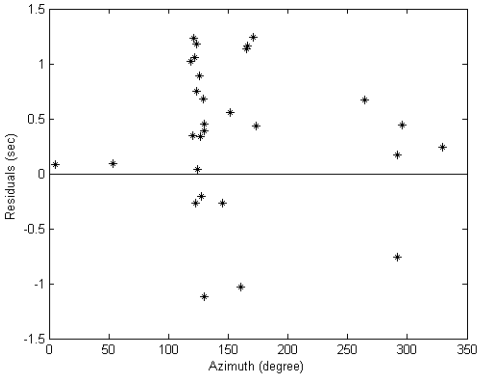

Station KIBO

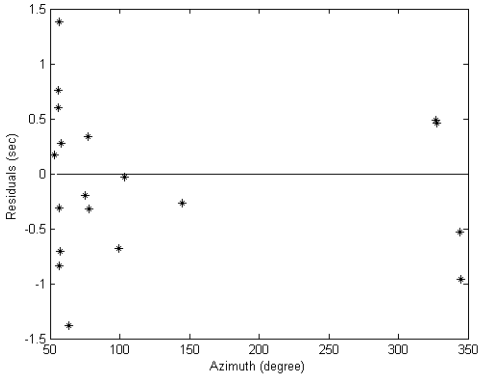

Station MALE

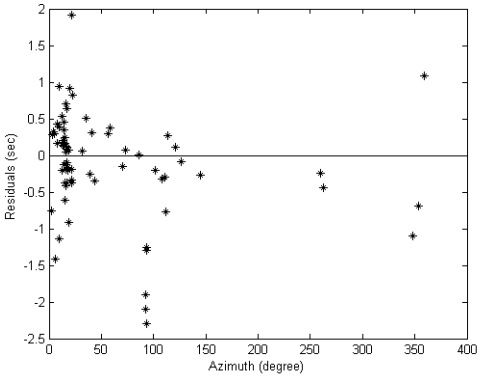

Station MAUS

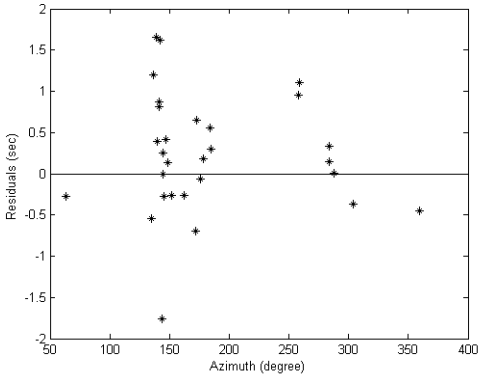

Station MKRE

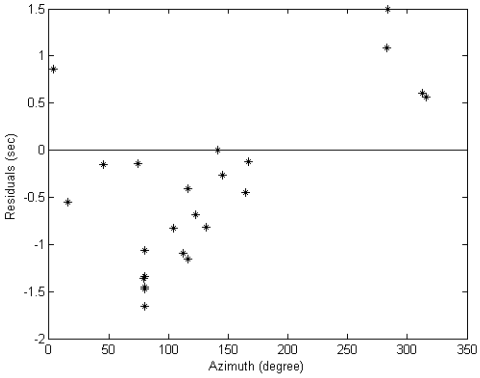

Station MLBA

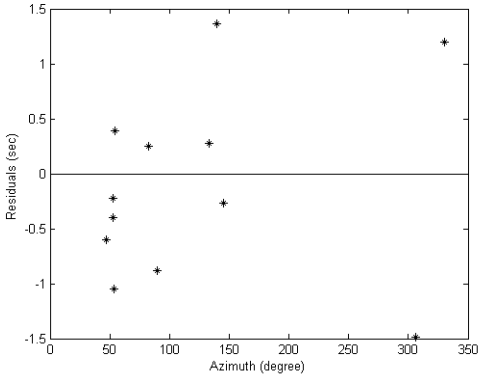

Station PIGI

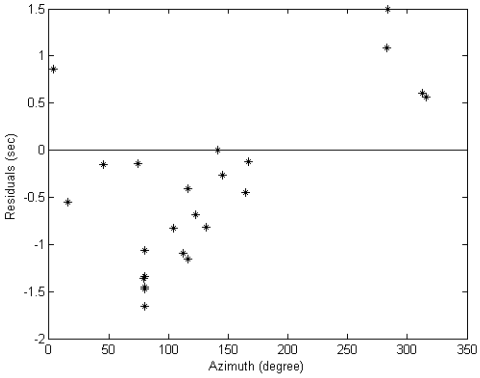

Station SROTI

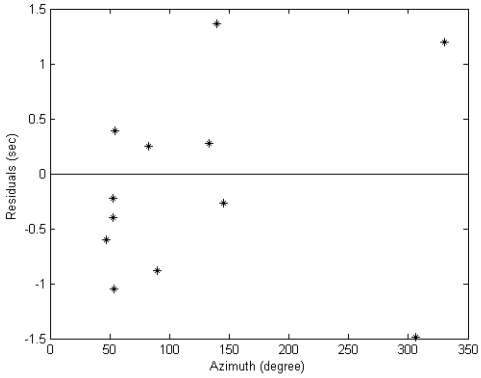

Station SAKA

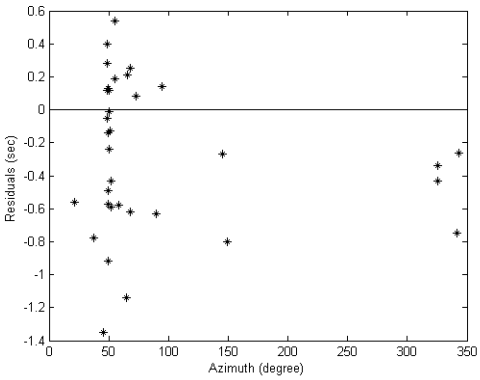

Station SULU

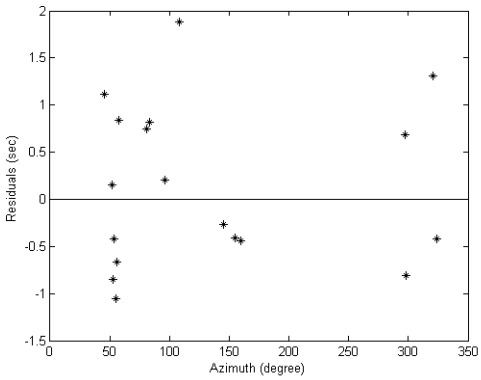

Station UVZA

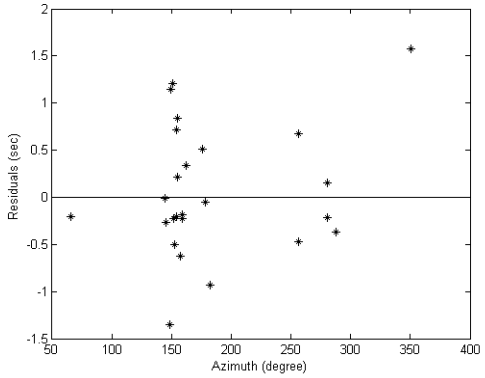

Station PNDA

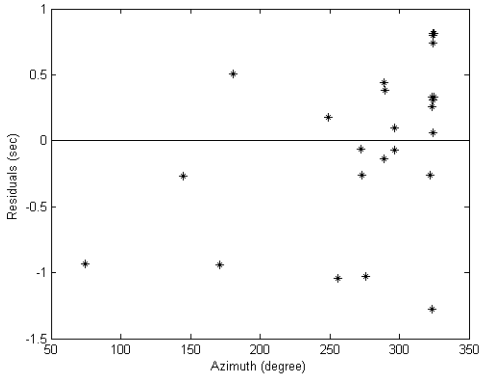

Station NAMA

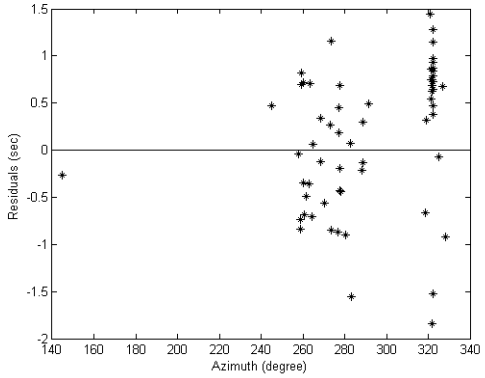

Station CHIM

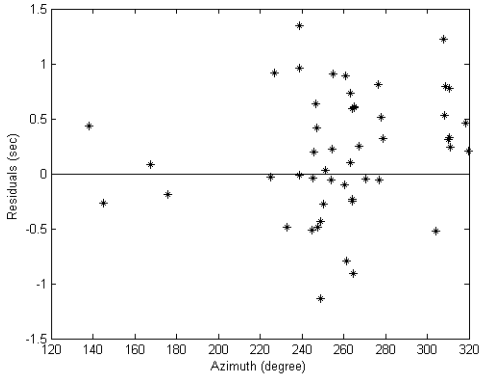

Station KYLA

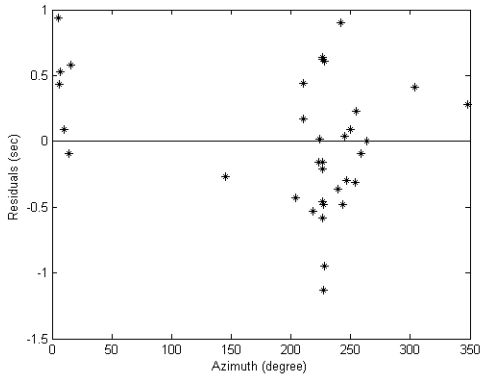

Station NJOM

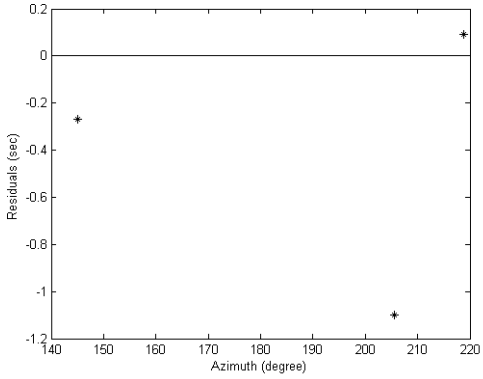

Station LALE

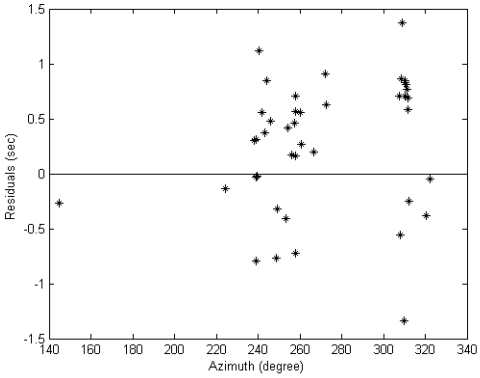

Station SUMB

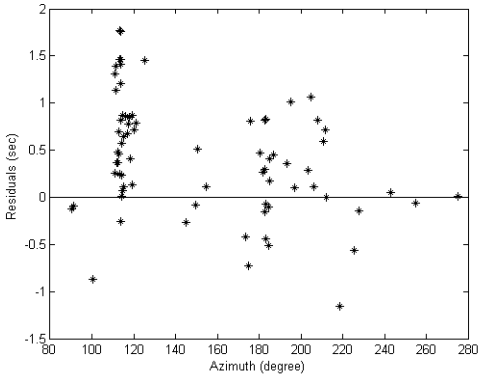

Station SONG

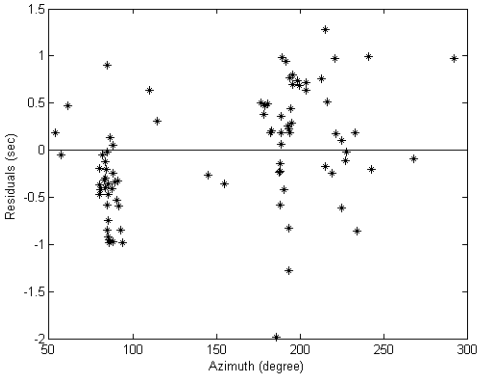

Station WINO

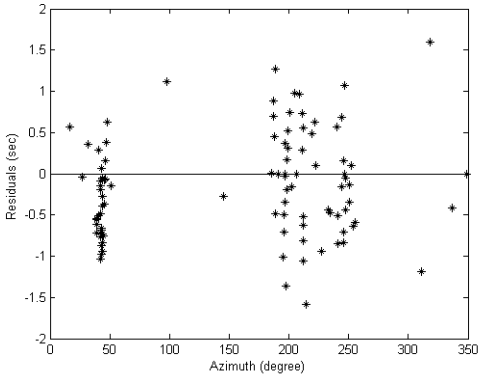

Station MAKA

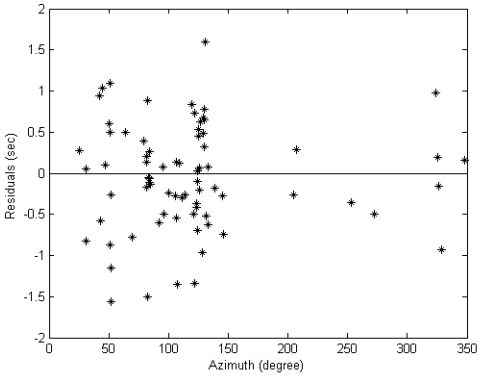

Station MGOR

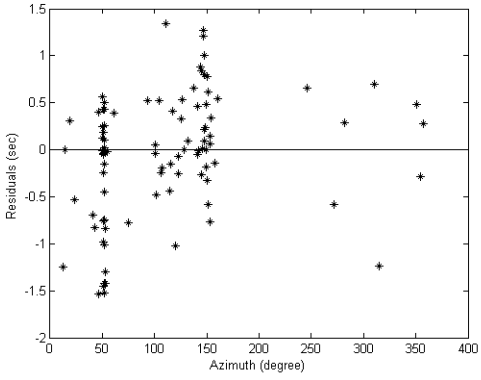

Station MIKU

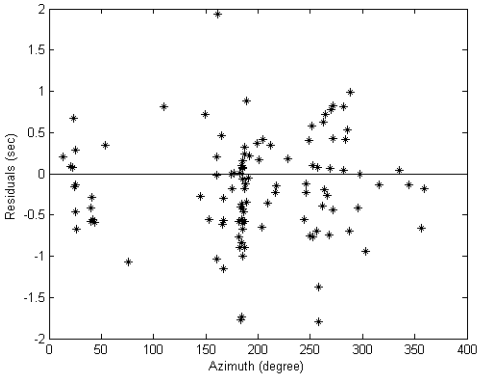

Station IRIN

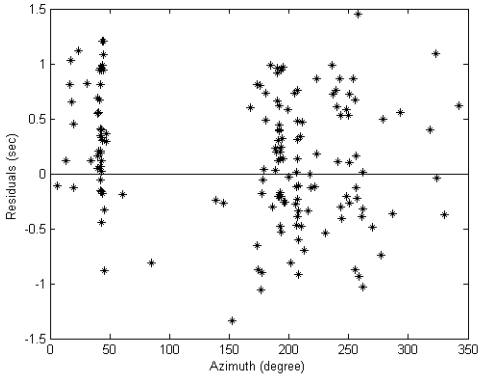

Station MAFI

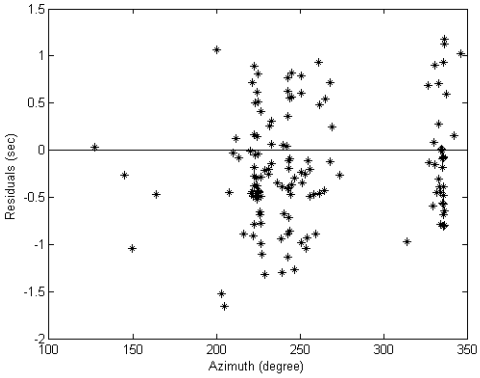

Station LOSS

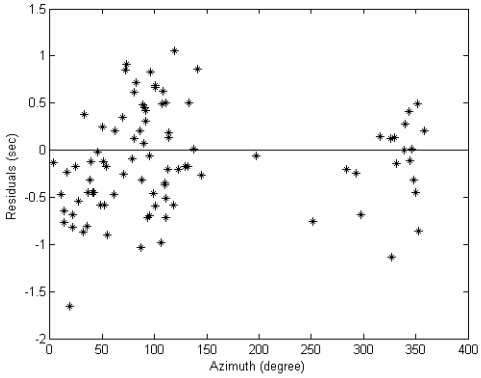

Station CHAL

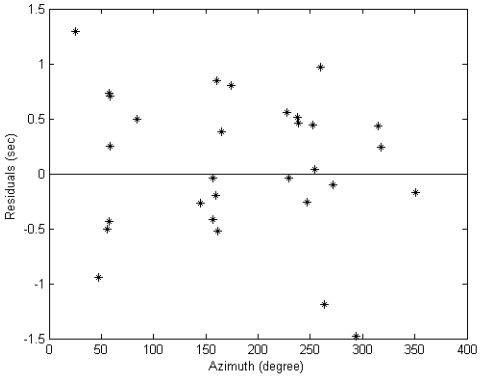

Station IFAK

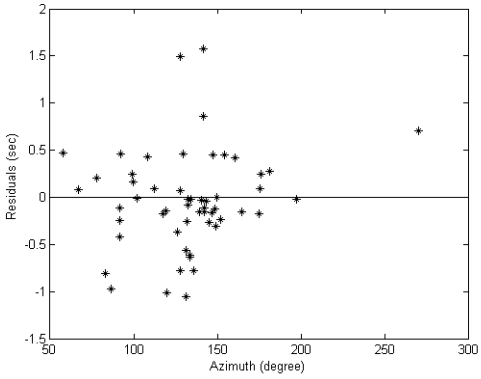

Station INDI

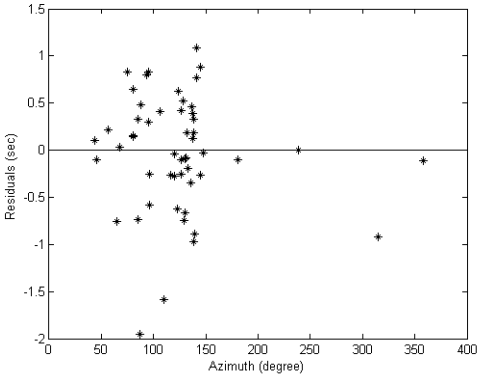

Station KIMA

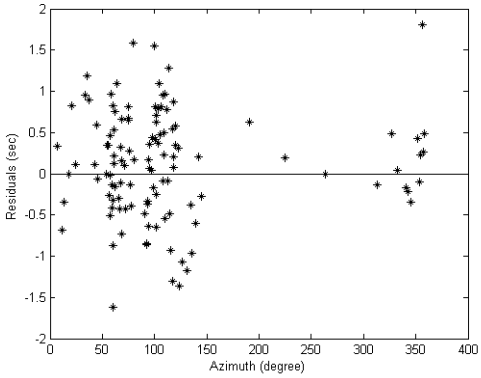

Station MANG

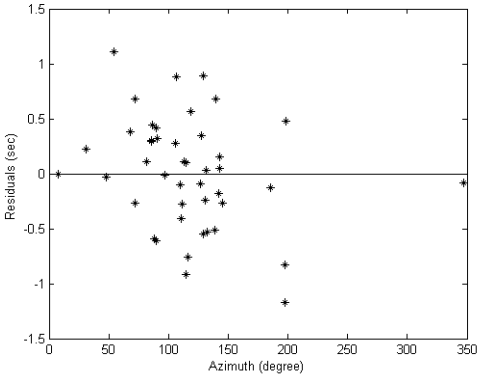

Station MOHO

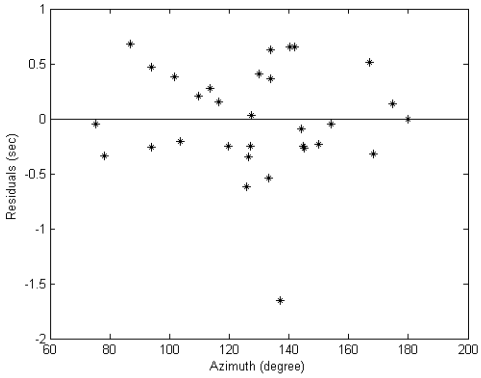

Station MTWA

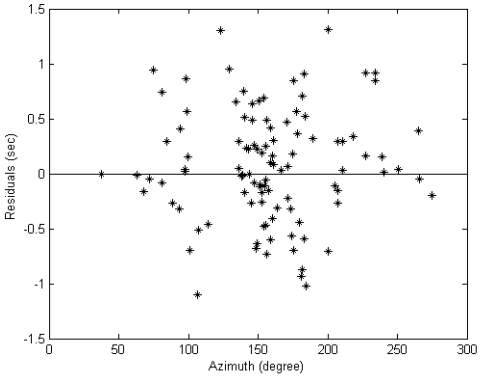

Station WALE

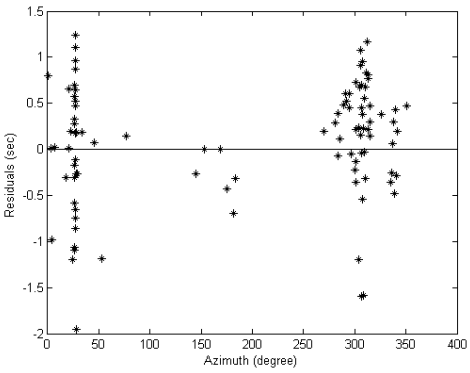

Station DODT

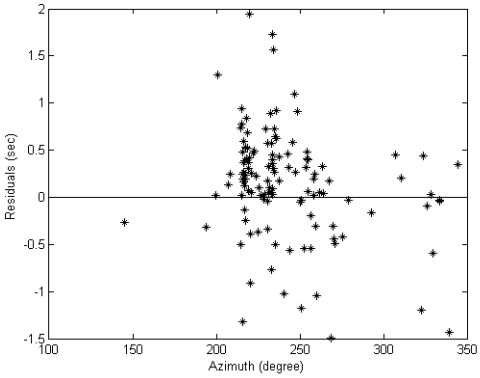

Station MBEY

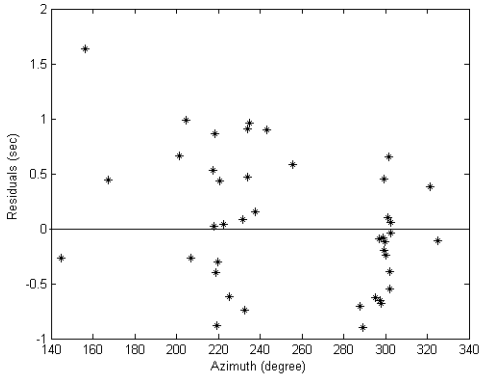

Station TUND

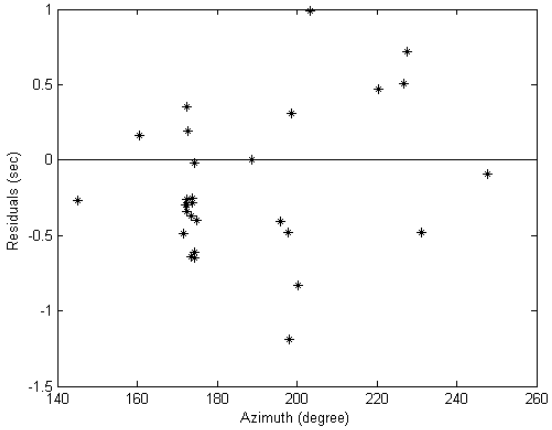

Station MZM